Maximum Likelihood Training of Implicit Nonlinear Diffusion Models

Dongjun Kim[*]
KAIST
dongjoun57@kaist.ac.kr

Byeonghu Na[*]
KAIST
wp03052@kaist.ac.kr

Se Jung Kwon
NAVER CLOVA

Dongsoo Lee
NAVER CLOVA

Wanmo Kang
KAIST

Il-Chul Moon
KAIST / Summary.AI

Abstract

Whereas diverse variations of diffusion models exist, extending the linear diffusion into a nonlinear diffusion process is investigated by very few works. The nonlinearity effect has been hardly understood, but intuitively, there would be promising diffusion patterns to efficiently train the generative distribution towards the data distribution. This paper introduces a data-adaptive nonlinear diffusion process for score-based diffusion models. The proposed Implicit Nonlinear Diffusion Model (INDM) learns by combining a normalizing flow and a diffusion process. Specifically, INDM implicitly constructs a nonlinear diffusion on the *data space* by leveraging a linear diffusion on the *latent space* through a flow network. This flow network is key to forming a nonlinear diffusion, as the nonlinearity depends on the flow network. This flexible nonlinearity improves the learning curve of INDM to nearly Maximum Likelihood Estimation (MLE) against the non-MLE curve of DDPM++, which turns out to be an inflexible version of INDM with the flow fixed as an identity mapping. Also, the discretization of INDM shows the sampling robustness. In experiments, INDM achieves the state-of-the-art FID of 1.75 on CelebA. We release our code at https://github.com/byeonghu-na/INDM.

1 Introduction

Diffusion models have recently achieved success on the task of sample generation, and some works [1, 2] claim state-of-the-art performance over Generative Adversarial Networks (GAN) [3]. This success is highlighted particularly in likelihood-based models, including normalizing flows [4], autoregressive models [5], and Variational Auto-Encoders (VAE) [6]. Moreover, this success is noteworthy because it is achieved merely using linear diffusion processes, such as Variance Exploding (VE) Stochastic Differential Equation (SDE) [7], and Variance Preserving (VP) SDE [8].

This paper extends linear diffusions of VE/VP SDEs to a data-adaptive trainable nonlinear diffusion. To motivate the extension, though there are structural similarities between diffusion models and VAEs, the inference part of a linear diffusion process has not been trained while its counterpart of VAE (the encoder) has been trained. We introduce Implicit Nonlinear Diffusion Models (INDM) to train its *forward* SDE, the inference part in diffusion models. INDM constructs the nonlinearity of the data diffusion by transforming a linear *latent* diffusion back to the data space.

We implement the transformation between the data and latent spaces with a normalizing flow. The invertibility of the flow mapping is key to learning a nonlinear inference part. Invertibility is necessary

[*]Equal contribution

36th Conference on Neural Information Processing Systems (NeurIPS 2022).

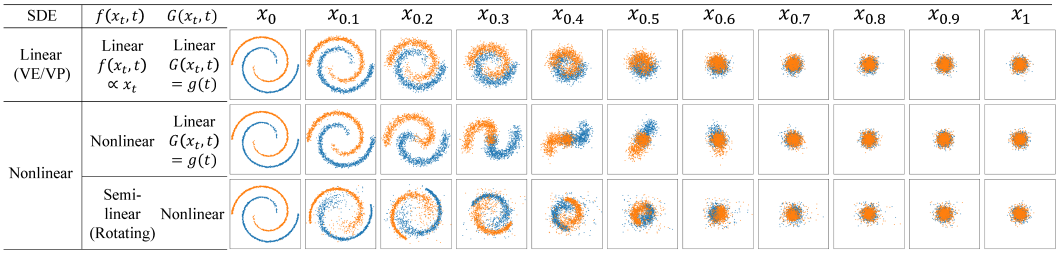

Figure 1: Examples of linear (top row) and nonlinear (middle/bottom rows) diffusion processes.

for constructing the nonlinearity, and we clarify this by comparing INDM with LSGM [9], a latent diffusion model with VAE. Altogether, INDM provides the following advantages over the existing models.

- INDM achieves fast and tractable optimization with *implicit* modeling.
- INDM learns not only drift but *volatility* coefficients of the forward SDE.
- INDM trains its network with *Maximum Likelihood Estimation* (MLE).
- INDM is *robust* on the sampling discretization.

2 Preliminary

A diffusion model is constructed with bidirectional *forward* and *reverse* stochastic processes.

Forward and Reverse Diffusions A forward diffusion process diffuses an input data variable, $\mathbf{x}_0 \sim p_r$, to a noise variable, and the corresponding reverse diffusion process [10] of this forward diffusion denoises a noise variable to regenerate the input variable. The forward diffusion is fully described by an SDE of $\mathrm{d}\mathbf{x}_t = \mathbf{f}(\mathbf{x}_t, t)\,\mathrm{d}t + \mathbf{G}(\mathbf{x}_t, t)\,\mathrm{d}\mathbf{w}_t$, and the corresponding reverse SDE becomes $\mathrm{d}\mathbf{x}_t = \left[\mathbf{f}(\mathbf{x}_t, t) - \mathrm{div}(\mathbf{G}\mathbf{G}^T)(\mathbf{x}_t, t) - (\mathbf{G}\mathbf{G}^T)(\mathbf{x}_t, t)\nabla_{\mathbf{x}_t} \log p_t(\mathbf{x}_t)\right] \mathrm{d}\bar{t} + \mathbf{G}(\mathbf{x}_t, t)\,\mathrm{d}\bar{\mathbf{w}}_t$. Here, $\mathbf{w}_t \in \mathbb{R}^d$ is an abstraction of a random walk process with independent increments, where d is the data dimension, and $\mathrm{d}\bar{\mathbf{w}}_t$ is the standard Wiener processes with backwards in time.

Generative Diffusion Having that the drift ($\mathbf{f} \in \mathbb{R}^d$) and the volatility ($\mathbf{G} \in \mathbb{R}^{d \times d}$) terms are given a-priori, diffusion models [1] estimate the data score, $\nabla_{\mathbf{x}_t} \log p_t(\mathbf{x}_t)$, with the score network, $\mathbf{s}_{\boldsymbol{\theta}}(\mathbf{x}_t, t)$. By plugging the score network in the data score, we obtain another diffusion process, called the *generative* SDE, described by $\mathrm{d}\mathbf{x}_t^{\boldsymbol{\theta}} = \left[\mathbf{f}(\mathbf{x}_t^{\boldsymbol{\theta}}, t) - \mathrm{div}(\mathbf{G}\mathbf{G}^T)(\mathbf{x}_t^{\boldsymbol{\theta}}, t) - (\mathbf{G}\mathbf{G}^T)(\mathbf{x}_t^{\boldsymbol{\theta}}, t)\mathbf{s}_{\boldsymbol{\theta}}(\mathbf{x}_t^{\boldsymbol{\theta}}, t)\right] \mathrm{d}\bar{t} + \mathbf{G}(\mathbf{x}_t^{\boldsymbol{\theta}}, t)\,\mathrm{d}\bar{\mathbf{w}}_t$. Starting from a prior distribution of $\mathbf{x}_T^{\boldsymbol{\theta}} \sim \pi$ and solving the SDE time backwards, Song et al. [1] construct the generative stochastic process of $\{\mathbf{x}_t^{\boldsymbol{\theta}}\}_{t=0}^T$ that perfectly reconstructs the reverse process of $\{\mathbf{x}_t\}_{t=0}^T$ under two conditions: 1) $\mathbf{s}_{\boldsymbol{\theta}}(\mathbf{x}_t, t) = \nabla_{\mathbf{x}_t} \log p_t(\mathbf{x}_t)$ and 2) $\mathbf{x}_T \sim \pi$. We define a generative distribution, $p_{\boldsymbol{\theta}}$, as the distribution of $\mathbf{x}_0^{\boldsymbol{\theta}}$.

Score Estimation The diffusion model estimates the data score with the score network by minimizing the denoising score loss [1], given by $\mathcal{L}(\{\mathbf{x}_t\}_{t=0}^T, \lambda; \boldsymbol{\theta}) = \int_0^T \lambda(t)\mathbb{E}_{\mathbf{x}_0, \mathbf{x}_t}[\|\mathbf{s}_{\boldsymbol{\theta}}(\mathbf{x}_t, t) - \nabla_{\mathbf{x}_t} \log p_{0t}(\mathbf{x}_t|\mathbf{x}_0)\|_2^2]\,\mathrm{d}t$, where $p_{0t}(\mathbf{x}_t|\mathbf{x}_0)$ is a transition probability of $\mathbf{x}_t$ given $\mathbf{x}_0$; and λ is the weighting function that determines the level of contribution for each diffusion time. When $\mathbf{G}(\mathbf{x}_t, t) = g(t)$, Song et al. [11], Huang et al. [12] proved that this loss with the likelihood weighting ($\lambda = g^2$) turns out to be a variational bound of the negative log-likelihood: $\mathbb{E}_{\mathbf{x}_0}[-\log p_{\boldsymbol{\theta}}(\mathbf{x}_0)] \leq \mathcal{L}(\{\mathbf{x}_t\}_{t=0}^T, g^2; \boldsymbol{\theta}) - \mathbb{E}_{\mathbf{x}_T}[\log \pi(\mathbf{x}_T)]$, up to a constant, see Appendix A.1 for a detailed discussion.

Choice of Drift ($\mathbf{f}$) and Volatility ($\mathbf{G}$) Terms The original diffusion model strictly limits the scope of diffusion process to be a family of linear diffusions that $\mathbf{f}$ is a linear function of $\mathbf{x}_t$ and $\mathbf{G}$ is an identity matrix multiplied by a t-function. For instance, VESDE [1, 7] satisfies $\mathbf{f} \equiv 0$ with $\mathbf{G} = \sqrt{\mathrm{d}\sigma^2(t)/\mathrm{d}t}\mathbf{I}$ and VPSDE [1, 8] satisfies $\mathbf{f} = -\frac{1}{2}\beta(t)\mathbf{x}_t \propto \mathbf{x}_t$ with $\mathbf{G} = \sqrt{\beta(t)}\mathbf{I}$. Few concurrent works have extended linear diffusions to nonlinear diffusions by 1) applyng a latent diffusion using VAE in LSGM [9], 2) applying a flow network to nonlinearize the drift term in DiffFlow [13], and 3) reformulating the diffusion model into a Schrodinger Bridge Problem (SBP) [14–16]. We further analyze these approaches in Section 5.

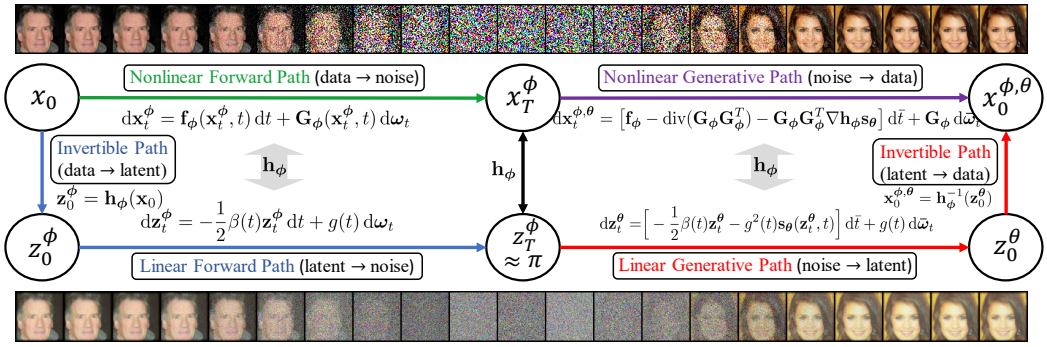

Figure 3: INDM attains a ladder structure between the data space and the latent space. The latent vector is visualized by normalizing the latent value, see Appendix F.5.2 for further visualization.

3 Motivation of Nonlinear Diffusion Process

Figure 1 illustrates various diffusion processes on a spiral toy dataset. In the top row, the diffusion path of VPSDE keeps its overall structure of the initial data manifold during the data deformation procedure to $\mathcal{N}(0, \mathbf{I})$. The drift vector field illustrated in Figure 2-(a) as black arrows presents that VPSDE *linearly* deforms its data distribution.

Unlike the linear diffusion, the middle row of Figure 1 with a nonlinear drift shows that the data is not linearly deformed to $\mathcal{N}(0, \mathbf{I})$. Figure 2-(b) illustrates the corresponding vector field, in which two distinctive components (orange/blue) are forced to separate each other. The nonlinearity of the drift term represented as rotating black arrows is the source of such nonlinear deformation at the intermediate steps, $\mathbf{x}_{0.2} \sim \mathbf{x}_{0.6}$. When it comes to the volatility term, the last row of Figure 1 presents the process with nonlinear $\mathbf{G}$. Figure 2-(c) illustrates the covariance matrices of the perturbation distribution at $t = 0$ with linear and nonlinear volatility terms, where the perturbation distribution induced by the volatility term is $\mathcal{N}(0, \mathbf{G}(\mathbf{x}_t, t)\mathbf{G}^T(\mathbf{x}_t, t))$[1]. It shows the non-diagonal and data-dependent covariances of $\mathbf{G}\mathbf{G}^T$ in red ellipses of a nonlinear volatility term, and the isotropic blue circles of linear diffusions.

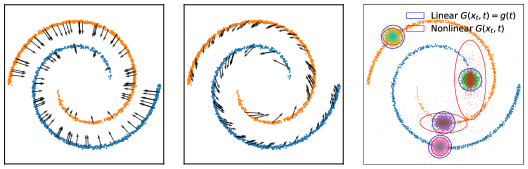

(a) Linear $\mathbf{f} \propto \mathbf{x}_t$ (b) Nonlinear $\mathbf{f}$ (c) Nonlinear $\mathbf{G}$

Figure 2: Vector fields on various SDEs at $t = 0$.

4 Implicit Nonlinear Diffusion Model

There are two ways to nonlinearize the drift and volatility coefficients in SDE: explicit and implicit parametrizations. While explicit is a straightforward way to model the nonlinearity, it becomes impractical particularly in the training procedure. Concretely, in each of the training iteration, the denoising loss $\mathcal{L}(\{\mathbf{x}_t\}_{t=0}^T, \lambda; \boldsymbol{\theta})$ requires 1) the perturbed samples $\mathbf{x}_t$ from $p_{0t}(\mathbf{x}_t|\mathbf{x}_0)$ and 2) the calculation of $\nabla \log p_{0t}(\mathbf{x}_t|\mathbf{x}_0)$, and these two steps require long execution time because the transition probability $p_{0t}(\mathbf{x}_t|\mathbf{x}_0)$ is intractable for nonlinear diffusions in general. Therefore, we parametrize $\mathbf{f}_\phi$ and $\mathbf{G}_\phi$ *implicitly* for fast and tractable optimization. As visualized in Figure 3, we impose a linear diffusion model on the latent space, and connect this latent variable with the data variable through a normalizing flow. The nonlinear diffusion on the data space, then, is induced from the latent diffusion leveraged to the data space.

4.1 Data and Latent Diffusion Processes

Latent Diffusion Processes Let us define $\mathbf{z}_0^\phi$ to be a transformed latent variable $\mathbf{z}_0^\phi = \mathbf{h}_\phi(\mathbf{x}_0)$, where $\mathbf{h}_\phi$ is a transformation of the normalizing flow. Then, a forward linear diffusion

(Latent Forward SDE) $$\mathrm{d}\mathbf{z}_t^\phi = -\frac{1}{2}\beta(t)\mathbf{z}_t^\phi \,\mathrm{d}t + g(t)\,\mathrm{d}\mathbf{w}_t,$$

[1]The covariance is $\frac{\mathrm{d}}{\mathrm{d}t}\mathbb{E}_{\mathbf{x}_{t+\mathrm{d}t}|\mathbf{x}_t}[(\mathbf{x}_{t+\mathrm{d}t} - \mathbf{x}_t - \mathbf{f}\,\mathrm{d}t)(\mathbf{x}_{t+\mathrm{d}t} - \mathbf{x}_t - \mathbf{f}\,\mathrm{d}t)^T] = \mathbf{G}(\mathbf{x}_t, t)\mathbf{G}^T(\mathbf{x}_t, t)$.

starting at $\mathbf{z}_0^{\phi} = \mathbf{h}_{\phi}(\mathbf{x}_0)$ with $\mathbf{x}_0 \sim p_r$, describes the forward diffusion process on the latent space (blue diffusion path in Figure 3). The corresponding reverse latent diffusion is given by $\mathrm{d}\mathbf{z}_t^{\phi} = [-\frac{1}{2}\beta(t)\mathbf{z}_t^{\phi} - g^2(t)\nabla_{\mathbf{z}_t^{\phi}} \log p_t^{\phi}(\mathbf{z}_t^{\phi})]\,\mathrm{d}\bar{t} + g(t)\,\mathrm{d}\bar{\mathbf{w}}_t$, where p_t^{ϕ} is the probability of $\mathbf{z}_t^{\phi}$.

Forward Data Diffusion We have not defined the data diffusion process yet. We build the data diffusion from the latent diffusion and the normalizing flow. From the invertibility, we define random variables on the data space by transforming the latent linear diffusion back to the data space: $\mathbf{x}_t^{\phi} := \mathbf{h}_{\phi}^{-1}(\mathbf{z}_t^{\phi})$ for any $t \in [0, T]$. Then, from the Ito's formula [17], the process $\{\mathbf{x}_t^{\phi}\}_{t=0}^{T}$ follows

$$\text{(Data Forward SDE)} \qquad \mathrm{d}\mathbf{x}_t^{\phi} = \mathbf{f}_{\phi}(\mathbf{x}_t^{\phi}, t)\,\mathrm{d}t + \mathbf{G}_{\phi}(\mathbf{x}_t^{\phi}, t)\,\mathrm{d}\mathbf{w}_t,$$

starting with $\mathbf{x}_0^{\phi} = \mathbf{h}_{\phi}^{-1}(\mathbf{z}_0^{\phi})$. From $\mathbf{x}_0^{\phi} = \mathbf{h}_{\phi}^{-1}(\mathbf{h}_{\phi}(\mathbf{x}_0)) = \mathbf{x}_0 \sim p_r$, we call this process by *induced diffusion* that permeates the data variable on the data space. We emphasize that this induced diffusion collapses to a linear diffusion if $\mathbf{h}_{\phi_{id}} = id$. See Appendix A.2 for details on drift and volatility terms.

Generative Data Diffusion A diffusion model estimates the forward latent score $\mathbf{s}_{\phi}(\mathbf{z}, t) = \nabla \log p_t^{\phi}(\mathbf{z})$ with the score network, $\mathbf{s}_{\theta}(\mathbf{z}, t)$, to mimic the forward linear diffusion on the latent space. Then, the generative SDE on the latent space becomes

$$\text{(Latent Gen. SDE)} \qquad \mathrm{d}\mathbf{z}_t^{\theta} = \left[-\frac{1}{2}\beta(t)\mathbf{z}_t^{\theta} - g^2(t)\mathbf{s}_{\theta}(\mathbf{z}_t^{\theta}, t) \right] \mathrm{d}\bar{t} + g(t)\,\mathrm{d}\bar{\mathbf{w}}_t$$

with a starting variable $\mathbf{z}_T^{\theta} \sim \pi$. Thus, the process $\{\mathbf{x}_t^{\phi,\theta}\}_{t=0}^{T}$ of $\mathbf{x}_t^{\phi,\theta} := \mathbf{h}_{\phi}^{-1}(\mathbf{z}_t^{\theta})$ becomes a generative data diffusion (purple path in Figure 3) with SDE of

$$\text{(Data Gen. SDE)} \quad \mathrm{d}\mathbf{x}_t^{\phi,\theta} = \left[\mathbf{f}_{\phi} - \mathrm{div}(\mathbf{G}_{\phi}\mathbf{G}_{\phi}^T) - (\mathbf{G}_{\phi}\mathbf{G}_{\phi}^T \nabla \mathbf{h}_{\phi})\mathbf{s}_{\theta}\big(\mathbf{h}_{\phi}(\mathbf{x}_t^{\phi,\theta}), t\big)\right] \mathrm{d}\bar{t} + \mathbf{G}_{\phi}\,\mathrm{d}\bar{\mathbf{w}}_t.$$

4.2 Model Training and Sampling

Likelihood Training Theorem 1 estimates Negative Evidence Lower Bound (NELBO) of Negaitve Log-Likelihood (NLL). For the notational simplicity, we define the targetted score function by

$$\text{(Target of Score Estimation)} \qquad \mathbf{s}_{\phi}(\mathbf{z}_t^{\phi}, t) := \nabla \log p_t^{\phi}(\mathbf{z}_t^{\phi}).$$

Also, suppose $\mathcal{L}\big(\{\mathbf{z}_t^{\phi}\}_{t=0}^{T}, g^2; \theta\big) = \frac{1}{2}\int_0^T g^2(t)\mathbb{E}_{\mathbf{z}_0^{\phi}, \mathbf{z}_t^{\phi}}\big[\|\mathbf{s}_{\theta}(\mathbf{z}_t^{\phi}, t) - \nabla \log p_{0t}(\mathbf{z}_t^{\phi}|\mathbf{z}_0^{\phi})\|_2^2\big]\,\mathrm{d}t$, where $p_{0t}(\mathbf{z}_t^{\phi}|\mathbf{z}_0^{\phi})$ is the transition probability of the latent forward diffusion. In Theorem 1, we drop the constant terms that do not hurt the essence of the theorem to keep the simplicity. See full details and the proof in Appendix G.

Theorem 1. *Suppose that $p_{\phi,\theta}$ is the likelihood of a generative random variable $\mathbf{x}_0^{\phi,\theta}$. Then, the negative log-likelihood is upper bounded by*

$$\mathbb{E}_{\mathbf{x}_0}\big[-\log p_{\phi,\theta}(\mathbf{x}_0)\big] \le \mathcal{L}\big(\{\mathbf{x}_t\}_{t=0}^{T}, g^2; \{\phi, \theta\}\big),$$

where

$$\mathcal{L}\big(\{\mathbf{x}_t\}_{t=0}^{T}, g^2; \{\phi, \theta\}\big) = \frac{1}{2}\int_0^T g^2(t)\mathbb{E}_{\mathbf{z}_t^{\phi}}\big[\|\mathbf{s}_{\theta}(\mathbf{z}_t^{\phi}, t) - \mathbf{s}_{\phi}(\mathbf{z}_t^{\phi}, t)\|_2^2\big]\,\mathrm{d}t + D_{KL}(p_T^{\phi}\|\pi) \quad (1)$$

$$= -\mathbb{E}_{\mathbf{x}_0}\big[\log\big|\det\big(\nabla \mathbf{h}_{\phi}(\mathbf{x}_0)\big)\big|\big] + \mathcal{L}\big(\{\mathbf{z}_t^{\phi}\}_{t=0}^{T}, g^2; \theta\big) - \mathbb{E}_{\mathbf{z}_T^{\phi}}\big[\log \pi(\mathbf{z}_T^{\phi})\big]. \quad (2)$$

Eq. (1) is the KL divergence $D_{KL}(\boldsymbol{\mu}_{\phi}\|\boldsymbol{\nu}_{\phi,\theta})$, where $\boldsymbol{\mu}_{\phi}$ and $\boldsymbol{\nu}_{\phi,\theta}$ are the path measures of the forward and generative diffusions on the data space. Eq. (1) explains the reasoning of why $\mathbf{s}_{\phi}$ is the target of the score estimation. However, the KL divergence is intractable, and Theorem 1 provides an equivalent tractable loss by Eq. (2), the summation of the flow loss with the denoising loss.

Algorithm 1 describes the line-by-line algorithm of INDM training. We obtain the flow loss by taking a flow evaluation. Afterward, we compute the denoising loss. We train the flow with Eq. (2). However, we train the score with $\mathcal{L}\big(\{\mathbf{x}_t\}_{t=0}^{T}, \lambda; \{\phi, \theta\}\big)$ with various λ settings for a better Fréchet Inception Distance (FID) [18].

Latent Sampling While either of red or purple path in Figure 3 could synthesize the samples, we choose the red path for the fast sampling (because the red path feed-forwards the flow only once). Starting from a pure noise $\mathbf{z}_T^{\theta} \sim \pi$, we denoise $\mathbf{z}_T^{\theta}$ to $\mathbf{z}_0^{\theta}$ by solving the generative process backward on the latent space. Then, we transform the fully denoised latent $\mathbf{z}_0^{\theta}$ to the data space $\mathbf{x}_0^{\phi,\theta} = \mathbf{h}_{\phi}^{-1}(\mathbf{z}_0^{\theta})$.

Table 1: Comparison of INDM with previous works. N is the number of random variables.

Model	Nonlinear Diffusion	Implemented Data Diffusion	Latent Diffusion	Nonlinear $\mathbf{f}$-Modeling	Nonlinear $\mathbf{G}$-Modeling	Explicit $\mathbf{f}$&$\mathbf{G}$ Derived	Training Complexity	Sampling Cost
DDPM++	✗	Continuous	✗	✗	✗	✓	$O(1)$	$\downarrow$
LSGM	✗	✗	Continuous	✗	✗	✗	$O(1)$	$\downarrow$
SBP	△	Discrete	✗	Explicit	✗	✓	$O(N)$	$\downarrow$
DiffFlow	✓	Discrete	✗	Explicit	✗	✓	$O(N)$	$\uparrow$
INDM	✓	Continuous	Continuous	Implicit	Implicit	✓	$O(1)$	$\downarrow$

5 Related Work

In this section, we compare INDM with previous works, and summarize our arguments in Table 1.

Algorithm 1 Implicit Nonlinear Diffusion Model

repeat
  Get latent with flow by $\mathbf{z}_0^{\boldsymbol{\phi}} = \mathbf{h}_{\boldsymbol{\phi}}(\mathbf{x}_0)$ for $\mathbf{x}_0 \sim p_r$
  Compute $-\mathbb{E}_{\mathbf{x}_0}\left[\log\left|\det\left(\nabla \mathbf{h}_{\boldsymbol{\phi}}(\mathbf{x}_0)\right)\right|\right]$
  Get diffused latents $\{\mathbf{z}_t^{\boldsymbol{\phi}}\}_{t=0}^T$ with a linear SDE
  Compute $\mathcal{L}\left(\{\mathbf{z}_t^{\boldsymbol{\phi}}\}_{t=0}^T, g^2; \boldsymbol{\theta}\right) - \mathbb{E}_{\mathbf{z}_T^{\boldsymbol{\phi}}}\left[\log \pi(\mathbf{z}_T^{\boldsymbol{\phi}})\right]$
  Compute flow loss $\mathcal{L}_f = \mathcal{L}\left(\{\mathbf{x}_t\}_{t=0}^T, g^2; \{\boldsymbol{\phi}, \boldsymbol{\theta}\}\right)$
  Update $\boldsymbol{\phi} \leftarrow \boldsymbol{\phi} - \eta \frac{\partial \mathcal{L}_f}{\partial \boldsymbol{\phi}}$
  Compute $\mathcal{L}\left(\{\mathbf{z}_t^{\boldsymbol{\phi}}\}_{t=0}^T, \lambda; \boldsymbol{\theta}\right) - \mathbb{E}_{\mathbf{z}_T^{\boldsymbol{\phi}}}\left[\log \pi(\mathbf{z}_T^{\boldsymbol{\phi}})\right]$
  Compute score loss $\mathcal{L}_s = \mathcal{L}\left(\{\mathbf{x}_t\}_{t=0}^T, \lambda; \{\boldsymbol{\phi}, \boldsymbol{\theta}\}\right)$
  Update $\boldsymbol{\theta} \leftarrow \boldsymbol{\theta} - \eta \frac{\partial \mathcal{L}_s}{\partial \boldsymbol{\theta}}$
until converged

LSGM Vahdat et al. [9] put a linear diffusion on the latent space like INDM but uses an auto-encoder structure. From this modeling choice, LSGM cannot be categorized as a nonlinear diffusion model in a strict sense. Concretely, recall that a diffusion process is (mathematically) defined as a sequence of random variables connected via a Markov chain. From this definition, one needs to satisfy two requirements to call it a diffusion process: 1) there must be multiple (possibly infinite) numbers of random variables; 2) the random variables should be connected via a Markov chain. Unlike INDM, LSGM cannot build forward data variables from the forward latent variables because there is no exact inverse function of the encoder map, as long as the data dimension differs to the latent dimension (Lemma 3 of Appendix D.1). This leads that LSGM has no forward data diffusion process. From this point, analyzing the data nonlinearity becomes infeasible in LSGM.

Moreover, LSGM has a pair of key differences in its training. First, the latent dimension of LSGM is 40,080, which is *15× higher* dimension than the data dimension (3,072) on CIFAR-10 [19]. In contrast, INDM always keeps its latent dimension by the data dimension. See Table 9 to compare the latent dimensions of INDM with LSGM on benchmark datasets. Furthermore, LSGM is repeatedly reported [9, 20] for its training instability on the best FID setting of $\lambda = \sigma^2$ (i.e., L_{simple} [8]). Meanwhile, INDM is consistently stable for any of training configurations, see Table 8.

DiffFlow Zhang and Chen [13] explicitly model the drift term $\mathbf{f}_{\boldsymbol{\phi}}$ as a flow network, so the forward diffusion becomes $\mathrm{d}\mathbf{x}_t = \mathbf{f}_{\boldsymbol{\phi}}\,\mathrm{d}t + g\,\mathrm{d}\mathbf{w}_t$. However, there are differences between DiffFlow and INDM: 1) DiffFlow does not nonlinearize the volatility; 2) DiffFlow is too slow for its explicit parametrization (Table 18); 3) the flexibility of $\mathbf{f}_{\boldsymbol{\phi}}$ is too restricted; 4) DiffFlow has a larger loss variance (Table 10). See Appendix D.2 for the full details of our arguments. Focusing on the slow training, observe that the denoising loss $\mathbb{E}_{\mathbf{x}_0, \mathbf{x}_t^{\boldsymbol{\phi}}}[\|\mathbf{s}_{\boldsymbol{\theta}}(\mathbf{x}_t^{\boldsymbol{\phi}}, t) - \nabla \log p_{0t}(\mathbf{x}_t^{\boldsymbol{\phi}}|\mathbf{x}_0)\|_2^2]$ requires a pair of heavy computations: (A) sampling from $\mathbf{x}_t^{\boldsymbol{\phi}}$, and (B) computation of $\nabla \log p_{0t}(\mathbf{x}_t^{\boldsymbol{\phi}}|\mathbf{x}_0)$. Intractable transition probability $p_{0t}(\mathbf{x}_t^{\boldsymbol{\phi}}|\mathbf{x}_0)$ is the major bottleneck of the slow training.

To overcome the bottleneck, DiffFlow discretizes the continuous diffusion with N variables of a discrete diffusion and uses the DDPM-style loss [8], which does not need to calculate the transition probability. Under the discretization, however, the forward sampling of $\mathbf{x}_t^{\boldsymbol{\phi}}$ takes $O(N)$ flow evaluations for every network update. This sampling issue is an inevitable fundamental problem when we parametrize the coefficients explicitly. Having that the flow evaluation is generally more expensive than score evaluation given the same number of parameters, a fast sampling is achievable only if we reduce N. However, it hurts the flexibility of a diffusion process, so DiffFlow suffers from the trade-off between training speed and model flexibility. On the other hand, the training of INDM is invariant of N, and INDM is free from such a trade-off. Analogously, DiffFlow generates a sample with the purple path in Figure 3, so it takes $O(N)$ flow evaluations, contrastive to INDM with a single flow evaluation in its sampling with the red path.

SBP De Bortoli et al. [15] learn the diffusion process with a problem of $\min_{\boldsymbol{\rho}_{\boldsymbol{\theta}} \in \mathcal{P}(p_r, \pi)} D_{KL}(\boldsymbol{\rho}_{\boldsymbol{\theta}} \| \boldsymbol{\mu})$, where $\mathcal{P}(p_r, \pi)$ is the collection of path measure with p_r and π as its marginal distributions at $t = 0$ and $t = T$, respectively. It is a bi-constrained optimization problem as any path measure on the search space that should satisfy boundary conditions at both $t = 0$ and $t = T$. $\boldsymbol{\mu}$ is the reference measure of a linear diffusion $\mathrm{d}\mathbf{x}_t = \mathbf{f}(\mathbf{x}_t, t)\,\mathrm{d}t + g(t)\mathbf{w}_t$; and the forward and reverse SDEs of $\boldsymbol{\rho}_{\boldsymbol{\theta}}$ are $\mathrm{d}\mathbf{x}_t = [\mathbf{f}(\mathbf{x}_t, t) + g^2(t)\nabla \log \Psi(\mathbf{x}_t, t)]\,\mathrm{d}t + g(t)\,\mathrm{d}\mathbf{w}_t$ and $\mathrm{d}\mathbf{x}_t = [\mathbf{f}(\mathbf{x}_t, t) - g^2(t)\nabla \log \hat{\Psi}(\mathbf{x}_t, t)]\,\mathrm{d}\bar{t} + g(t)\,\mathrm{d}\bar{\mathbf{w}}_t$, respectively, where $(\Psi, \hat{\Psi})$ is the solution of a coupled PDE, called Hopf-Cole transform [21]. Solving this coupled PDE is intractable, so the estimation target of SBP is $\nabla \log \Psi$ and $\nabla \log \hat{\Psi}$. As $\mathbf{f}$ and g are assumed to be linear functions, the nonlinearity of SBP is fully determined by $(\Psi, \hat{\Psi})$.

Analogous to DiffFlow, sampling from $\mathbf{x}_t$ in SBP needs a long time. Few works [15, 16] detour this training issue using the experience replay memory. Aside from the training time, the KL minimization puts the global optimal nonlinear diffusion $\boldsymbol{\rho}_{\boldsymbol{\theta}^*}$ near a neighborhood of the linear diffusion $\boldsymbol{\mu}$. In other words, the optimal $\boldsymbol{\rho}_{\boldsymbol{\theta}^*}$ is the closest path measure on $\mathcal{P}(p_r, \pi)$ to $\boldsymbol{\mu}$, so the inferred nonlinear diffusion would be the *most* linear diffusion on the space of $\mathcal{P}(p_r, \pi)$. For the demonstration, we illustrate $\|g^2(t)\nabla \log \Psi(\mathbf{x}_t, t)\Delta t\|_2 / \|g(t)\Delta \mathbf{w}_t\|_2$ in Figure 4. We used the released checkpoint of SB-FBSDE [16], an algorithm for solving SBP, trained with VESDE on CIFAR-10. As $\mathbf{f} \equiv 0$ in VESDE, this norm ratio measures how much nonlinearity is counted on a diffusion trajectory compared to the linear effect. Figure 4 shows that the ratio approaches zero except at the small range around $t \approx 0$, meaning that the nonlinear effect is virtually ignorable than the linear effect. Therefore, Figure 4 implies that the diffusion process is nearly linear in most of the diffusion time. We give a detailed discussion of SBP in Appendix D.3.

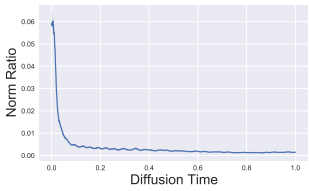

Figure 4: Norm Ratio of SBP.

6 Discussion

This section investigates characteristics of INDM. We show that INDM training is faster and nearly MLE in Section 6.1, and INDM sampling is robust on discretization step sizes in Section 6.2.

6.1 Benefit of INDM in Training

Having that DDPM++ is a collapsed INDM with a fixed identity transformation $\mathbf{h}_{\boldsymbol{\phi}_{id}} = id$, the difference lies in whether to train $\boldsymbol{\phi}$ or not. This trainable nonlinearity provides the better optimization of INDM, as evidenced in Figure 5-(a), experimented on CIFAR-10 using VPSDE. It shows a pair of critical characteristics of INDM training: 1) it is faster than DDPM++ training, and 2) it is asymptotically an MLE training. For the training speed, recall that the regression target of the score estimation is $\mathbf{s}_{\boldsymbol{\phi}}$, and this target is fixed in DDPM++ while keep moving in INDM. The target is constantly updated through the direction of $\mathbf{s}_{\boldsymbol{\theta}}$ in Eq. (1) by optimizing $\|\mathbf{s}_{\boldsymbol{\phi}} - \mathbf{s}_{\boldsymbol{\theta}}\|_2^2$. This *bidirectional* attraction between $\mathbf{s}_{\boldsymbol{\theta}}$ and $\mathbf{s}_{\boldsymbol{\phi}}$ is what flow learning does in the optimization.

For the MLE training, as the flow training is intricately entangled with the score training, we analyze INDM training for a specific class of score networks. First, we define $\mathbf{S}_{sol}$ (Definition 1 in Appendix B) to be the class of forward score functions of a linear diffusion with some initial distribution. Then, it turns out that it is the whole class of zero variational gap (=NLL-NELBO).

Theorem 2. $\mathrm{Gap}(\boldsymbol{\mu}_{\boldsymbol{\phi}}, \boldsymbol{\nu}_{\boldsymbol{\phi},\boldsymbol{\theta}}) := D_{KL}(\boldsymbol{\mu}_{\boldsymbol{\phi}} \| \boldsymbol{\nu}_{\boldsymbol{\phi},\boldsymbol{\theta}}) - D_{KL}(p_r \| p_{\boldsymbol{\phi},\boldsymbol{\theta}}) = 0$ *if and only if* $\mathbf{s}_{\boldsymbol{\theta}} \in \mathbf{S}_{sol}$.

Song et al. [11] partially reveal the connection between the gap with $\mathbf{S}_{sol}$, by proving the *if* part of Theorem 2, in Theorem 2 of Song et al. [11] (see Lemma 2 in Appendix B). We completely characterize this connection by proving the *only-if* part in Theorem 2. Surprisingly, the variational gap is irrelevant to the flow parameters, and the MLE training of INDM implies that the score network is nearby $\mathbf{S}_{sol}$ throughout the training. Combining Theorem 2 with the global optimality analysis raises a qualitative discrepancy in the optimization of DDPM++ and INDM by Theorem 3.

Theorem 3. *For any fixed* $\mathbf{s}_{\boldsymbol{\theta}} \in \mathbf{S}_{sol}$, *if* $\boldsymbol{\phi}^* \in \arg\min_{\boldsymbol{\phi}} D_{KL}(\boldsymbol{\mu}_{\boldsymbol{\phi}} \| \boldsymbol{\nu}_{\boldsymbol{\phi},\boldsymbol{\theta}})$, *then* $\mathbf{s}_{\boldsymbol{\phi}^*}(\mathbf{z}, t) = \nabla \log p_t^{\boldsymbol{\phi}^*}(\mathbf{z}) = \mathbf{s}_{\boldsymbol{\theta}}(\mathbf{z}, t)$, *and* $D_{KL}(\boldsymbol{\mu}_{\boldsymbol{\phi}^*} \| \boldsymbol{\nu}_{\boldsymbol{\phi}^*,\boldsymbol{\theta}}) = D_{KL}(p_r \| p_{\boldsymbol{\phi}^*,\boldsymbol{\theta}}) = \mathit{Gap}(\boldsymbol{\mu}_{\boldsymbol{\phi}^*}, \boldsymbol{\nu}_{\boldsymbol{\phi}^*,\boldsymbol{\theta}}) = 0$.

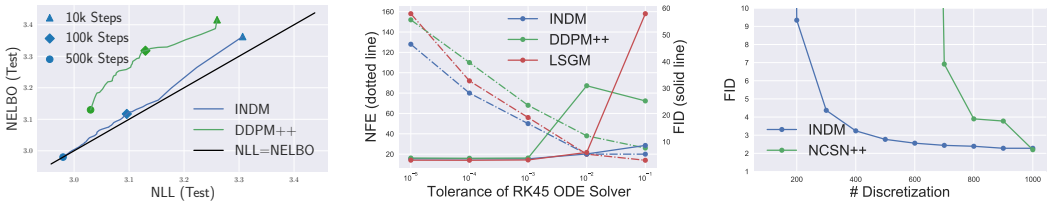

(a) Training Curve (b) FID by Tolerance (c) FID by Discretization

Figure 5: Comparison of INDM with baseline models, experimented on CIFAR-10.

Theorem 3 implies that there exists an optimal flow that the forward and generative SDEs on the latent space coincide, for any score network in $\mathbf{S}_{sol}$, if the flow is flexible enough. Therefore, INDM attains infinitely many ($= |\mathbf{S}_{sol}|$) global optimums in its optimization space. On the other hand, DDPM++ has only a unique optimal score network, i.e., $\mathbf{s}_{\boldsymbol{\theta}^*} = \mathbf{s}_{\boldsymbol{\phi}_{id}}$. Thus, Theorem 3 potentially explains the faster convergence of INDM. We give a detailed analysis in Appendix B.

6.2 Benefit of INDM in Sampling

Figure 5-(b,c) equally illustrate that INDM is more robust on the discretization step sizes in FID than DDPM++/NCSN++. To analyze the sample quality with respect to discretizations, recall that the Euler-Maruyama discretization of the generative SDE (or called the reverse diffusion sampler, or simply the predictor [1]) iteratively updates the sample $\tilde{\mathbf{z}}_k$ with

$$\tilde{\mathbf{z}}_{t_{k-1}} = \tilde{\mathbf{z}}_{t_k} + \gamma_k \left(\frac{1}{2}\beta(t_k)\tilde{\mathbf{z}}_{t_k} + g^2(t_k)\mathbf{s}_{\boldsymbol{\theta}}(\tilde{\mathbf{z}}_{t_k}, t_k) \right) + g(t_k)\sqrt{\gamma_k}\boldsymbol{\epsilon},$$

until time reaches to zero, where $\gamma_k = t_k - t_{k-1}$ is the step size of the discretized sampler and $\boldsymbol{\epsilon} \sim \mathcal{N}(0, \mathbf{I})$. The sampling error is the distributional discrepancy between the sample distribution of $\mathbf{h}_{\boldsymbol{\phi}}^{-1}(\tilde{\mathbf{z}}_0)$ and the data distribution. Theorem 4 decomposes the sampling error with three factors: 1) the prior error E_{pri}, 2) the discretization error E_{dis}, and 3) the score error E_{est}. Note that Theorem 4 is a straightforward application of the analysis done by De Bortoli et al. [15] and Guth et al. [22]. We omit regularity conditions to avoid unnecessary complications; see Appendix C.1.

Theorem 4 (De Bortoli et al. [15] and Guth et al. [22])**.** *Assume that 1)* $\sup_{\mathbf{z},t} \|\mathbf{s}_{\boldsymbol{\theta}^*}(\mathbf{z}, t) - \nabla \log p_t^{\boldsymbol{\phi}}(\mathbf{z})\| \leq M$*, 2)* $\sup_{\mathbf{z},t} \|\nabla^2 \log p_t^{\boldsymbol{\phi}}(\mathbf{z})\| \leq K$*, and 3)* $\sup_{\mathbf{z},t} \|\partial_t \nabla \log p_t^{\boldsymbol{\phi}}(\mathbf{z})\| / \|\mathbf{z}\| \leq Le^{-\alpha t}$*, for some* $K, L, M, \alpha > 0$*. Then*

$$\|p_r - (\mathbf{h}_{\boldsymbol{\phi}}^{-1})_{\#} \circ p_{0,N}^{\boldsymbol{\theta}}\|_{TV} \leq E_{pri}(\boldsymbol{\phi}) + E_{dis}(\boldsymbol{\phi}) + E_{est}(\boldsymbol{\phi}, \boldsymbol{\theta}) + o(\sqrt{\delta} + e^{-T}),$$

where $E_{pri}(\boldsymbol{\phi}) = \sqrt{2}e^{-T} D_{KL}(p_T^{\boldsymbol{\phi}} \| \pi)^{1/2}$*,* $E_{dis}(\boldsymbol{\phi}) = 6\sqrt{\delta}(1 + \mathbb{E}[\|\mathbf{z}\|^4]^{1/4})(1 + K + L(1 + 1/\sqrt{2\alpha}))$*, and* $E_{est}(\boldsymbol{\phi}, \boldsymbol{\theta}) = 2TM^2$ *with* $\delta = \max \gamma_k{}^2 / \min \gamma_k$*.*

There are a pair of implications from Theorem 4.

- ✓ $E_{pri}(\boldsymbol{\phi})$ and $E_{est}(\boldsymbol{\phi}, \boldsymbol{\theta})$ are independent of the discretization steps.
- ✓ $E_{dis}(\boldsymbol{\phi})/\sqrt{\delta}$ is the discretization sensitivity, entirely determined by the latent distribution's smoothness.

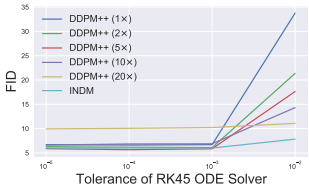

Figure 6: Sensitivity analysis on scaled-up scenario.

To the deep understanding of the second implication, let us assume $\mathbf{h}_{\boldsymbol{\phi}_a}(\mathbf{x}) = a\mathbf{x}$ for some scalar $a > 1$, then the sensitivity is anti-proportional to a with the identical discretizations, i.e., $E_{dis}(\boldsymbol{\phi}_a) \approx \frac{1}{a} E_{dis}(\boldsymbol{\phi}_{id})$. With a smaller sensitivity of $\boldsymbol{\phi}_a$, there is more room to reduce the number of discretization steps for $\boldsymbol{\phi}_a$. Figure 6 empirically supports the theory, showing that the sampler (at the large tolerance with 10^{-2}) becomes more robust as a increases, on CIFAR-10.

Before we derive a concrete result from the implication, observe that the flow $\mathbf{h}_{\boldsymbol{\phi}}$ is maximizing $\det(\nabla \mathbf{h}_{\boldsymbol{\phi}})$ in Eq. (2). To understand the effect of flow training on the discretization sensitivity, let us restrict the hypothesis class of the transformation to be linear mappings of $\mathbf{h}_{\boldsymbol{\phi}_a}(\mathbf{x}) = a\mathbf{x}$. Then, as the determinant increases by a, the trained diffusion model would be insensitive to the discretizations. Now, for the general case, Figure 7-(a,b) illustrate $\|\nabla^2 \log p_t^{\boldsymbol{\phi}}(\mathbf{z})\|$ and $\|\partial_t \nabla \log p_t^{\boldsymbol{\phi}}(\mathbf{z})\| / \|\mathbf{z}\|$ on

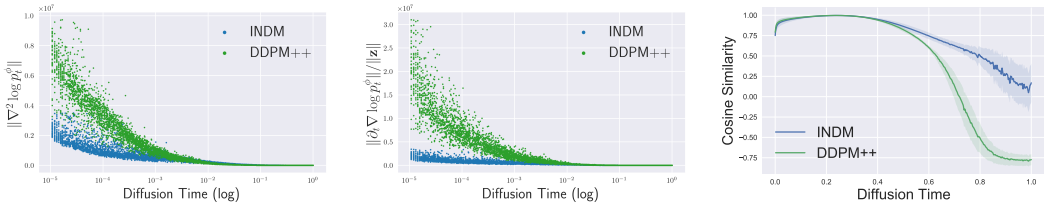

(a) $\|\nabla^2 \log p_t^{\phi}(\mathbf{z})\|$ (b) $\|\partial_t \nabla \log p_t^{\phi}(\mathbf{z})\|/\|\mathbf{z}\|$ (c) Cosine Similarity

Figure 7: (a,b) Comparison of INDM with DDPM++ for K, L, α. (c) Cosine similarity of forward diffusion trajectories on CIFAR-10.

CIFAR-10, respectively. Also, $\mathbb{E}[\|\mathbf{z}\|^4]^{1/4}$ of INDM is slightly larger (1.3x) than DDPM++. Therefore, with these observations combined, we conclude that INDM is less sensitive to the discretization steps than DDPM++, from its loss design.

Second, the robustness could originate from the geometry of the diffusion trajectory. The forward solution of VPSDE is $\mathbf{x}_t = \mu(t)\mathbf{x}_0 + \sqrt{1-\mu^2(t)}\boldsymbol{\epsilon}$ with $\mu(t) = e^{-\frac{1}{2}\int_0^t \beta(s)\,\mathrm{d}s}$, where the first term is a contraction mapping and the second term is the random perturbation. The contraction mapping points toward the origin, but the overall vector field of the diffusion path points outward because the prior manifold lies outside the data manifold, as shown in Table 2. This contrastive force leads the drift and volatility coefficients works in repulsive and raises a highly nonlinear diffusion trajectory in DDPM++, see Figure 11 for a toy illustration. On the other hand, the flow mapping of INDM pushes the latent manifold outside the prior manifold, and the drift and volatility coefficients act coherently. Hence, INDM has the relatively linear diffusion path; see Figures 12, 13, and 14 for a quick intuition. Figure 7-(c) measures the cosine similarity of the ODE's diffusion trajectory with the straight line connecting the initial-final points of each trajectory. Figure 7-(c) implies that DDPM++ is under an inefficient nonlinear trajectory that reverts backward near the end of the trajectory, as in Figure 11. In contrast, INDM trajectory is relatively efficient and linear (Figure 15), which yields robust sampling by discretization steps; see Appendix C.2 for details.

Table 2: Average L_2^2 Norm.

Manifold	Norm
Data	776
Latent	5,385
Prior	3,072

7 Experiments

This section quantitatively analyzes suggested INDM on CIFAR-10 and CelebA 64×64. Throughout the experiments, we use NCSN++ with VESDE and DDPM++ with VPSDE [1] as the backbones of diffusion models, and a ResNet-based flow model [23, 24] as the backbone of the flow model. See Appendix F for experimental details. We experiment with a pair of weighting functions for the score training. One is the likelihood weighting [11] with $\lambda(t) = g^2(t)$, and we denote INDM (NLL) for this weighing choice. The other is the variance weighting [8] $\lambda(t) = \sigma^2(t)$ with an emphasis on FID, and we denote INDM (FID) for this weighting choice.

We use either the Predictor-Corrector (PC) sampler [1] or a numerical ODE solver (RK45 [25]) of the probability flow ODE [1]. For a better FID, we find the optimal signal-to-noise value (Table 14), sampling temperature (Table 15), and stopping time (Table 16). Moreover, sampling from $\mathbf{z}_T^{\phi}$ rather than π improves FID because $E_{pri}(\phi)$ collapses to zero in Theorem 4, see Appendix F.2.2. We compute NLL/NELBO for performances of density estimation with Bits Per Dimension (BPD). We compute NLL with the uniform dequantization, instead of the variational dequantization [26] because it requires training an auxiliary network [11] only for the evaluation after the model training.

7.1 Correction on Likelihood Evaluation

A continuous diffusion model truncates the time horizon from $[0, T]$ to $[\epsilon, T]$ to avoid training instability [27]. In the model evaluation, this positive truncation could potentially be the primary source of poor evaluation (Figure 1-(c) of Kim et al. [27]), so we fix $\epsilon = 10^{-5}$ as default in our training and evaluation. In the model evaluation, as the score network is untrained on $[0, \epsilon)$, we calculate NLL by the Right-Hand-Side (RHS) of Eq. (3),

$$\text{NLL} = \mathbb{E}_{\mathbf{x}_0}[-\log p_0^m(\mathbf{x}_0)] \leq \mathbb{E}_{\mathbf{x}_0, \mathbf{x}_\epsilon}\left[-\log p_\epsilon^m(\mathbf{x}_\epsilon) + \log \frac{p_{\epsilon 0}^m(\mathbf{x}_0|\mathbf{x}_\epsilon)}{p_{0\epsilon}(\mathbf{x}_\epsilon|\mathbf{x}_0)}\right]. \tag{3}$$

Table 4: Performance comparison to linear/nonlinear diffusion models on CIFAR-10. We report the performance of linear diffusions by training our PyTorch implementation based on Song et al. [1, 11] with identical hyperparameters and score networks on both linear/nonlinear diffusions to quantify the effect of nonlinearity in a fair setting. Boldface numbers represent the best performance in a column.

SDE	Model	Nonlinear Data Diffusion	# Params	NLL (↓) after correction	NLL (↓) before correction	NELBO (↓) w/ residual (after)	NELBO (↓) w/o residual (before)	Gap (↓) (=NELBO-NLL) after	Gap (↓) (=NELBO-NLL) before	FID (↓) ODE	FID (↓) PC
VE	NCSN++ (FID)	✗	63M	4.86	3.66	4.89	4.45	0.03	0.79	-	2.38
	INDM (FID)	✓	76M	3.22	3.13	3.28	3.24	0.06	0.11	-	**2.29**
VP	DDPM++ (FID)	✗	62M	3.21	3.16	3.34	3.32	0.13	0.16	3.90	2.89
	INDM (FID)	✓	75M	3.17	3.11	3.23	3.18	0.06	0.07	**3.61**	2.90
	DDPM++ (NLL)	✗	62M	3.03	2.97	3.13	3.11	0.10	0.14	6.70	5.17
	INDM (NLL)	✓	75M	**2.98**	**2.95**	**2.98**	**2.97**	**0.00**	**0.02**	6.01	5.30

Table 5: Performance comparison on CIFAR-10.

SDE	Type	Model	# Params	NLL	FID
Linear		NCSN++ (FID) [1]	108M	4.85	2.20
		DDPM++ (FID) [1]	108M	3.19	2.64
		DDPM++ (NLL) [1]	108M	3.01	4.88
		VDM [28]	-	**2.65**	7.41
		CLD-SGM [20]	108M	3.31	2.25
Nonlinear	SBP	SB-FBSDE [16]	102M	2.98	3.18
	VAE -based	LSGM (FID) [9]	476M	3.45	**2.10**
		LSGM (NLL) [9]	269M	2.97	6.15
		LSGM (NLL) [9]	506M	2.87	6.89
		LSGM (balanced) [9]	109M	2.96	4.60
		LSGM (balanced) [9]	476M	2.98	2.17
	Flow -based	DiffFlow (FID) [13]	≈36M	3.04	14.14
		INDM (FID)	118M	3.09	2.28
		INDM (NLL)	121M	2.97	4.79
		INDM (NLL) + ST	75M	3.01	3.25

Table 6: Performance comparison on CelebA 64×64.

Model	NLL	NELBO	Gap	FID
UNCSN++ [27]	**1.93**	-	-	1.92
DDGM [29]	-	-	-	2.92
Efficient-VDVAE [30]	-	**1.83**	-	-
CR-NVAE [31]	-	1.86	-	-
DenseFlow-74-10 [4]	1.99	-	-	-
StyleFormer [32]	-	-	-	3.66
NCSN++ (VE, FID)	3.41	3.42	0.01	3.95
INDM (VE, FID)	2.31	2.33	0.02	2.54
DDPM++ (VP, FID)	2.14	2.21	0.07	2.32
INDM (VP, FID)	2.27	2.31	0.04	**1.75**
DDPM++ (VP, NLL)	2.00	2.09	0.09	3.95
INDM (VP, NLL)	2.05	2.05	**0.00**	3.06

Here, p_0^m and p_ϵ^m are the model probability distributions at $t = 0$ and $t = \epsilon$, respectively; and $p_{\epsilon 0}^m(\cdot|\mathbf{x}_\epsilon)$ is the model's reconstruction probability of $\mathbf{x}_0$ given $\mathbf{x}_\epsilon$. RHS of Eq. (3) is a generic formula to compute NLL in continuous diffusion models, including DDPM++, LSGM, and INDM. Previous continuous models [1, 11, 9] have approximated $\mathbb{E}_{\mathbf{x}_0}[-\log p_0^m(\mathbf{x}_0)]$ by $\mathbb{E}_{\mathbf{x}_0}[-\log p_\epsilon^m(\mathbf{x}_0)]$.

There are two significant differences between our and the previous calculation: 1) the input of p_ϵ^m is replaced with $\mathbf{x}_\epsilon$ from $\mathbf{x}_0$ (Table 11); 2) the residual term of $\log \frac{p_{\epsilon 0}^m(\mathbf{x}_0|\mathbf{x}_\epsilon)}{p_{0\epsilon}(\mathbf{x}_\epsilon|\mathbf{x}_0)}$ is added. With this modification, our NLL differs from the previous NLL of $\mathbb{E}_{\mathbf{x}_0}[-\log p_\epsilon^m(\mathbf{x}_0)]$ by about 0.03-0.06 in VPSDE, see Table 4. We report both previous/corrected ways in Table 4 and report corrected NLL/NELBO as default; see Appendix E for theoretical justification of our NLL/NELBO corrections.

7.2 Quantitative Results on Image Generation

FID Boost with Pre-training Training INDM from scratch improves NLL with the sacrifice of FID compared to DDPM++ in Table 3. Therefore, we pre-train the score network by DDPM++ as default. This pre-training is intended to search the data nonlinearity near well-trained linear diffusions. Table 3 shows that training INDM after 500k of pre-training steps performs better than DDPM++ on both NLL and FID. Appendix F.3 conducts the ablation study of pre-training steps.

Table 3: Effect of Pre-training.

Model	NLL	FID
DDPM++	3.03	6.70
INDM (w/ pre)	2.98	6.01
INDM (w/o pre)	2.98	8.49

Effect of Flow Training Table 4 investigates how the flow training affects to performances, under the various linear diffusions and weighting functions. It compares the pre-trained NCSN++/DDPM++ with INDM, of which these pre-trained models initialize the score network of INDM. Experiments in Table 4 presents that INDM improves NELBO in any setting, and minimizes the variational gap to zero if we train the score network with the likelihood weighting.

SOTA on CelebA Tables 5 and 6 compare INDM to baseline models. With the emphasis on FID, LSGM is the State-Of-The-Art (SOTA) model on CIFAR-10, but INDM-118M (FID) is on par with LSGM-476M (FID). Moreover, we use Soft Truncation [27] to compare with LSGM (balanced). Soft Truncation softens the smallest diffusion time as a random variable in the training stage to boost sample performance by improving the score accuracy, particularly on large diffusion time. In the inference stage, Soft Truncation uses the fixed smallest diffusion time (ϵ). INDM (NLL) + ST

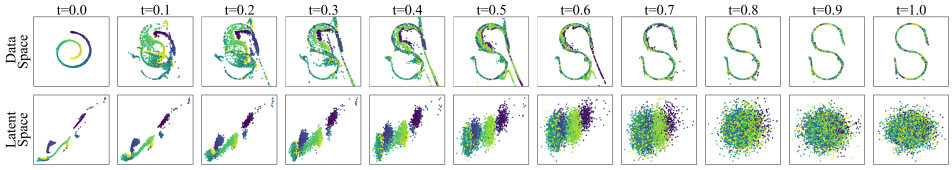

Figure 8: INDM enables to learn a diffusion bridge between two distinctive data distributions.

outperforms LSGM-109M (balanced) in terms of FID with comparable NLL. Also, INDM-121M (NLL) outperforms LSGM-269M (NLL) in FID with identical NLLs. We achieve SOTA FID of 1.75 on CelebA in Table 6. See Appendix F.8 for an extended comparison and Appendix F.9 for samples.

7.3 Application Task: Dataset Interpolation

The linear SDEs fixedly perturb data variables, so such SDEs should have the end distribution $p_T(\mathbf{x}_T)$ as an easy-to-compute distribution. With the nonlinear extension, a complex diffusion process exists to transport $p_r^{(1)}$ to another arbitrary $p_r^{(2)}$. However, a common practice of diffusion models constrains only the starting variable by $\mathbf{x}_0^{\phi} \sim p_r^{(1)}$, so the ending variable of $\mathbf{x}_T^{\phi}$ is free to deviate from $p_r^{(2)}$. Previous works have tackled this data interpolation task by using a conditional diffusion model [33] or a couple of jointly trained source-and-target diffusion models [34] on paired datasets. Among unconditional diffusion models using unpaired datasets, SBP [15] is a natural approach for the task by imposing bi-constraints with $\mathcal{P}(p_r, \pi)$ replaced by $\mathcal{P}(p_r^{(1)}, p_r^{(2)})$.

INDM can alternatively train the nonlinear diffusion from $p_r^{(1)}$ to $p_r^{(2)}$ with unpaired datasets. We train the score and flow networks with a loss

$$\underbrace{D_{KL}(\boldsymbol{\mu}_{\phi} \| \boldsymbol{\nu}_{\phi,\theta})}_{\text{INDM NELBO}} + \underbrace{D_{KL}(p_r^{(2)} \| p_{\phi})}_{\text{Interpolation Loss}},$$

where p_{ϕ} is the probability distribution of $\mathbf{x}_T^{\phi}$, which is calculated by a single feed-forward computation of the flow network, see Algorithm 2 in Appendix F.2.3. The additional interpolation loss forces the diffusion bridge $\{\mathbf{x}_t^{\phi}\}_{t=0}^{T}$ to ahead towards $p_r^{(2)}$ by minimizing the KL divergence between $\mathbf{x}_T^{\phi} \sim p_{\phi}$ and $p_r^{(2)}$. As the destined variable of the bridge becomes $\mathbf{x}_T^{\phi} = \mathbf{h}_{\phi}^{-1}(\mathbf{z}_T) \approx \mathbf{h}_{\phi}^{-1}(\pi)$, the flow network is what constructs the interpolated bridge between a couple of data variables, see Figures 8 and 9. Particularly, Figure 9 shows that LSGM fails to interpolate a letter to a digit, and we attribute this failure to the non-existence of a diffusion bridge in LSGM. Also, INDM models $p_r^{(1)}$ with $p_{\phi,\theta}$ and $p_r^{(2)}$ with p_{ϕ}, so we could compute NLL of each dataset *separately*: 1.10 BPD for MNIST and 1.56 BPD for EMNIST. In contrast, SBP cannot separately estimate densities on each dataset. We emphasize that no additional neural network is needed for the interpolation task with INDM.

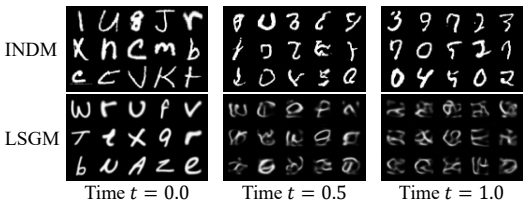

Figure 9: Image-to-image translation from EMNIST letters dataset to MNIST digits dataset.

8 Conclusion

This paper expands the linear diffusion to trainable nonlinear diffusion by combining an invertible transformation and a diffusion model, where the nonlinear diffusion learns the forward diffusion out of variational family of inference measures. A limitation of INDM lies in the training/evaluation time. Potential risk from this work is the negative use of deep generative models, such as deepfake images.

Acknowledgements

This research was supported by AI Technology Development for Commonsense Extraction, Reasoning, and Inference from Heterogeneous Data(IITP) funded by the Ministry of Science and ICT(2022-0-00077). Also, this work was supported by the National Research Foundation of Korea (NRF) grant funded by the Korea government(MSIT) (NRF-2019R1A5A1028324).

References

[1] Yang Song, Jascha Sohl-Dickstein, Diederik P Kingma, Abhishek Kumar, Stefano Ermon, and Ben Poole. Score-based generative modeling through stochastic differential equations. In *International Conference on Learning Representations*, 2020.

[2] Prafulla Dhariwal and Alexander Nichol. Diffusion models beat gans on image synthesis. *Advances in Neural Information Processing Systems*, 34, 2021.

[3] Tero Karras, Samuli Laine, and Timo Aila. A style-based generator architecture for generative adversarial networks. In *Proceedings of the IEEE/CVF Conference on Computer Vision and Pattern Recognition*, pages 4401–4410, 2019.

[4] Matej Grcić, Ivan Grubišić, and Siniša Šegvić. Densely connected normalizing flows. *Advances in Neural Information Processing Systems*, 34, 2021.

[5] Niki Parmar, Ashish Vaswani, Jakob Uszkoreit, Lukasz Kaiser, Noam Shazeer, Alexander Ku, and Dustin Tran. Image transformer. In *International Conference on Machine Learning*, pages 4055–4064. PMLR, 2018.

[6] Arash Vahdat and Jan Kautz. Nvae: A deep hierarchical variational autoencoder. *Advances in Neural Information Processing Systems*, 33:19667–19679, 2020.

[7] Yang Song and Stefano Ermon. Improved techniques for training score-based generative models. *Advances in neural information processing systems*, 33:12438–12448, 2020.

[8] Jonathan Ho, Ajay Jain, and Pieter Abbeel. Denoising diffusion probabilistic models. *Advances in Neural Information Processing Systems*, 33:6840–6851, 2020.

[9] Arash Vahdat, Karsten Kreis, and Jan Kautz. Score-based generative modeling in latent space. *Advances in Neural Information Processing Systems*, 34, 2021.

[10] Brian DO Anderson. Reverse-time diffusion equation models. *Stochastic Processes and their Applications*, 12(3):313–326, 1982.

[11] Yang Song, Conor Durkan, Iain Murray, and Stefano Ermon. Maximum likelihood training of score-based diffusion models. *Advances in Neural Information Processing Systems*, 34, 2021.

[12] Chin-Wei Huang, Jae Hyun Lim, and Aaron C Courville. A variational perspective on diffusion-based generative models and score matching. *Advances in Neural Information Processing Systems*, 34, 2021.

[13] Qinsheng Zhang and Yongxin Chen. Diffusion normalizing flow. *Advances in Neural Information Processing Systems*, 34, 2021.

[14] Francisco Vargas, Pierre Thodoroff, Austen Lamacraft, and Neil Lawrence. Solving schrödinger bridges via maximum likelihood. *Entropy*, 23(9):1134, 2021.

[15] Valentin De Bortoli, James Thornton, Jeremy Heng, and Arnaud Doucet. Diffusion schrödinger bridge with applications to score-based generative modeling. *Advances in Neural Information Processing Systems*, 34, 2021.

[16] Tianrong Chen, Guan-Horng Liu, and Evangelos Theodorou. Likelihood training of schrödinger bridge using forward-backward SDEs theory. In *International Conference on Learning Representations*, 2022.

[17] Bernt Oksendal. *Stochastic differential equations: an introduction with applications*. Springer Science & Business Media, 2013.

[18] Martin Heusel, Hubert Ramsauer, Thomas Unterthiner, Bernhard Nessler, and Sepp Hochreiter. Gans trained by a two time-scale update rule converge to a local nash equilibrium. *Advances in neural information processing systems*, 30, 2017.

[19] Alex Krizhevsky, Geoffrey Hinton, et al. Learning multiple layers of features from tiny images. 2009.

[20] Tim Dockhorn, Arash Vahdat, and Karsten Kreis. Score-based generative modeling with critically-damped langevin diffusion. In *International Conference on Learning Representations*, 2022.

[21] Flavien Léger and Wuchen Li. Hopf–cole transformation via generalized schrödinger bridge problem. *Journal of Differential Equations*, 274:788–827, 2021.

[22] Florentin Guth, Simon Coste, Valentin De Bortoli, and Stephane Mallat. Wavelet score-based generative modeling. *Advances in Neural Information Processing Systems*, 35, 2022.

[23] Ricky TQ Chen, Jens Behrmann, David K Duvenaud, and Jörn-Henrik Jacobsen. Residual flows for invertible generative modeling. *Advances in Neural Information Processing Systems*, 32, 2019.

[24] Xuezhe Ma, Xiang Kong, Shanghang Zhang, and Eduard H Hovy. Decoupling global and local representations via invertible generative flows. In *International Conference on Learning Representations*, 2021.

[25] John R Dormand and Peter J Prince. A family of embedded runge-kutta formulae. *Journal of computational and applied mathematics*, 6(1):19–26, 1980.

[26] Jonathan Ho, Xi Chen, Aravind Srinivas, Yan Duan, and Pieter Abbeel. Flow++: Improving flow-based generative models with variational dequantization and architecture design. In *International Conference on Machine Learning*, pages 2722–2730. PMLR, 2019.

[27] Dongjun Kim, Seungjae Shin, Kyungwoo Song, Wanmo Kang, and Il-Chul Moon. Soft truncation: A universal training technique of score-based diffusion model for high precision score estimation. In *International Conference on Machine Learning*, pages 11201–11228. PMLR, 2022.

[28] Diederik P Kingma, Tim Salimans, Ben Poole, and Jonathan Ho. Variational diffusion models. In *Advances in Neural Information Processing Systems*, 2021.

[29] Eliya Nachmani, Robin San Roman, and Lior Wolf. Non gaussian denoising diffusion models. *arXiv preprint arXiv:2106.07582*, 2021.

[30] Louay Hazami, Rayhane Mama, and Ragavan Thurairatnam. Efficient-vdvae: Less is more. *arXiv preprint arXiv:2203.13751*, 2022.

[31] Samarth Sinha and Adji Bousso Dieng. Consistency regularization for variational auto-encoders. *Advances in Neural Information Processing Systems*, 34, 2021.

[32] Jeeseung Park and Younggeun Kim. Styleformer: Transformer based generative adversarial networks with style vector. In *Proceedings of the IEEE/CVF Conference on Computer Vision and Pattern Recognition*, pages 8983–8992, 2022.

[33] Chitwan Saharia, William Chan, Huiwen Chang, Chris A. Lee, Jonathan Ho, Tim Salimans, David J. Fleet, and Mohammad Norouzi. Palette: Image-to-image diffusion models. In *NeurIPS 2021 Workshop on Deep Generative Models and Downstream Applications*, 2021.

[34] Hiroshi Sasaki, Chris G Willcocks, and Toby P Breckon. Unit-ddpm: Unpaired image translation with denoising diffusion probabilistic models. *arXiv preprint arXiv:2104.05358*, 2021.

[35] Simo Särkkä and Arno Solin. *Applied stochastic differential equations*, volume 10. Cambridge University Press, 2019.

[36] John Duchi. Lecture notes for statistics 311/electrical engineering 377. *URL: https://stanford.edu/class/stats311/Lectures/full_notes. pdf. Last visited on*, 2:23, 2016.

[37] Haim Avron and Sivan Toledo. Randomized algorithms for estimating the trace of an implicit symmetric positive semi-definite matrix. *Journal of the ACM (JACM)*, 58(2):1–34, 2011.

[38] Walter Rudin et al. *Principles of mathematical analysis*, volume 3. McGraw-hill New York, 1964.

[39] Danilo Rezende and Shakir Mohamed. Variational inference with normalizing flows. In *International conference on machine learning*, pages 1530–1538. PMLR, 2015.

[40] Yuri Burda, Roger Grosse, and Ruslan Salakhutdinov. Importance weighted autoencoders. 2020.

[41] Erhard Glötzl and Oliver Richters. Helmholtz decomposition and rotation potentials in n-dimensional cartesian coordinates. *arXiv preprint arXiv:2012.13157*, 2020.

[42] Yang Song, Sahaj Garg, Jiaxin Shi, and Stefano Ermon. Sliced score matching: A scalable approach to density and score estimation. In *Uncertainty in Artificial Intelligence*, pages 574–584. PMLR, 2020.

[43] Michael F Hutchinson. A stochastic estimator of the trace of the influence matrix for laplacian smoothing splines. *Communications in Statistics-Simulation and Computation*, 18(3):1059–1076, 1989.

[44] J. D. Hunter. Matplotlib: A 2d graphics environment. *Computing in Science & Engineering*, 9 (3):90–95, 2007. doi: 10.1109/MCSE.2007.55.

[45] Avrim Blum, John Hopcroft, and Ravindran Kannan. *Foundations of data science*. Cambridge University Press, 2020.

[46] Rémi Flamary, Nicolas Courty, Alexandre Gramfort, Mokhtar Z. Alaya, Aurélie Boisbunon, Stanislas Chambon, Laetitia Chapel, Adrien Corenflos, Kilian Fatras, Nemo Fournier, Léo Gautheron, Nathalie T.H. Gayraud, Hicham Janati, Alain Rakotomamonjy, Ievgen Redko, Antoine Rolet, Antony Schutz, Vivien Seguy, Danica J. Sutherland, Romain Tavenard, Alexander Tong, and Titouan Vayer. Pot: Python optimal transport. *Journal of Machine Learning Research*, 22(78):1–8, 2021.

[47] Valentin Khrulkov and Ivan Oseledets. Understanding ddpm latent codes through optimal transport. *arXiv preprint arXiv:2202.07477*, 2022.

[48] Glen E Bredon. *Topology and geometry*, volume 139. Springer Science & Business Media, 2013.

[49] Desmond J Higham. An algorithmic introduction to numerical simulation of stochastic differential equations. *SIAM review*, 43(3):525–546, 2001.

[50] Diederik P. Kingma and Max Welling. Auto-encoding variational bayes. In Yoshua Bengio and Yann LeCun, editors, *2nd International Conference on Learning Representations, ICLR 2014, Banff, AB, Canada, April 14-16, 2014, Conference Track Proceedings*, 2014.

[51] Yongxin Chen, Tryphon T Georgiou, and Michele Pavon. On the relation between optimal transport and schrödinger bridges: A stochastic control viewpoint. *Journal of Optimization Theory and Applications*, 169(2):671–691, 2016.

[52] Ludger Ruschendorf. Convergence of the iterative proportional fitting procedure. *The Annals of Statistics*, pages 1160–1174, 1995.

[53] Matthew Tancik, Pratul Srinivasan, Ben Mildenhall, Sara Fridovich-Keil, Nithin Raghavan, Utkarsh Singhal, Ravi Ramamoorthi, Jonathan Barron, and Ren Ng. Fourier features let networks learn high frequency functions in low dimensional domains. *Advances in Neural Information Processing Systems*, 33:7537–7547, 2020.

[54] Ashish Vaswani, Noam Shazeer, Niki Parmar, Jakob Uszkoreit, Llion Jones, Aidan N Gomez, Łukasz Kaiser, and Illia Polosukhin. Attention is all you need. In *Advances in neural information processing systems*, pages 5998–6008, 2017.

[55] Olaf Ronneberger, Philipp Fischer, and Thomas Brox. U-net: Convolutional networks for biomedical image segmentation. In *International Conference on Medical image computing and computer-assisted intervention*, pages 234–241. Springer, 2015.

[56] Durk P Kingma and Prafulla Dhariwal. Glow: Generative flow with invertible 1x1 convolutions. *Advances in neural information processing systems*, 31, 2018.

[57] Sergey Ioffe and Christian Szegedy. Batch normalization: Accelerating deep network training by reducing internal covariate shift. In *International conference on machine learning*, pages 448–456. PMLR, 2015.

[58] Cheng Lu, Jianfei Chen, Chongxuan Li, Qiuhao Wang, and Jun Zhu. Implicit normalizing flows. In *International Conference on Learning Representations*, 2021.

[59] Prajit Ramachandran, Barret Zoph, and Quoc V Le. Searching for activation functions. *arXiv preprint arXiv:1710.05941*, 2017.

[60] Alexander Quinn Nichol and Prafulla Dhariwal. Improved denoising diffusion probabilistic models. In *International Conference on Machine Learning*, pages 8162–8171. PMLR, 2021.

[61] Lawrence F Shampine. Some practical runge-kutta formulas. *Mathematics of computation*, 46 (173):135–150, 1986.

[62] Alexia Jolicoeur-Martineau, Rémi Piché-Taillefer, Ioannis Mitliagkas, and Remi Tachet des Combes. Adversarial score matching and improved sampling for image generation. In *International Conference on Learning Representations*, 2020.

[63] Yang Song and Stefano Ermon. Generative modeling by estimating gradients of the data distribution. *Advances in Neural Information Processing Systems*, 32, 2019.

[64] Gaurav Parmar, Richard Zhang, and Jun-Yan Zhu. On aliased resizing and surprising subtleties in gan evaluation, 2022.

[65] Jean-David Benamou and Yann Brenier. A computational fluid mechanics solution to the monge-kantorovich mass transfer problem. *Numerische Mathematik*, 84(3):375–393, 2000.

[66] Cédric Villani. *Optimal transport: old and new*, volume 338. Springer, 2009.

[67] Bharath K Sriperumbudur, Arthur Gretton, Kenji Fukumizu, Bernhard Schölkopf, and Gert RG Lanckriet. Hilbert space embeddings and metrics on probability measures. *The Journal of Machine Learning Research*, 11:1517–1561, 2010.

[68] Lawrence C Evans. Partial differential equations. *Graduate studies in mathematics*, 19(2), 1998.

[69] Valentin De Bortoli. Convergence of denoising diffusion models under the manifold hypothesis. *arXiv preprint arXiv:2208.05314*, 2022.

[70] Tero Karras, Miika Aittala, Janne Hellsten, Samuli Laine, Jaakko Lehtinen, and Timo Aila. Training generative adversarial networks with limited data. In H. Larochelle, M. Ranzato, R. Hadsell, M. F. Balcan, and H. Lin, editors, *Advances in Neural Information Processing Systems*, volume 33, pages 12104–12114. Curran Associates, Inc., 2020.

[71] Abdul Fatir Ansari, Ming Liang Ang, and Harold Soh. Refining deep generative models via discriminator gradient flow. In *International Conference on Learning Representations*, 2020.

[72] Yifan Jiang, Shiyu Chang, and Zhangyang Wang. Transgan: Two pure transformers can make one strong gan, and that can scale up. *Advances in Neural Information Processing Systems*, 34, 2021.

[73] Aaron Van Oord, Nal Kalchbrenner, and Koray Kavukcuoglu. Pixel recurrent neural networks. In *International Conference on Machine Learning*, pages 1747–1756. PMLR, 2016.

[74] Rewon Child, Scott Gray, Alec Radford, and Ilya Sutskever. Generating long sequences with sparse transformers. *arXiv preprint arXiv:1904.10509*, 2019.

[75] Jianfei Chen, Cheng Lu, Biqi Chenli, Jun Zhu, and Tian Tian. Vflow: More expressive generative flows with variational data augmentation. In *International Conference on Machine Learning*, pages 1660–1669. PMLR, 2020.

[76] Rewon Child. Very deep vaes generalize autoregressive models and can outperform them on images. In *International Conference on Learning Representations*, 2020.

[77] Ali Razavi, Aaron van den Oord, Ben Poole, and Oriol Vinyals. Preventing posterior collapse with delta-vaes. In *International Conference on Learning Representations*, 2018.

[78] Gaurav Parmar, Dacheng Li, Kwonjoon Lee, and Zhuowen Tu. Dual contradistinctive generative autoencoder. In *Proceedings of the IEEE/CVF Conference on Computer Vision and Pattern Recognition*, pages 823–832, 2021.

[79] Jiaming Song, Chenlin Meng, and Stefano Ermon. Denoising diffusion implicit models. In *International Conference on Learning Representations*, 2020.

Checklist

1. For all authors...
   (a) Do the main claims made in the abstract and introduction accurately reflect the paper's contributions and scope? [Yes] We have reflected the contribution of this work claimed in the abstract and introduction in the main sections.
   (b) Did you describe the limitations of your work? [Yes] See Section 7 and 8.
   (c) Did you discuss any potential negative societal impacts of your work? [Yes] See Section 8.
   (d) Have you read the ethics review guidelines and ensured that your paper conforms to them? [Yes] I have read the ethics review guidelines and ensured that our paper conforms to them.
2. If you are including theoretical results...
   (a) Did you state the full set of assumptions of all theoretical results? [Yes] See Appendix B, C, and G.
   (b) Did you include complete proofs of all theoretical results? [Yes] See Appendix G.
3. If you ran experiments...
   (a) Did you include the code, data, and instructions needed to reproduce the main experimental results (either in the supplemental material or as a URL)? [Yes] We have released our code and instructions at `https://github.com/byeonghu-na/INDM`.
   (b) Did you specify all the training details (e.g., data splits, hyperparameters, how they were chosen)? [Yes] See Appendix F.
   (c) Did you report error bars (e.g., with respect to the random seed after running experiments multiple times)? [Yes] Figures 4, 7-(c), and 19 report the error bars.
   (d) Did you include the total amount of compute and the type of resources used (e.g., type of GPUs, internal cluster, or cloud provider)? [Yes] See Appendix F.4.
4. If you are using existing assets (e.g., code, data, models) or curating/releasing new assets...
   (a) If your work uses existing assets, did you cite the creators? [Yes] See Appendix F.
   (b) Did you mention the license of the assets? [No]
   (c) Did you include any new assets either in the supplemental material or as a URL? [Yes] We have released the asset on CelebA pool-3 features at `https://github.com/byeonghu-na/INDM`.
   (d) Did you discuss whether and how consent was obtained from people whose data you're using/curating? [Yes] Our asset is a representative asset in the field of diffusion models.
   (e) Did you discuss whether the data you are using/curating contains personally identifiable information or offensive content? [No]
5. If you used crowdsourcing or conducted research with human subjects...
   (a) Did you include the full text of instructions given to participants and screenshots, if applicable? [N/A]
   (b) Did you describe any potential participant risks, with links to Institutional Review Board (IRB) approvals, if applicable? [N/A]
   (c) Did you include the estimated hourly wage paid to participants and the total amount spent on participant compensation? [N/A]

Contents

1 Introduction **1**

2 Preliminary **2**

3 Motivation of Nonlinear Diffusion Process **3**

4 Implicit Nonlinear Diffusion Model **3**

4.1 Data and Latent Diffusion Processes 3

4.2 Model Training and Sampling 4

5 Related Work **5**

6 Discussion **6**

6.1 Benefit of INDM in Training 6

6.2 Benefit of INDM in Sampling 7

7 Experiments **8**

7.1 Correction on Likelihood Evaluation 8

7.2 Quantitative Results on Image Generation 9

7.3 Application Task: Dataset Interpolation 10

8 Conclusion **10**

A Derivations **18**

A.1 Derivation of Variational Bound for Nonlinear Diffusion 18

A.2 Derivation of Nonlinear Drift and Volatility Terms for INDM 19

B Details on Section 6.1 **20**

B.1 Restricting Search Space of $\mathbf{s}_{\boldsymbol{\theta}}$ into $\mathbf{S}_{div}$ 23

C Details on Section 6.2 **24**

C.1 Full Statement of Theorem 4 24

C.2 Geometric Interpretation of Latent Diffusion 24

D Related Work **27**

D.1 Latent Score-based Generative Model (LSGM) 27

D.2 Diffusion Normalizing Flow (DiffFlow) 28

D.3 Schrödinger Bridge Problem (SBP) 32

E Correction of Density Estimation Metrics of Diffusion Models with Time Truncation **33**

E.1 Equivalent Reverse SDEs 33

E.2 Log-Likelihood for Diffusion Models with Time Truncation 34

E.3 NELBO Correction 34

E.4 NLL Correction 35
E.5 Calculating the Residual Term 36

F Experimental Details and Additional Results **37**
F.1 Model Architecture 37
F.2 Experimental details 37
F.2.1 Variance Reduction 38
F.2.2 Sampling Tricks to Improve FID 39
F.2.3 Interpolation Task 41
F.3 Effect of Pre-training 41
F.4 Training Time 42
F.5 Visualization of Latent 42
F.5.1 Visualization of 2d Latent Manifold 42
F.5.2 Visualization of High-dimensional Latent Vector on Benchmark Datasets . 42
F.6 Nonlinear Diffusion Coefficient 43
F.7 Relative Energy 43
F.8 Full Quantitative Tables 43
F.9 Random samples 43

G Proofs of Theorems and Propositions **43**

A Derivations

A.1 Derivation of Variational Bound for Nonlinear Diffusion

The variational bound derived in Song et al. [11] is only applicable when $\mathbf{G}(\mathbf{x}_t, t)$ is reduced to $g(t)\mathbf{I}$. This section, therefore, derives the variational bound of a general diffusion SDE of $\mathrm{d}\mathbf{x}_t = \mathbf{f}(\mathbf{x}_t, t)\,\mathrm{d}t + \mathbf{G}(\mathbf{x}_t, t)\,\mathrm{d}\mathbf{w}_t$, and we analyze why learning $\mathbf{f}$ and $\mathbf{G}$ is infeasible if 1) the transition probability of $p_{0t}(\mathbf{x}_t|\mathbf{x}_0)$ is intractable and 2) $\mathbf{G}$ is anisotropic by $\mathbf{x}_t$.

From Anderson [10], the corresponding reverse SDE of $\mathrm{d}\mathbf{x}_t = \mathbf{f}(\mathbf{x}_t, t)\,\mathrm{d}t + \mathbf{G}(\mathbf{x}_t, t)\,\mathrm{d}\mathbf{w}_t$ is

$$\mathrm{d}\mathbf{x}_t = \left[\mathbf{f}(\mathbf{x}_t, t) - \mathrm{div}(\mathbf{G}\mathbf{G}^T) - \mathbf{G}\mathbf{G}^T \nabla \log p_t(\mathbf{x}_t)\right] \mathrm{d}\bar{t} + \mathbf{G}(\mathbf{x}_t, t)\,\mathrm{d}\bar{\mathbf{w}}_t, \tag{4}$$

and the generative SDE becomes

$$\mathrm{d}\mathbf{x}_t = \left[\mathbf{f}(\mathbf{x}_t, t) - \mathrm{div}(\mathbf{G}\mathbf{G}^T) - \mathbf{G}\mathbf{G}^T \mathbf{s}(\mathbf{x}_t, t)\right] \mathrm{d}\bar{t} + \mathbf{G}(\mathbf{x}_t, t)\,\mathrm{d}\bar{\mathbf{w}}_t. \tag{5}$$

Then, from the Girsanov theorem [35] and the martingale property [17], using the disintegration property of the KL divergence, we have

$$\begin{aligned} D_{KL}(\boldsymbol{\mu}\|\boldsymbol{\nu}) &= D_{KL}(p_T(\mathbf{x}_T)\|\pi(\mathbf{x}_T)) \\ &+ \frac{1}{2}\int_0^T \mathbb{E}_{\mathbf{x}_t}\left[\left(\mathbf{s}(\mathbf{x}_t, t) - \nabla \log p_t(\mathbf{x}_t)\right)^T \mathbf{G}\mathbf{G}^T \left(\mathbf{s}(\mathbf{x}_t, t) - \nabla \log p_t(\mathbf{x}_t)\right)\right] \mathrm{d}t, \end{aligned} \tag{6}$$

where $\boldsymbol{\mu}$ is the path measure of Eq. (4) and $\boldsymbol{\nu}$ is the path measure of Eq. (5). Therefore, from the data processing inequality [36], we get

$$\begin{aligned} D_{KL}(p_r\|p) \leq D_{KL}(\boldsymbol{\mu}\|\boldsymbol{\nu}) &= D_{KL}(p_T(\mathbf{x}_T)\|\pi(\mathbf{x}_T)) \\ &+ \frac{1}{2}\int_0^T \mathbb{E}_{\mathbf{x}_t}\left[\left(\mathbf{s}(\mathbf{x}_t, t) - \nabla \log p_t(\mathbf{x}_t)\right)^T \mathbf{G}\mathbf{G}^T \left(\mathbf{s}(\mathbf{x}_t, t) - \nabla \log p_t(\mathbf{x}_t)\right)\right] \mathrm{d}t, \end{aligned}$$

where p is the generative distribution at $t = 0$.

Now, from the Fokker-Planck equation, the density function satisfies

$$\frac{\partial p_t}{\partial t} = -\sum_j \frac{\partial}{\partial x_{t,j}}\left[f_j(\mathbf{x}_t, t)p_t(\mathbf{x}_t) - \sum_i \frac{\partial}{\partial x_{t,j}}(H_{ij}(\mathbf{x}_t, t)p_t(\mathbf{x}_t))\right],$$

where $\mathbf{H}(\mathbf{x}_t, t) = \frac{1}{2}\mathbf{G}(\mathbf{x}_t, t)\mathbf{G}(\mathbf{x}_t, t)^T$. Then, analogous to Theorem 4 of Song et al. [11], the entropy becomes

$$\begin{aligned} \mathcal{H}(p_r) - \mathcal{H}(p_T) &= -\int_0^T \frac{\partial}{\partial t}\mathcal{H}(p_t)\,\mathrm{d}t \\ &= \int_0^T \int \frac{\partial p_t}{\partial t} \log p_t(\mathbf{x}_t)\,\mathrm{d}\mathbf{x}_t\,\mathrm{d}t \\ &= -\int_0^T \int \sum_j \frac{\partial}{\partial x_{t,j}}\left[f_j(\mathbf{x}_t, t)p_t(\mathbf{x}_t) - \sum_i \frac{\partial}{\partial x_{t,i}}(H_{ij}(\mathbf{x}_t, t)p_t(\mathbf{x}_t))\right] \log p_t(\mathbf{x}_t)\,\mathrm{d}\mathbf{x}_t\,\mathrm{d}t \\ &= \int_0^T \int \sum_j \left[f_j(\mathbf{x}_t, t)p_t(\mathbf{x}_t) - \sum_i \frac{\partial}{\partial x_{t,i}}(H_{ij}(\mathbf{x}_t, t)p_t(\mathbf{x}_t))\right] \frac{\partial \log p_t(\mathbf{x}_t)}{\partial x_{t,j}}\,\mathrm{d}\mathbf{x}_t\,\mathrm{d}t \\ &= \int_0^T \int p_t(\mathbf{x}_t) \sum_j f_j(\mathbf{x}_t, t) \frac{\partial \log p_t(\mathbf{x}_t)}{\partial x_{t,j}}\,\mathrm{d}\mathbf{x}_t\,\mathrm{d}t \\ &\quad - \int_0^T \int \sum_j \sum_i \left(\frac{\partial H_{ij}}{\partial x_{t,i}} p_t + H_{ij}\frac{\partial p_t}{\partial x_{t,i}}\right) \frac{\partial \log p_t}{\partial x_{t,j}}\,\mathrm{d}\mathbf{x}_t\,\mathrm{d}t \\ &= -\int_0^T \mathbb{E}_{\mathbf{x}_t}[\mathrm{div}(\mathbf{f}(\mathbf{x}_t, t))]\,\mathrm{d}t \\ &\quad - \int_0^T \mathbb{E}_{\mathbf{x}_t}[\mathrm{div}(\mathbf{H}(\mathbf{x}_t, t))^T \nabla \log p_t(\mathbf{x}_t)] + \mathbb{E}_{\mathbf{x}_t}[\nabla \log p_t(\mathbf{x}_t)^T \mathbf{H}(\mathbf{x}_t, t) \nabla \log p_t(\mathbf{x}_t)]\,\mathrm{d}t \end{aligned}$$

$$= -\frac{1}{2}\int_0^T \mathbb{E}_{\mathbf{x}_t}\Big[2\text{div}(\mathbf{f}(\mathbf{x}_t,t)) + \text{div}(\mathbf{G}(\mathbf{x}_t,t)\mathbf{G}(\mathbf{x}_t,t)^T)^T\nabla\log p_t(\mathbf{x}_t) + \nabla\log p_t(\mathbf{x}_t)^T\mathbf{G}(\mathbf{x}_t,t)\mathbf{G}(\mathbf{x}_t,t)^T\nabla\log p_t(\mathbf{x}_t)\Big]\,\mathrm{d}t.$$

Therefore, the variational bound of the model log-likelihood is derived by

$$\begin{aligned}
\mathbb{E}_{p_r(\mathbf{x}_0)}\big[-\log p(\mathbf{x}_0)\big] &= D_{KL}(p_r\|p) + \mathcal{H}(p_r) \le D_{KL}(\boldsymbol{\mu}\|\boldsymbol{\nu}) + \mathcal{H}(p_r)\\
&= \frac{1}{2}\int_0^T \mathbb{E}_{\mathbf{x}_t}\big[(\nabla\log p_t(\mathbf{x}_t) - \mathbf{s}(\mathbf{x}_t,t))^T\mathbf{G}\mathbf{G}^T(\nabla\log p_t(\mathbf{x}_t) - \mathbf{s}(\mathbf{x}_t,t))\big]\,\mathrm{d}t\\
&\quad + \mathbb{E}_{\mathbf{x}_T}\big[-\log\pi(\mathbf{x}_T)\big] + \mathcal{H}(p_r) - \mathcal{H}(p_T)\\
&= \frac{1}{2}\int_0^T \mathbb{E}_{\mathbf{x}_t}\Big[\big(\mathbf{s}(\mathbf{x}_t,t) - \nabla\log p_t(\mathbf{x}_t)\big)^T\mathbf{G}\mathbf{G}^T\big(\mathbf{s}(\mathbf{x}_t,t) - \nabla\log p_t(\mathbf{x}_t)\big)\\
&\quad - \nabla\log p_t(\mathbf{x}_t)^T\mathbf{G}\mathbf{G}^T\nabla\log p_t(\mathbf{x}_t) - \text{div}(\mathbf{G}\mathbf{G}^T)^T\nabla\log p_t(\mathbf{x}_t) - 2\text{div}(\mathbf{f}(\mathbf{x}_t,t))\Big]\,\mathrm{d}t\\
&\quad + \mathbb{E}_{\mathbf{x}_T}\big[-\log\pi(\mathbf{x}_T)\big].
\end{aligned}$$

Using the integration by parts, this variational bound transforms to

$$\mathbb{E}_{p_r(\mathbf{x}_0)}\big[-\log p_{\boldsymbol{\theta}}(\mathbf{x}_0)\big] \le \frac{1}{2}\int_0^T \mathbb{E}_{\mathbf{x}_t}\Big[\mathbf{s}^T\mathbf{G}\mathbf{G}^T\mathbf{s} + 2\text{div}(\mathbf{G}\mathbf{G}^T\mathbf{s}) - \text{div}(\mathbf{G}\mathbf{G}^T)\nabla\log p_t - 2\text{div}(\mathbf{f})\Big]\,\mathrm{d}t + \mathbb{E}_{\mathbf{x}_T}\big[-\log\pi(\mathbf{x}_T)\big]$$

Also, this variational bound is equivalently formulated as

$$\begin{aligned}
&\mathbb{E}_{p_r(\mathbf{x}_0)}\big[-\log p(\mathbf{x}_0)\big]\\
&\le \frac{1}{2}\int_0^T \mathbb{E}_{\mathbf{x}_0,\mathbf{x}_t}\Big[\big(\mathbf{s}(\mathbf{x}_t,t) - \nabla\log p_{0t}(\mathbf{x}_t|\mathbf{x}_0)\big)^T\mathbf{G}\mathbf{G}^T\big(\mathbf{s}(\mathbf{x}_t,t) - \nabla\log p_{0t}(\mathbf{x}_t|\mathbf{x}_0)\big)\\
&\quad - \nabla\log p_{0t}(\mathbf{x}_t|\mathbf{x}_0)^T\mathbf{G}\mathbf{G}^T\nabla\log p_{0t}(\mathbf{x}_t|\mathbf{x}_0) - \text{div}(\mathbf{G}\mathbf{G}^T)^T\nabla\log p_{0t}(\mathbf{x}_t|\mathbf{x}_0) - 2\text{div}(\mathbf{f})\Big]\,\mathrm{d}t\\
&\quad + \mathbb{E}_{\mathbf{x}_T}\big[-\log\pi(\mathbf{x}_T)\big].
\end{aligned}$$

Therefore, optimizing the nonlinear drift ($\mathbf{f}$) and diffusion ($\mathbf{G}$) terms are intractable in general for two reasons. First, the transition probability of $p_{0t}(\mathbf{x}_t|\mathbf{x}_0)$ is intractable for nonlinear SDEs. To compute $p_{0t}(\mathbf{x}_t|\mathbf{x}_0)$, one needs the Feynman-Kac formula [12] which requires expectation on every sample paths, see Appendix E.4.

Second, even if $p_{0t}(\mathbf{x}_t|\mathbf{x}_0)$ is tractable, computing the above variational bound would not be scalable due to the matrix multiplication of $\mathbf{G}\mathbf{G}^T$ that is of $O(d^2)$ complexity and the divergence computation [37]. These would become the main source of training bottleneck if dimension increases.

A.2 Derivation of Nonlinear Drift and Volatility Terms for INDM

Throughout this section, we omit $\boldsymbol{\phi}$ for notational simplicity. With the linear SDE on latent space

$$\mathrm{d}\mathbf{z}_t = -\frac{1}{2}\beta(t)\mathbf{z}_t\,\mathrm{d}t + g(t)\,\mathrm{d}\mathbf{w}_t, \quad \mathbf{z}_0 = \mathbf{h}(\mathbf{x}_0) \text{ with } \mathbf{x}_0 \sim p_r, \tag{7}$$

from $\mathbf{x}_t = \mathbf{h}^{-1}(\mathbf{z}_t)$, the k-th component of the induced variable satisfies

$$\mathrm{d}\mathrm{x}_{t,k} = \frac{\partial \mathrm{h}_k^{-1}}{\partial t}\,\mathrm{d}t + \big[\nabla_{\mathbf{z}_t}\mathrm{h}_k^{-1}(\mathbf{z}_t)\big]^T\,\mathrm{d}\mathbf{z}_t + \frac{1}{2}\text{tr}\left(\nabla^2_{\mathbf{z}_t}\mathrm{h}_k^{-1}(\mathbf{z}_t)\,\mathrm{d}\mathbf{z}_t\,\mathrm{d}\mathbf{z}_t^T\right) \tag{8}$$

by the multivariate Ito's Lemma [17]. Plugging the linear SDE of Eq. (7), Eq. (8) is transformed to

$$\begin{aligned}
\mathrm{d}\mathrm{x}_{t,k} &= \big[\nabla_{\mathbf{z}_t}\mathrm{h}_k^{-1}(\mathbf{z}_t)\big]^T\left\{-\frac{1}{2}\beta(t)\mathbf{z}_t\,\mathrm{d}t + g(t)\,\mathrm{d}\mathbf{w}_t\right\} + \frac{1}{2}g^2(t)\text{tr}\left(\nabla^2_{\mathbf{z}_t}\mathrm{h}_k^{-1}(\mathbf{z}_t)\right)\mathrm{d}t\\
&= \left\{-\frac{1}{2}\beta(t)\big[\nabla_{\mathbf{z}_t}\mathrm{h}_k^{-1}(\mathbf{z}_t)\big]^T\mathbf{z}_t + \frac{1}{2}g^2(t)\text{tr}\left(\nabla^2_{\mathbf{z}_t}\mathrm{h}_k^{-1}(\mathbf{z}_t)\right)\right\}\mathrm{d}t + g(t)\big[\nabla_{\mathbf{z}_t}\mathrm{h}_k^{-1}(\mathbf{z}_t)\big]^T\,\mathrm{d}\mathbf{w}_t,
\end{aligned} \tag{9}$$

because $\frac{\partial \mathrm{h}_k^{-1}}{\partial t} = 0$. Then, Eq. (9) in vector form becomes

$$\mathrm{d}\mathbf{x}_t = \mathbf{f}(\mathbf{x}_t, t)\,\mathrm{d}t + \mathbf{G}(\mathbf{x}_t, t)\,\mathrm{d}\mathbf{w}_t,$$

where the vector-valued drift and the matrix-valued volatility terms are given by

$$\begin{cases} \mathbf{f}(\mathbf{x}_t, t) = -\frac{1}{2}\beta(t)\nabla_{\mathbf{z}_t}\mathbf{h}^{-1}(\mathbf{z}_t)\mathbf{z}_t + \frac{1}{2}g^2(t)\mathrm{tr}\left(\nabla^2_{\mathbf{z}_t}\mathbf{h}^{-1}(\mathbf{z}_t)\right) \\ \mathbf{G}(\mathbf{x}_t, t) = g(t)\nabla_{\mathbf{z}_t}\mathbf{h}^{-1}(\mathbf{z}_t). \end{cases} \tag{10}$$

Here, $\nabla^2_{\mathbf{z}_t}\mathbf{h}^{-1}(\mathbf{z}_t)$ is a 3-dimensional tensor with (i, j, k)-th element to be $\left(\nabla^2_{\mathbf{z}_t}\mathrm{h}_k^{-1}(\mathbf{z}_t)\right)_{i,j}$, and the trace operator applied on this tensor is defined as a vector of $\left[\mathrm{tr}\left(\nabla^2_{\mathbf{z}_t}\mathrm{h}_1^{-1}(\mathbf{z}_t)\right), ..., \mathrm{tr}\left(\nabla^2_{\mathbf{z}_t}\mathrm{h}_d^{-1}(\mathbf{z}_t)\right)\right]^T$. From the inverse function theorem [38], the Jacobian of the inverse function $\nabla_{\mathbf{z}_t}\mathbf{h}^{-1}(\mathbf{z}_t)$ equals to the inverse Jacobian $\left[\nabla_{\mathbf{x}_t}\mathbf{h}(\mathbf{x}_t)\right]^{-1}$. Therefore, Eq. (10) is transformed to

$$\begin{cases} \mathbf{f}(\mathbf{x}_t, t) = -\frac{1}{2}\beta(t)\left[\nabla_{\mathbf{x}_t}\mathbf{h}(\mathbf{x}_t)\right]^{-1}\mathbf{h}(\mathbf{x}_t) + \frac{1}{2}g^2(t)\mathrm{tr}\left(\nabla^2_{\mathbf{z}_t}\mathbf{h}^{-1}(\mathbf{z}_t)\right) \\ \mathbf{G}(\mathbf{x}_t, t) = g(t)\left[\nabla_{\mathbf{x}_t}\mathbf{h}(\mathbf{x}_t)\right]^{-1}. \end{cases} \tag{11}$$

Now, we derive the second term of $\mathbf{f}$ in terms of $\mathbf{x}_t$ as follows: observe that $\sum_k \frac{\partial \mathrm{h}_i^{-1}}{\partial \mathrm{z}_{t,k}}\frac{\partial \mathrm{h}_k}{\partial \mathrm{x}_{t,j}} = \delta_{i,j}$, where $\delta_{i,j} = 1$ if $i = j$ and 0 otherwise. Differentiating both sides with respect to $\mathrm{x}_{t,l}$, we have

$$\sum_k \left\{\frac{\partial}{\partial \mathrm{x}_{t,l}}\left(\frac{\partial \mathrm{h}_i^{-1}}{\partial \mathrm{z}_{t,k}}\right)\right\}\frac{\partial \mathrm{h}_k}{\partial \mathrm{x}_{t,j}} + \frac{\partial \mathrm{h}_i^{-1}}{\partial \mathrm{z}_{t,k}}\left\{\frac{\partial}{\partial \mathrm{x}_{t,l}}\left(\frac{\partial \mathrm{h}_k}{\partial \mathrm{x}_{t,j}}\right)\right\} = 0,$$

where the first term is

$$\sum_{k,m}\frac{\partial \mathrm{h}_m}{\partial \mathrm{x}_{t,l}}\left\{\frac{\partial}{\partial \mathrm{z}_{t,m}}\left(\frac{\partial \mathrm{h}_i^{-1}}{\partial \mathrm{z}_{t,k}}\right)\right\}\frac{\partial \mathrm{h}_k}{\partial \mathrm{x}_{t,j}} = \sum_{k,m}\left(\nabla_{\mathbf{x}_t}\mathbf{h}(\mathbf{x}_t)\right)^T_{l,m}\left(\nabla^2_{\mathbf{z}_t}\mathbf{h}_i^{-1}(\mathbf{z}_t)\right)_{m,k}\left(\nabla_{\mathbf{x}_t}\mathbf{h}(\mathbf{x}_t)\right)_{k,j},$$

using the chain rule, and the second term becomes

$$\sum_k \frac{\partial \mathrm{h}_i^{-1}}{\partial \mathrm{z}_{t,k}}\left\{\frac{\partial}{\partial \mathrm{x}_{t,l}}\left(\frac{\partial \mathrm{h}_k}{\partial \mathrm{x}_{t,j}}\right)\right\} = \sum_k \left(\nabla_{\mathbf{z}_t}\mathbf{h}^{-1}(\mathbf{z}_t)\right)_{i,k}\left(\nabla^2_{\mathbf{x}_t}\mathbf{h}_k(\mathbf{x}_t)\right)_{l,j}.$$

From the above, we derive the trace term of $\mathbf{f}$ in Eq. (11) as

$$\mathrm{tr}\left(\nabla^2_{\mathbf{z}_t}\mathbf{h}^{-1}(\mathbf{z}_t)\right) = -\mathrm{tr}\left(\left[\nabla_{\mathbf{x}_t}\mathbf{h}(\mathbf{x}_t)\right]^{-T}\left(\left[\nabla_{\mathbf{x}_t}\mathbf{h}(\mathbf{x}_t)\right]^{-1} * \nabla^2_{\mathbf{x}_t}\mathbf{h}(\mathbf{x}_t)\right)\left[\nabla_{\mathbf{x}_t}\mathbf{h}(\mathbf{x}_t)\right]^{-1}\right),$$

where $\nabla^2_{\mathbf{x}_t}\mathbf{h}(\mathbf{x}_t)$ is a 3-dimensional tensor with (i, j, k)-th element to be $\left(\nabla^2_{\mathbf{x}_t}\mathbf{h}_k(\mathbf{x}_t)\right)_{i,j}$. Also, we define $*$ operation as the element-wise matrix multiplication given by

$$\left(\left[\nabla_{\mathbf{x}_t}\mathbf{h}(\mathbf{x}_t)\right]^{-1} * \nabla^2_{\mathbf{x}_t}\mathbf{h}(\mathbf{x}_t)\right)_{i,j} := \nabla_{\mathbf{x}_t}\left[\mathbf{h}(\mathbf{x}_t)\right]^{-1}\left(\nabla^2_{\mathbf{x}_t}\mathbf{h}(\mathbf{x}_t)\right)_{i,j}.$$

Combining all together, thus, we derive the nonlinear drift term in Eq. (11) as a function of $\mathbf{x}_t$ given by

$$\begin{aligned}\mathbf{f}(\mathbf{x}_t, t) = &-\frac{1}{2}\beta(t)\left[\nabla_{\mathbf{x}_t}\mathbf{h}(\mathbf{x}_t)\right]^{-1}\mathbf{h}(\mathbf{x}_t) \\ &-\frac{1}{2}g^2(t)\mathrm{tr}\left(\left[\nabla_{\mathbf{x}_t}\mathbf{h}(\mathbf{x}_t)\right]^{-T}\left(\left[\nabla_{\mathbf{x}_t}\mathbf{h}(\mathbf{x}_t)\right]^{-1} * \nabla^2_{\mathbf{x}_t}\mathbf{h}(\mathbf{x}_t)\right)\left[\nabla_{\mathbf{x}_t}\mathbf{h}(\mathbf{x}_t)\right]^{-1}\right).\end{aligned}$$

B Details on Section 6.1

It is one of central topics in the community of VAE to obtain a tighter ELBO [39, 40]. This section analyzes the variational gap and further theoretical analysis in diffusion models. Before we start, we remind the generalized Helmholtz decomposition in Lemma 1.

Lemma 1 (Helmholtz Decomposition [41])**.** *Any twice continuously differentiable vector field* $\mathbf{s}$ *that decays faster than* $\|\mathbf{z}\|_2^{-c}$ *for* $\|\mathbf{z}\|_2 \to \infty$ *and* $c > 0$ *can be uniquely decomposed into two vector fields, one rotation-free and one divergence-free:* $\mathbf{s} = \nabla \log p + \mathbf{u}$.

A rotation-free vector field $\nabla \log p$, or the divergence part, is a score function of a probability density p, and a divergence-free vector field $\mathbf{u}$, or the rotation part, satisfies $\mathrm{div}(\mathbf{u}) \equiv 0$. From this decomposition, any score network is decomposed by $\mathbf{s}_{\boldsymbol{\theta}}(\mathbf{z}_t, t) = \nabla \log p_t^{\boldsymbol{\theta}}(\mathbf{z}_t) + \mathbf{u}_t^{\boldsymbol{\theta}}(\mathbf{z}_t)$ for some probability $p_t^{\boldsymbol{\theta}}$ and vector field $\mathbf{u}_t^{\boldsymbol{\theta}}$, for any $t \in (0, T]$. Then, the generative SDE of the full score network

$$\mathrm{d}\mathbf{z}_t = \left[\mathbf{f}(\mathbf{z}_t, t) - g^2(t)\mathbf{s}_{\boldsymbol{\theta}}(\mathbf{z}_t, t)\right] \mathrm{d}\bar{t} + g(t)\, \mathrm{d}\bar{\mathbf{w}}_t \tag{12}$$

and the generative SDE of the divergence part

$$\mathrm{d}\mathbf{z}_t = \left[\mathbf{f}(\mathbf{z}_t, t) - g^2(t)\nabla \log p_t^{\boldsymbol{\theta}}(\mathbf{z}_t)\right] \mathrm{d}\bar{t} + g(t)\, \mathrm{d}\bar{\mathbf{w}}_t \tag{13}$$

has distinctive path measures. Throughout this section, $\mathbf{f}(\mathbf{z}_t, t)$ does not have to be a linear vector field, such as $-\frac{1}{2}\beta(t)\mathbf{z}_t$. If $\boldsymbol{\nu}_{\boldsymbol{\theta}}$ and $\boldsymbol{\rho}_{\boldsymbol{\theta}}$ are the path measures of SDEs of Eqs. (12) and (13), respectively, then using the Girsanov theorem [11, 35] and the martingale property [17], we have

$$\begin{aligned} D_{KL}(\boldsymbol{\nu}_{\boldsymbol{\theta}} \| \boldsymbol{\rho}_{\boldsymbol{\theta}}) =& \frac{1}{2}\int_0^T g^2(t)\mathbb{E}_{\mathbf{z}_t \sim \boldsymbol{\nu}_{\boldsymbol{\theta}}|_t}\left[\|\nabla \log p_t^{\boldsymbol{\theta}}(\mathbf{z}_t) - \mathbf{s}_{\boldsymbol{\theta}}(\mathbf{z}_t, t)\|_2^2\right] \mathrm{d}t \\ =& \frac{1}{2}\int_0^T g^2(t)\mathbb{E}_{\mathbf{z}_t \sim \boldsymbol{\nu}_{\boldsymbol{\theta}}|_t}\left[\|\mathbf{u}_{\boldsymbol{\theta}}(\mathbf{z}_t, t)\|_2^2\right] \mathrm{d}t. \end{aligned} \tag{14}$$

This KL divergence of two path measures quantifies how much the score network contains the rotation part $\mathbf{u}_t^{\boldsymbol{\theta}}$. Recall that the forward SDE satisfies

$$\mathrm{d}\mathbf{z}_t = \mathbf{f}(\mathbf{z}_t, t)\, \mathrm{d}t + g(t)\, \mathrm{d}\mathbf{w}_t,$$

which starts at $p_0^{\boldsymbol{\phi}}$, and the marginal distribution of its path measure $\boldsymbol{\mu}_{\boldsymbol{\phi}}$ at t is $p_t^{\boldsymbol{\phi}}$. As NELBO is equivalent to

$$D_{KL}(\boldsymbol{\mu}_{\boldsymbol{\phi}} \| \boldsymbol{\nu}_{\boldsymbol{\phi},\boldsymbol{\theta}}) = \frac{1}{2}\int_0^T g^2(t)\mathbb{E}_{p_t^{\boldsymbol{\phi}}(\mathbf{z}_t)}\left[\|\mathbf{s}_{\boldsymbol{\theta}}(\mathbf{z}_t, t) - \nabla \log p_t^{\boldsymbol{\phi}}(\mathbf{z}_t)\|_2^2\right] \mathrm{d}t + D_{KL}\big(p_T^{\boldsymbol{\phi}}(\mathbf{z}_T) \| \pi(\mathbf{z}_T)\big), \tag{15}$$

for $\boldsymbol{\theta}$-optimization, the optimal $\boldsymbol{\theta}^*$ satisfies $\mathbf{s}_{\boldsymbol{\theta}^*}(\mathbf{z}_t, t) = \nabla \log p_t^{\boldsymbol{\phi}}(\mathbf{z}_t)$. At this optimality, $\boldsymbol{\theta}$ should satisfy a pair of constraints: 1) the zero-rotation part $\mathbf{u}_t^{\boldsymbol{\theta}^*} \equiv 0$, which is equivalent to $D_{KL}(\boldsymbol{\nu}_{\boldsymbol{\theta}^*} \| \boldsymbol{\rho}_{\boldsymbol{\theta}^*}) = 0$; 2) the coincidence of $\nabla \log p_t^{\boldsymbol{\phi}}(\mathbf{z}_t) \equiv \nabla \log p_t^{\boldsymbol{\theta}}(\mathbf{z}_t)$. The starting point to analyze the variational gap with respect to the Helmholtz decomposition is the next theorem. We defer the proofs in Section G.

Proposition 1. *Suppose $q_t^{\boldsymbol{\theta}}$ is the marginal distribution of $\boldsymbol{\nu}_{\boldsymbol{\theta}}$ at t. The variational gap is*

$$\begin{aligned} \mathrm{Gap}\big(\boldsymbol{\mu}_{\boldsymbol{\phi}}(\{\mathbf{x}_t\}), \boldsymbol{\nu}_{\boldsymbol{\phi},\boldsymbol{\theta}}(\{\mathbf{x}_t\})\big) :=& D_{KL}\big(\boldsymbol{\mu}_{\boldsymbol{\phi}}(\{\mathbf{x}_t\}) \| \boldsymbol{\nu}_{\boldsymbol{\phi},\boldsymbol{\theta}}(\{\mathbf{x}_t\})\big) - D_{KL}\big(p_0^{\boldsymbol{\phi}}(\mathbf{x}_0) \| q_0^{\boldsymbol{\theta}}(\mathbf{x}_0)\big) \\ =& \frac{1}{2}\int_0^T g^2(t)\mathbb{E}_{p_t^{\boldsymbol{\phi}}(\mathbf{z}_t)}\big[\underbrace{\|\nabla \log q_t^{\boldsymbol{\theta}}(\mathbf{z}_t) - \mathbf{s}_{\boldsymbol{\theta}}(\mathbf{z}_t, t)\|_2^2}_{\textit{Score-only error}}\big] \mathrm{d}t. \end{aligned}$$

Remark 1. The generative SDE of $\mathrm{d}\mathbf{z}_t^{\boldsymbol{\theta}} = [-\frac{1}{2}\beta(t)\mathbf{z}_t^{\boldsymbol{\theta}} - g^2(t)\mathbf{s}_{\boldsymbol{\theta}}(\mathbf{z}_t^{\boldsymbol{\theta}}, t)]\, \mathrm{d}\bar{t} + g(t)\, \mathrm{d}\bar{\mathbf{w}}_t$ does not necessarily start from the prior π. Proposition 1 holds for an arbitrary distribution $p_T^{\boldsymbol{\theta}}$. At the same spirit, Proposition 1 holds for any distribution $p_0^{\boldsymbol{\phi}}$.

Remark 2. Throughout the section, we follow the assumptions made in Appendix A of Song et al. [11]. On top of that, we assume that both $\mathbf{s}_{\boldsymbol{\theta}}$ and $q_t^{\boldsymbol{\theta}}$ are continuously differentiable.

The variational gap derived in Proposition 1 does not include the forward score, $\nabla \log p_t^{\boldsymbol{\phi}}(\mathbf{z}_t)$, except for taking the expectation, $\mathbb{E}_{p_t^{\boldsymbol{\phi}}(\mathbf{z}_t)}$. Therefore, the gap is intuitively connected to the score training, rather than the flow training. To elucidate the logic, we decompose the variational gap in Proposition 1 into

$$\begin{aligned} \mathrm{Gap}\big(\boldsymbol{\mu}_{\boldsymbol{\phi}}, \boldsymbol{\nu}_{\boldsymbol{\phi},\boldsymbol{\theta}}\big) =& \frac{1}{2}\int_0^T g^2(t)\mathbb{E}_{p_t^{\boldsymbol{\phi}}(\mathbf{z}_t)}\left[\|\nabla \log q_t^{\boldsymbol{\theta}}(\mathbf{z}_t) - \mathbf{s}_{\boldsymbol{\theta}}(\mathbf{z}_t, t)\|_2^2\right] \mathrm{d}t \\ \leq& \frac{1}{2}\int_0^T g^2(t)\mathbb{E}_{p_t^{\boldsymbol{\phi}}(\mathbf{z}_t)}\left[\left\|\nabla \log q_t^{\boldsymbol{\theta}}(\mathbf{z}_t) - \nabla \log p_t^{\boldsymbol{\theta}}(\mathbf{z}_t)\right\|_2^2 + \left\|\nabla \log p_t^{\boldsymbol{\theta}}(\mathbf{z}_t) - \mathbf{s}_{\boldsymbol{\theta}}(\mathbf{z}_t, t)\right\|_2^2\right] \mathrm{d}t. \end{aligned} \tag{16}$$

$$= \frac{1}{2}\int_0^T g^2(t)\mathbb{E}_{p_t^{\phi}(\mathbf{z}_t)}\Big[\underbrace{\left\|\nabla \log q_t^{\boldsymbol{\theta}}(\mathbf{z}_t) - \nabla \log p_t^{\boldsymbol{\theta}}(\mathbf{z}_t)\right\|_2^2}_{\text{How close is } \boldsymbol{\nu}_{\boldsymbol{\theta}} \text{ to forward measure}} + \underbrace{\left\|\mathbf{u}_t^{\boldsymbol{\theta}}(\mathbf{z}_t)\right\|_2^2}_{\text{How close is } \mathbf{u}_t^{\boldsymbol{\theta}} \text{ to zero}}\Big]\,\mathrm{d}t.$$

The second term, $\|\nabla \log p_t^{\boldsymbol{\theta}}(\mathbf{z}_t) - \mathbf{s}_{\boldsymbol{\theta}}(\mathbf{z}_t, t)\|_2^2$ (see Eq. (14)), equals to the L^2-norm of the rotation term, $\|\mathbf{u}_t^{\boldsymbol{\theta}}(\mathbf{z}_t, t)\|_2^2$, so it measures how close is the score network to the space of

$$\mathbf{S}_{div} := \{\mathbf{s} : \mathbb{R}^d \to \mathbb{R}^d | \text{ the rotation term of } \mathbf{s} \text{ is zero}\}.$$

On the other hand, having assumed the rotation part to be zero, the first term, $\|\nabla \log q_t^{\boldsymbol{\theta}}(\mathbf{z}_t) - \nabla \log p_t^{\boldsymbol{\theta}}(\mathbf{z}_t)\|_2^2$, becomes zero only if the generative score $\nabla \log q_t^{\boldsymbol{\theta}}$ equals to a forward score $\nabla \log q_t$ with certain initial distribution q_0, meaning that if there exists a q_0 and q_t is a marginal density of the forward SDE starting from q_0, then

$$\nabla \log q_t(\mathbf{z}_t) = \nabla \log q_t^{\boldsymbol{\theta}}(\mathbf{z}_t) \text{ is equivalent to } \nabla \log q_t(\mathbf{z}_t) = \nabla \log p_t^{\boldsymbol{\theta}}(\mathbf{z}_t),$$

and only in that case, $\nabla \log q_t^{\boldsymbol{\theta}}(\mathbf{z}_t) = \nabla \log p_t^{\boldsymbol{\theta}}(\mathbf{z}_t)$. Therefore, the gap becomes tight if 1) $\mathbf{u}_t^{\boldsymbol{\theta}} \equiv 0$ and 2) $\nabla \log q_t^{\boldsymbol{\theta}} = \nabla \log q_t$ for some q_t following the forward SDE, which is concretely proved in Lemma 2. It turns out that this is the only case of the gap being zero proved in Theorem 2. For that, we provide a rigorous definition of the class of score functions of interest as below.

Definition 1. Let $\mathbf{S}_{sol} \subseteq \mathbf{S}_{div}$ be a sub-family of rotation-free score functions $\mathbf{s} : \mathbb{R}^d \to \mathbb{R}^d$ such that $\mathbf{s}(\mathbf{z}_t, t) = \nabla \log p_t(\mathbf{z}_t)$ almost everywhere for p_t that is the marginal distribution of the path measure of $\mathrm{d}\mathbf{z}_t = \mathbf{f}(\mathbf{z}_t, t)\,\mathrm{d}t + g(t)\,\mathrm{d}\mathbf{w}_t$ at t.

Remark 3. Analogous to Theorem 1, no condition for the starting and ending variables is imposed in Definition 1.

Remark 4. $\mathbf{S}_{sol}$ is the space of score functions of the forward SDE $\mathrm{d}\mathbf{z}_t = \mathbf{f}(\mathbf{z}_t, t)\,\mathrm{d}t + g(t)\,\mathrm{d}\mathbf{w}_t$ with arbitrary initial variable.

Although Song et al. [11] focused on the data diffusion, their theory is applicable for a diffusion process that starts with an arbitrary initial distribution. Lemma 2 describes the theoretic analysis done by Song et al. [11].

Lemma 2 (Theorem 2 of Song et al. [11])**.** $\mathrm{Gap}(\boldsymbol{\mu}_{\boldsymbol{\phi}}, \boldsymbol{\nu}_{\boldsymbol{\phi},\boldsymbol{\theta}}) = 0$ *if* $\mathbf{s}_{\boldsymbol{\theta}} \in \mathbf{S}_{sol}$.

With Lemma 2, however, we cannot certainly be sure that the score network $\mathbf{s}_{\boldsymbol{\theta}}$ of INDM falls to $\mathbf{S}_{sol}$ when the variational gap is zero. Thus, we take a step further to identify the connection of zero variational gap and the class of rotation-free score functions $\mathbf{S}_{sol}$ in Theorem 2. This Theorem 2 completely characterizes all admissible score networks that achieve the zero variational gaps, and we are certain that the zero variational gap implies $\mathbf{s}_{\boldsymbol{\theta}} \in \mathbf{S}_{sol}$, which turns out to be a solution space in Theorem 3.

Theorem 2. $\mathrm{Gap}(\boldsymbol{\mu}_{\boldsymbol{\phi}}, \boldsymbol{\nu}_{\boldsymbol{\phi},\boldsymbol{\theta}}) = 0$ *if and only if* $\mathbf{s}_{\boldsymbol{\theta}} \in \mathbf{S}_{sol}$.

From Theorem 2, the variational gap is strictly positive as long as the rotation part of the score network remains to be nonzero. NELBO of Eq. (15) optimizes its score network towards $\mathbf{s}_{\boldsymbol{\theta}}(\mathbf{z}_t, t) \to \nabla \log p_t^{\boldsymbol{\phi}}(\mathbf{z}_t) := \mathbf{s}_{\boldsymbol{\phi}}(\mathbf{z}_t, t)$, which is equivalent to $\log p_t^{\boldsymbol{\theta}}(\mathbf{z}_t) \to \nabla \log p_t^{\boldsymbol{\phi}}(\mathbf{z}_t)$ (or equivalently, $\log q_t^{\boldsymbol{\theta}}(\mathbf{z}_t) \to \nabla \log p_t^{\boldsymbol{\phi}}(\mathbf{z}_t)$) and $\mathbf{u}_t^{\boldsymbol{\theta}}(\mathbf{z}_t, t) \to 0$. In contrast to DDPM++ with fixed $\boldsymbol{\phi}$, optimizing $D_{KL}(\boldsymbol{\mu}_{\boldsymbol{\phi}} \| \boldsymbol{\nu}_{\boldsymbol{\phi},\boldsymbol{\theta}})$ w.r.t $\boldsymbol{\phi}$ finds the closest $\mathbf{s}_{\boldsymbol{\phi}}$ among $\mathbf{S}_{sol}$ to $\mathbf{s}_{\boldsymbol{\theta}}$. Thus, if $\mathbf{s}_{\boldsymbol{\theta}} \in \mathbf{S}_{sol}$, then $\mathbf{s}_{\boldsymbol{\phi}^*} = \mathbf{s}_{\boldsymbol{\theta}}$, which is proved in Theorem 3. If $\mathbf{s}_{\boldsymbol{\theta}} \notin \mathbf{S}_{sol}$, then $\mathbf{s}_{\boldsymbol{\phi}^*}$ is not equal to $\mathbf{s}_{\boldsymbol{\theta}}$, anymore, but $\mathbf{s}_{\boldsymbol{\phi}^*}$ will be the closest among $\mathbf{S}_{sol}$ to $\mathbf{s}_{\boldsymbol{\theta}}$ because $D_{KL}(\boldsymbol{\mu}_{\boldsymbol{\phi}} \| \boldsymbol{\nu}_{\boldsymbol{\phi},\boldsymbol{\theta}})$ is the weighted L^2-norm of $\mathbf{s}_{\boldsymbol{\phi}} - \mathbf{s}_{\boldsymbol{\theta}}$.

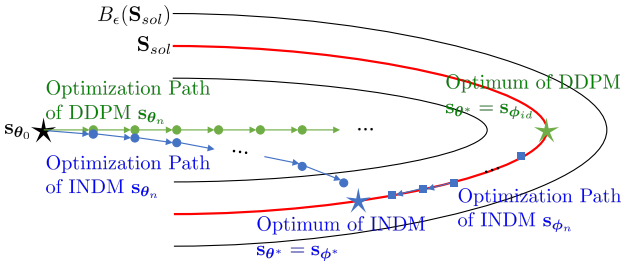

Figure 10: Descriptive Illustration On Nearly MLE Training.

Theorem 3. *For any fixed* $\mathbf{s}_{\bar{\boldsymbol{\theta}}} \in \mathbf{S}_{sol}$*, if* $\boldsymbol{\phi}^* \in \arg\min_{\boldsymbol{\phi}} D_{KL}(\boldsymbol{\mu}_{\boldsymbol{\phi}} \| \boldsymbol{\nu}_{\boldsymbol{\phi},\bar{\boldsymbol{\theta}}})$*, then* $\mathbf{s}_{\boldsymbol{\phi}^*}(\mathbf{z}_t, t) = \nabla \log p_t^{\boldsymbol{\phi}^*}(\mathbf{z}_t) = \mathbf{s}_{\bar{\boldsymbol{\theta}}}(\mathbf{z}_t, t)$*, and* $D_{KL}(\boldsymbol{\mu}_{\boldsymbol{\phi}^*} \| \boldsymbol{\nu}_{\boldsymbol{\phi}^*,\bar{\boldsymbol{\theta}}}) = D_{KL}(p_r \| p_{\boldsymbol{\phi}^*,\bar{\boldsymbol{\theta}}}) = Gap(\boldsymbol{\mu}_{\boldsymbol{\phi}^*}, \boldsymbol{\nu}_{\boldsymbol{\phi}^*,\bar{\boldsymbol{\theta}}}) = 0$.

Indeed, Theorem 3 implies that the whole class of $\mathbf{S}_{sol}$ is the solution space, which means that any $\mathbf{s}_{\boldsymbol{\theta}}$ in $\mathbf{S}_{sol}$ is a candidate for an optimal score function as there always exists ϕ^* corresponding to a given $\boldsymbol{\theta}$ that achieves the perfect match of the model distribution to the data distribution. This is contrastive to DDPM++ that only has a unique optimal point of $\mathbf{s}_{\boldsymbol{\theta}^*}(\mathbf{z}_t, t) = \nabla \log p_t^{\phi_{id}}(\mathbf{z}_t) \in \mathbf{S}_{sol}$. Figure 10 illustrates that the optimal point of DDPM is a single point in $\mathbf{S}_{sol}$, whereas any $\mathbf{s}_{\boldsymbol{\theta}} \in \mathbf{S}_{sol}$ is a candidate for the optimal point of INDM by Theorem 3. In other words, the number of DDPM optimality is one, while INDM has infinite number of optimalities.

B.1 Restricting Search Space of $\mathbf{s}_{\boldsymbol{\theta}}$ into $\mathbf{S}_{div}$

Due to the space limit, the argument in this section has not been included in the main paper. Below, we provide the rationale that it is the number of optimal points that affect the NLL performance. For that, we optimize DDPM++ with a regularization, suggested in Proposition 5. This regularization restricts the score network from not deviating $\mathbf{S}_{div}$ too far by keeping the rotation term, $\mathbf{u}_t^{\boldsymbol{\theta}}$, being consistently small. Consequently, a fastly converging rotation term is advantageous in reducing the variational gap (see Inequality (16)), and this regularization helps the MLE training of DDPM++.

Proposition 2 proves that $\mathbf{S}_{div}$ is identical to a class of score functions that have symmetric derivatives. From this, Proposition 3 provides a motivation of the regularization by proving that a symmetric matrix satisfies a certain equality. Then, Proposition 4 implies that the formula suggested in Proposition 3 indeed measures how close is the matrix symmetric. Lastly, Proposition 5 provides the minimum variance estimator of the formula. With these propositions, we conclude that the constraint of

$$\mathbb{E}_{\boldsymbol{\epsilon}_1, \boldsymbol{\epsilon}_2}\left[\left(\boldsymbol{\epsilon}_2^T\left(\nabla \mathbf{s}_{\boldsymbol{\theta}}(\mathbf{z}_t, t) - (\nabla \mathbf{s}_{\boldsymbol{\theta}})^T(\mathbf{z}_t, t)\right)\boldsymbol{\epsilon}_1\right)^2\right] = 0 \tag{17}$$

with $\boldsymbol{\epsilon}_1$ and $\boldsymbol{\epsilon}_2$ sampled from the random variable suggested in Proposition 5 would optimize $\mathbf{s}_{\boldsymbol{\theta}}$ in the space of $\mathbf{S}_{div}$. Using the Lagrangian form, we could add the left-hand-side of Eq. (17) as a regularization term in NELBO to force the score network not deviate from $\mathbf{S}_{div}$ too much.

With the clear mathematical properties, however, obtaining the full matrix of $\nabla \mathbf{s}_{\boldsymbol{\theta}}$ is a bottleneck in the computation of the regularization term. Specifically, each row of $\nabla \mathbf{s}_{\boldsymbol{\theta}}$ needs to be computed separately [42], so it takes $O(d)$ complexity to compute $\nabla \mathbf{s}_{\boldsymbol{\theta}}$, which is prohibitively expensive. Therefore, we use a trick to reduce $O(d)$ to $O(1)$ motivated from the Hutchinson's estimator [43, 23]: first, we compute the gradient of $\boldsymbol{\epsilon}_2^T \mathbf{s}_{\boldsymbol{\theta}}$ and $\boldsymbol{\epsilon}_1^T \mathbf{s}_{\boldsymbol{\theta}}$, separately. Afterwards, we apply vector multiplication between $\boldsymbol{\epsilon}_1$ and $\nabla(\boldsymbol{\epsilon}_2^T \mathbf{s}_{\boldsymbol{\theta}})$, which gives us $\boldsymbol{\epsilon}_2^T \nabla \mathbf{s}_{\boldsymbol{\theta}} \boldsymbol{\epsilon}_1$; and analogously, the multiplication of $\boldsymbol{\epsilon}_2$ with $\nabla(\boldsymbol{\epsilon}_1^T \mathbf{s}_{\boldsymbol{\theta}})$ yields $\boldsymbol{\epsilon}_2^T (\nabla \mathbf{s}_{\boldsymbol{\theta}})^T \boldsymbol{\epsilon}_1$. This trick requires only second time of gradient computations to estimate the regularization. Hence, the computational complexity of $\boldsymbol{\epsilon}_2^T(\nabla \mathbf{s}_{\boldsymbol{\theta}} - \nabla \mathbf{s}_{\boldsymbol{\theta}}^T)\boldsymbol{\epsilon}_1$ is $O(1)$.

Proposition 2. $\mathbf{s}_{\boldsymbol{\theta}} \in \mathbf{S}_{div}$ *if and only if* $\nabla_{\mathbf{z}_t} \mathbf{s}_{\boldsymbol{\theta}}(\mathbf{z}_t, t)$ *is symmetric.*

Proposition 3. *A matrix* $A \in \mathbb{R}^{d \times d}$ *is symmetric if and only if* $\mathbb{E}_{\boldsymbol{\epsilon}_1, \boldsymbol{\epsilon}_2 \sim \mathcal{N}(0, \mathbf{I})}\left[(\boldsymbol{\epsilon}_2^T(A - A^T)\boldsymbol{\epsilon}_1)^2\right] = 0$.

In fact, we can prove a bit stronger results in the next propositions.

Proposition 4. *Let* $\boldsymbol{\epsilon}_1$ *and* $\boldsymbol{\epsilon}_2$ *be vectors of* d *independent samples from a random variable* U *with mean zero. Then*

$$\mathbb{E}_{\boldsymbol{\epsilon}_1, \boldsymbol{\epsilon}_2}[(\boldsymbol{\epsilon}_2^T(A - A^T)\boldsymbol{\epsilon}_1)^2] = \mathbb{E}_U[U^2]^2 \|A - A^T\|_F^2$$

and

$$\begin{aligned}
Var\Big(\big(\boldsymbol{\epsilon}_2^T(A - A^T)\boldsymbol{\epsilon}_1\big)^2\Big) &= Var(U^2)\Big(Var(U^2) + 2\big(Var(U) + \mathbb{E}_U[U]^2\big)^2\Big)\sum_{a,b}(\Delta A)_{ab}^4 \\
&+ 2\big(Var(U) + \mathbb{E}_U[U]^2\big)^2\Big(3Var(U^2) + 2\big(Var(U) + \mathbb{E}_U[U]^2\big)^2\Big)\sum_{a}\sum_{b \neq d}(\Delta A)_{ab}^2(\Delta A)_{ad}^2 \\
&+ 2\big(Var(U) + \mathbb{E}_U[U]^2\big)^4\Big(\sum_{a \neq c}\sum_{b \neq d}(\Delta A)_{ab}^2(\Delta A)_{cd}^2 \\
&\qquad + 3\sum_{a \neq c}\sum_{b \neq d}(\Delta A)_{ab}(\Delta A)_{ad}(\Delta A)_{cb}(\Delta A)_{cd}\Big),
\end{aligned}$$

where $(\Delta A)_{ab} := A_{ab} - A_{ba}$.

Proposition 5. *Let U be the discrete random variable which takes the values $1, -1$ each with probability $1/2$. Then $(\boldsymbol{\epsilon}_2^T(A - A^T)\boldsymbol{\epsilon}_1)^2$ is the unbiased estimator of $\|A - A^T\|_F^2$. Moreover, U is the unique random variable amongst zero-mean random variables for which the estimator is an unbiased estimator, and attains a minimum variance.*

Summing altogether, if it is the main focus to eliminate the rotation term in the score estimation, we could optimize $D_{KL}(\boldsymbol{\mu}_{\boldsymbol{\phi}}\|\boldsymbol{\nu}_{\boldsymbol{\phi},\boldsymbol{\theta}}) + \lambda\mathbb{E}_{\boldsymbol{\epsilon}_1,\boldsymbol{\epsilon}_2}\left[(\boldsymbol{\epsilon}_2^T(\nabla\mathbf{s}_{\boldsymbol{\theta}} - \nabla\mathbf{s}_{\boldsymbol{\theta}}^T)\boldsymbol{\epsilon}_1^T)^2\right]$, where $\boldsymbol{\epsilon}_1$ and $\boldsymbol{\epsilon}_2$ are the random variables of minimum variance, as proposed in Proposition 5. In practice, we find that the above regularized training loss is unnecessary for INDM because we already achieves the nearly MLE training, but it helps DDPM++ to reduce the variational gap at the expense of $4\times$ slower training speed than the training with unregularized loss in DDPM++. Even with reduced variational gap, we find that NLL of DDPM++ is improved only marginally only on certain training scenarios, and has no effect in most trials, so we leave the detailed effect of MLE training in diffusion models as a future work. Notably, therefore, we conclude that the NLL gain in INDM, compared to DDPM++, essentially originates from ϕ-training and its consequential expanded solution space to $\mathbf{S}_{sol}$.

C Details on Section 6.2

C.1 Full Statement of Theorem 4

We provide a full statement of Theorem 4. Theorem 4 is heavily influenced by the theoretic analysis of De Bortoli et al. [15], Guth et al. [22], and it could be considered as merely an application of their results. It is possible that the inequality in Theorem 4 could not be tight, but empirically the robustness is significantly connected to the initial distribution's smoothness.

Theorem 4. *Assume that there exists $M \geq 0$ such that for any $t \in [0, T]$ and $\mathbf{z} \in \mathbb{R}^d$, the score estimation is close enough to the forward score by M, $\|\mathbf{s}_{\boldsymbol{\theta}}(\mathbf{x}, t) - \nabla \log p_t^{\boldsymbol{\phi}}(\mathbf{x})\| \leq M$, with $\mathbf{s}_{\boldsymbol{\theta}} \in C([0, T]\times\mathbb{R}^d, \mathbb{R}^d)$. Assume that $\nabla \log p_t^{\boldsymbol{\phi}}(\mathbf{z})$ is C^2 in both t and $\mathbf{z}$, and that $\sup_{\mathbf{z},t} \|\nabla^2 \log p_t^{\boldsymbol{\phi}}(\mathbf{z})\| \leq K$ and $\|\frac{\partial}{\partial t}\nabla \log p_t^{\boldsymbol{\phi}}(\mathbf{z})\| \leq Me^{-\alpha t}\|\mathbf{z}\|$ for some $K, M, \alpha > 0$. Suppose $(\mathbf{h}_{\boldsymbol{\phi}}^{-1})_{\#}$ s a push-forward map. Then $\|p_r - (\mathbf{h}_{\boldsymbol{\phi}}^{-1})_{\#}p_{0,N}^{\boldsymbol{\theta}}\|_{TV} \leq E_{pri}(\boldsymbol{\phi}) + E_{dis}(\boldsymbol{\phi}) + E_{est}(\boldsymbol{\phi}, \boldsymbol{\theta})$, where $E_{pri}(\boldsymbol{\phi}) = \sqrt{2}e^{-T}D_{KL}(p_T^{\boldsymbol{\phi}}\|\pi)^{1/2}$ is the error originating from the prior mismatch; $E_{dis}(\boldsymbol{\phi}) = 6\sqrt{\delta}(1 + \mathbb{E}_{p_0^{\boldsymbol{\phi}}(\mathbf{z})}[\|\mathbf{z}\|^4]^{1/4})(1 + K + M(1 + \frac{1}{\sqrt{2\alpha}}))$ is the discretization error with $\delta = \frac{\max \gamma_k}{\min \gamma_k}^2$; $E_{est}(\boldsymbol{\phi}, \boldsymbol{\theta}) = 2TM^2$ is the score estimation error.*

C.2 Geometric Interpretation of Latent Diffusion

Figure 11 illustrates the diffusion trajectories of the probability flow ODE of VPSDE. It shows that the trajectories are highly nonlinear, and this section is devoted to analyze why such nonlinear trajectory occurs. Figure 12 shows two diffusion paths differing only on their scales on (a) the two moons dataset and (b) the ring dataset. The standard Gaussian distribution at T has a larger variance than the initial data at the top row and has a smaller one at the bottom row on each dataset. For the visualization purpose, we zoom in the top row, and we zoom out the bottom row for each dataset, but we fix the xlim and ylim arguments in the matplotlib package [44] row-wisely. With this discrepancy of the initial data scale, the particle trajectory at the bottom row is much more straightforward than in the top row, and it implies that the scale of initial data matters to the straightness of the bridge even if the diffusion SDE is identically linear.

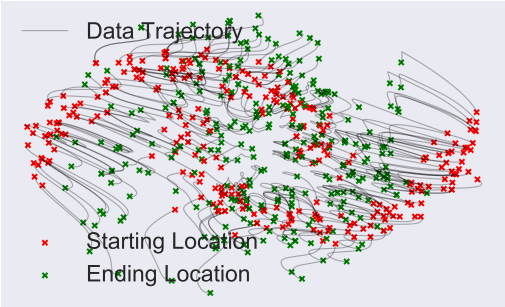

Figure 11: Particle trajectories of the probability flow ODE for VPSDE on the synthetic two moons 2d dataset.

A behind rationale for this observation comes from the closed-form solution of VPSDE. Suppose the forward diffusion follows VPSDE of $\mathrm{d}\mathbf{x}_t = -\frac{1}{2}\beta(t)\mathbf{x}_t\,\mathrm{d}t + \sqrt{\beta(t)}\,\mathrm{d}\mathbf{w}_t$. Then, the solution of this

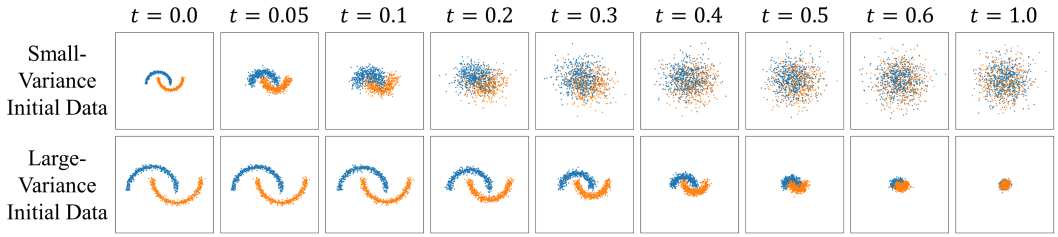

(a) Two Moons Dataset

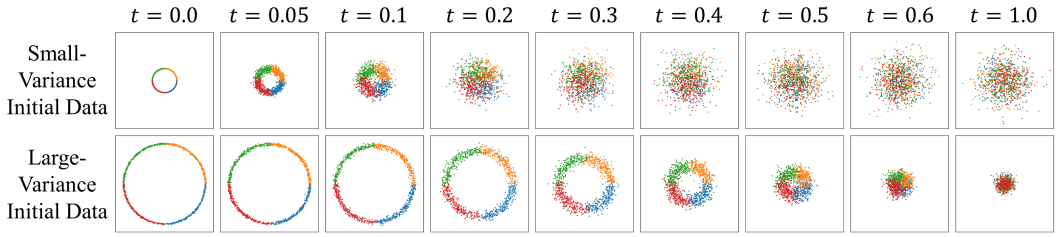

(b) Ring Dataset

Figure 12: Comparison of linear diffusion bridges on data and latent spaces in diverse datasets.

Table 7: Statistics of data variable and latent variable on CIFAR-10. All statistics are averaged by dimension.

	Mean	Variance	Min	Max
DDPM++ ($\mathbf{x}_0 = \mathbf{z}_0^{\boldsymbol{\phi}_{id}}$)	-0.05	0.25	-1	1
INDM ($\mathbf{z}_0^{\boldsymbol{\phi}}$)	0.70	9.74	-8.66	12.17

SDE becomes

$$\mathbf{x}_t = \underbrace{e^{-\frac{1}{2}\int_0^t \beta(s)\,\mathrm{d}s}\mathbf{x}_0}_{\text{linearly contraction mapping}} + \underbrace{\sqrt{1 - e^{-\int_0^t \beta(s)\,\mathrm{d}s}}\boldsymbol{\epsilon}}_{\text{random perturbation}}, \tag{18}$$

where $\boldsymbol{\epsilon} \sim \mathcal{N}(0, \mathbf{I})$. As the drift term $-\frac{1}{2}\beta(t)\mathbf{x}_t$ ahead towards the origin of $\mathbb{R}^d$, the solution in Eq. (18) is a summation of the contraction mapping to the origin, $0 \in \mathbb{R}^d$, with a random noise function, where the magnitude of the random perturbation depends solely on the diffusion coefficient, $g(t) = \sqrt{\beta(t)}$. If $\mathbf{x}_0$ is inflated by $c\mathbf{x}_0$, then it becomes $\mathbf{x}_t = c \times e^{-\frac{1}{2}\int_0^t \beta(s)\,\mathrm{d}s}\mathbf{x}_0 + \sqrt{1 - e^{-\int_0^t \beta(s)\,\mathrm{d}s}}\boldsymbol{\epsilon}$ with contraction mapping multiplied by c. Therefore, as c increases, the contraction force outweighs the random perturbing effect, and the particle trajectory is becoming straight.

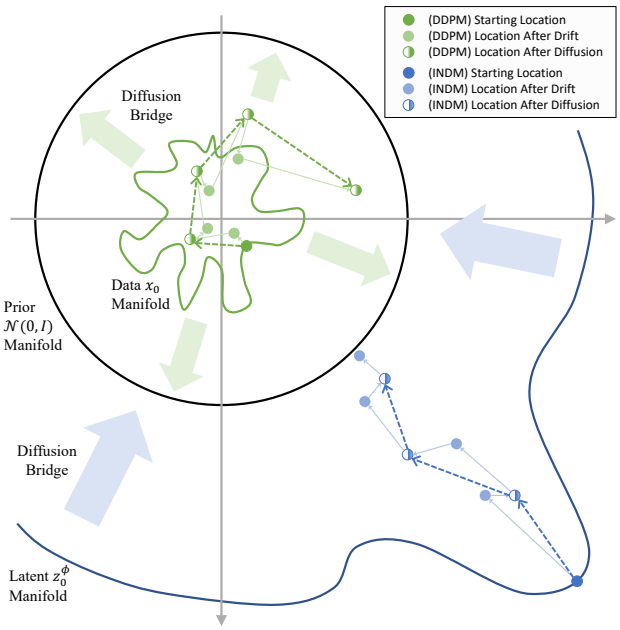

Figure 13: Descriptive Illustration On Diffusion Bridge.

On a high-dimensional dataset, most of the mass of the standard Gaussian $\pi = \mathcal{N}(0, \mathbf{I})$, which is the prior, is concentrated on a thin spherical shell with squared radius of d, according to the Gaussian annulus theorem [45], as described in the black circle of Figure 13. On CIFAR-10, the data distribution has the smaller average square radius of $\mathbb{E}_{p_r(\mathbf{x}_0)}\left[\|\mathbf{x}_0\|_2^2\right] = 776 < 3072 = d$, whereas the latent distribution has a larger

average square radius of $\mathbb{E}_{p_r(\mathbf{x}_0)}\left[\|\mathbf{h}_{\boldsymbol{\phi}}(\mathbf{x}_0)\|_2^2\right] = \mathbb{E}_{p_0^{\boldsymbol{\phi}}(\mathbf{z}_0^{\boldsymbol{\phi}})}\left[\|\mathbf{z}_0^{\boldsymbol{\phi}}\|_2^2\right] > d$ than a standard Gaussian distribution. The latent radius varies from $5,385$ to $31,399$ by experimental settings. Thus, the latent manifold is located outside of the prior on CIFAR-10 as depicted in Figure 13.

When the latent manifold envelops the prior manifold, i.e., $\|\mathbf{z}_0^{\boldsymbol{\phi}}\|_2 > \|\mathbf{z}_T^{\boldsymbol{\phi}}\|_2$, the drift term, $-\frac{1}{2}\beta(t)\mathbf{z}_t^{\boldsymbol{\phi}}$, and the vector of $\mathbf{z}_T^{\boldsymbol{\phi}} - \mathbf{z}_0^{\boldsymbol{\phi}}$ aligns towards the origin. On the other hand, if the initial manifold is located inside the prior manifold, i.e., $\|\mathbf{x}_0\|_2 < \|\mathbf{x}_T\|_2$, then the drift term points towards the opposite direction of $\mathbf{x}_T - \mathbf{x}_0$. This leads that the contraction mapping disturbs the particle to move towards $\mathbf{x}_T$, and it is the random perturbation that leads the particle to converge to $\mathbf{x}_T$. In latent trajectory, the contraction mapping driven by the drift term helps the particle moving towards $\mathbf{z}_T^{\boldsymbol{\phi}}$. Therefore, the particle trajectory is more straightforward in the latent trajectory, which moves *outside* of the prior manifold, compared to the data trajectory that lives *inside* of the prior manifold. This clarifies why the sampling-friendly bridge is constructed in INDM.

Figure 14 presents the 2d toy case of the two moons dataset. It illustrates a simple visualization of the flow training. Figure 14 shows that even though the latent manifold is located near the data manifold at the initial phase of training in Figure 14-(a), after the training, the latent manifold is inflated to the outside of the real data in Figure 14-(b). Therefore, the probability flow ODE (deterministic trajectory), after the training, transports the initial mass to the final mass with a nearly linear line in Figure 14-(d), in contrast to the curvy VPSDE trajectory at the initial phase of training in Figure 14-(c). In this example, the flow training puts the latent manifold out of the data manifold, and this helps the robust sampling.

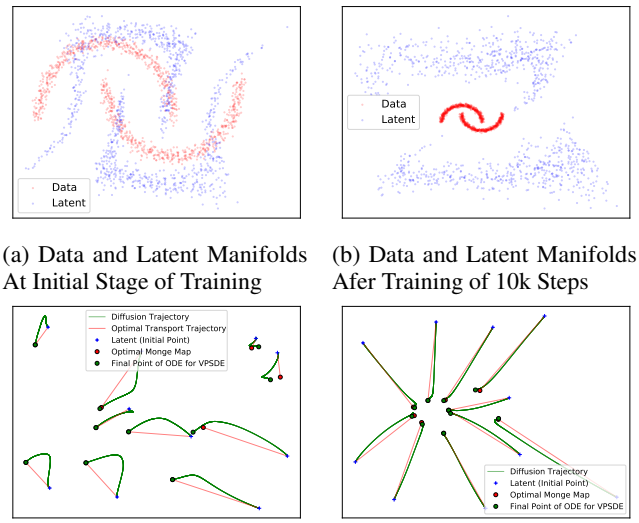

(a) Data and Latent Manifolds At Initial Stage of Training

(b) Data and Latent Manifolds Afer Training of 10k Steps

(c) Diffusion and (optimal) Monge Trajectories At Initial Stage of Training

(d) Diffusion and (optimal) Monge Trajectories After Training of 10k Steps

Figure 14: (a,b) Latent manifold by training iterations (c,d) Diffusion trajectories by training iterations. We use Python Optimal Transport (POT) library [46] to obtain the optimally transported Monge map between 1,000 samples from the latent starting variable and the latent ending variable. We only visualize 10 samples out of 1,000 transport maps for a clear implication. In (c), we train the score network further until converged (with the fixed flow) to visualize accurate diffusion paths.

In addition, Figure 14 illustrates the Monge trajectories between the latent initial distribution and the prior distribution. As theoretically demonstrated in Gaussian and empirically shown in general distribution in Khrulkov and Oseledets [47], the encoder map of VPSDE is nearly optimal transport under the squared Euclidean cost function, where the encoder map is the mapping from the initial point to the final point passed through the probability flow ODE. Figure 14 supports this, and the diffusion trajectory becomes more straight alike to the optimal Monge map after the training.

Figure 15 illustrates the concept of linearized diffusion path. As the flow inflates the latent manifold, the diffusion trajectory becomes more linear, and Figure 7 supports the conceptual illustration of Figure 15 on CIFAR-10.

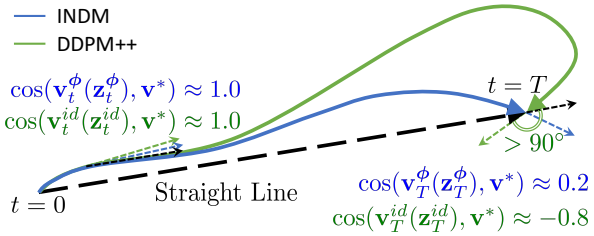

Figure 15: Illustrative Particle Trajectory.

D Related Work

D.1 Latent Score-based Generative Model (LSGM)

The diffusion process on latent space is firstly introduced in LSGM. LSGM transforms the data variable to a latent variable, and estimates the prior distribution with a diffusion model. Suppose $\boldsymbol{\theta}$, $\boldsymbol{\phi}$, and $\boldsymbol{\psi}$ represent for the parameters for the score network, the encoder network, and the decoder network, respectively. Then, LSGM optimizes the loss of

$$\begin{aligned}
D_{KL}(p_r \| p_{\boldsymbol{\theta},\boldsymbol{\psi}}) &\leq D_{KL}\big(p_r(\mathbf{x}_0) q_{\boldsymbol{\phi}}(\mathbf{z}_0|\mathbf{x}_0) \| p_{\boldsymbol{\theta}}(\mathbf{z}_0) p_{\boldsymbol{\psi}}(\mathbf{x}_0|\mathbf{z}_0)\big) \\
&= D_{KL}\big(p_r(\mathbf{x}_0) q_{\boldsymbol{\phi}}(\mathbf{z}_0|\mathbf{x}_0) \| q_{\boldsymbol{\phi}}(\mathbf{z}_0) p_{\boldsymbol{\psi}}(\mathbf{x}_0|\mathbf{z}_0)\big) + D_{KL}\big(q_{\boldsymbol{\phi}}(\mathbf{z}_0) \| p_{\boldsymbol{\theta}}(\mathbf{z}_0)\big) \\
&\leq D_{KL}\big(p_r(\mathbf{x}_0) q_{\boldsymbol{\phi}}(\mathbf{z}_0|\mathbf{x}_0) \| q_{\boldsymbol{\phi}}(\mathbf{z}_0) p_{\boldsymbol{\psi}}(\mathbf{x}_0|\mathbf{z}_0)\big) + D_{KL}\big(\boldsymbol{\mu}_{\boldsymbol{\phi}}(\{\mathbf{z}_t\}_{t=0}^T) \| \boldsymbol{\nu}_{\boldsymbol{\theta}}(\{\mathbf{z}_t\}_{t=0}^T)\big) \\
&= \mathcal{L}_{LSGM}(\boldsymbol{\theta}, \boldsymbol{\phi}, \boldsymbol{\psi})
\end{aligned}$$

where $q_{\boldsymbol{\phi}}(\mathbf{z}_0)$ is the marginal distribution of the encoder posterior, $q_{\boldsymbol{\phi}}(\mathbf{z}_0) = \int p_r(\mathbf{x}_0) q_{\boldsymbol{\phi}}(\mathbf{z}_0|\mathbf{x}_0)\, \mathrm{d}\mathbf{x}_0$.

As well as INDM, LSGM also optimizes the log-likelihood of the model distribution by using a diffusion model in the latent space. Though both INDM and LSGM losses include a denoising score loss on the latent space (which is the KL divergence between path measures on the latent space), $\mathcal{L}_{LSGM}(\boldsymbol{\theta}, \boldsymbol{\phi}, \boldsymbol{\psi})$ is not equivalent to the KL divergence between the forward and generative path measures on the data space, in contrast to INDM with $D_{KL}(\boldsymbol{\mu}_{\boldsymbol{\phi}}(\{\mathbf{x}_t\}_{t=0}^T) \| \boldsymbol{\nu}_{\boldsymbol{\phi},\boldsymbol{\theta}}(\{\mathbf{x}_t\}_{t=0}^T)$ as its loss function. In fact, there is no forward SDE (green path in Figure 3) on the data space in LSGM according to Lemma 3, which is a direct application of the Borsuk-Ulam theorem [48].

Lemma 3 ($\mathbb{R}^n$ **is not homeomorphic to** $\mathbb{R}^m$ [48])**.** *If $n \neq m$, there is no continuous map $E : \mathbb{R}^n \to \mathbb{R}^m$ that has the continuous inverse map $E^{-1} : \mathbb{R}^m \to \mathbb{R}^n$.*

Lemma 3 implies that there is no inverse function of the encoder as long as the latent dimension is different from the data dimension (and the activation function is continuous, such as ReLU). From this, LSGM cannot define a random variable on the data space by $\mathbf{x}_t^{\boldsymbol{\phi}} = E_{\boldsymbol{\phi}}^{-1}(\mathbf{z}_t)$, in contrast to INDM that defines $\mathbf{x}_t^{\boldsymbol{\phi}} = \mathbf{h}_{\boldsymbol{\phi}}^{-1}(\mathbf{z}_t)$. This non-existence of random variables on the data space implies that *the forward diffusion process does not exists as long as the latent dimension differs to the data dimension*.

With the above theoretic dilemma of LSGM, one could build a generative diffusion process on the data space. If $\mathbf{x}_t^{\boldsymbol{\psi},\boldsymbol{\theta}} := D_{\boldsymbol{\psi}}(\mathbf{z}_t^{\boldsymbol{\theta}})$, where $\mathbf{z}_t^{\boldsymbol{\theta}}$ is a generative random variable on the latent space, and $D_{\boldsymbol{\psi}}$ is a decoder map, then we could build a generative diffusion process on the data space through the Ito's formula in the same way as we did in INDM. Inspired by this, one could argue that the forward diffusion could be constructed by $\mathbf{x}_t^{\boldsymbol{\psi}} := D_{\boldsymbol{\psi}}(\mathbf{z}_t)$, where $\mathbf{z}_t$ is a forward random variable on the latent space. This construction enables to construct a forward diffusion process on the latent space, but there are a couple of caveats to this construction.

Table 8: LSGM training fails when using the variance weighting function.

	NLL	NELBO	FID
LSGM (VP, FID)	NaN	NaN	NaN
INDM (VP, FID)	3.23	3.17	2.90

Theoretically, this forward diffusion process starts from the reconstructed variable, $\mathbf{x}_0^{\boldsymbol{\psi}} = D_{\boldsymbol{\psi}}(\mathbf{z}_0) = D_{\boldsymbol{\psi}}(E_{\boldsymbol{\phi}}(\mathbf{x}_0)) = \mathbf{x}_{rec}$, where $\mathbf{x}_0$ and $\mathbf{x}_{rec}$ differs throughout the training procedure. In addition, even if we admit $\{\mathbf{x}_t^{\boldsymbol{\psi}}\}$ as a forward diffusion, $\mathcal{L}_{LSGM}(\boldsymbol{\theta}, \boldsymbol{\phi}, \boldsymbol{\psi})$ cannot be derived as the KL divergence of path measures for the forward diffusion (admittably $\{\mathbf{x}_t^{\boldsymbol{\psi}}\}$, but not true to be precise) and the generative diffusion ($\mathbf{x}_t^{\boldsymbol{\psi},\boldsymbol{\theta}}$) on the data space. Instead, the loss contains the encoder parameters to optimize, and the loss diverges from the KL divergence on the data space. Also, hypothetically, even if the loss is the KL divergence of the forward and generative path measures on the data space, the optimization could be drifted away from the optimal point because the forward diffusion starts from untrained reconstructed variable, $\mathbf{x}_{rec}$, which is not close to the data variable, $\mathbf{x}_0$. This analysis provides a clue to explain the training instability of LSGM as reported in Vahdat et al. [9] and Dockhorn et al. [20], in contrast to INDM that is stable to train in any training configuration. Table 8 shows a fast comparison of LSGM and INDM with variance weighting function, sampled from $t \in \mathcal{U}[0, 1]$. *NaN* indicates experiments that fail due to training instability, see Section 5.2 and Table 6 of Vahdat et al. [9] and Section E.2.7 of Dockhorn et al. [20].

Table 9: Comparison of latent dimension of INDM and LSGM.

Datset	Data Dimension	Latent Dimension of INDM	Latent Dimension of INDM
MNIST	784	784	2,560
CIFAR-10	3,072	3,072	46,080
CelebA-HQ 256	196,608	196,608	819,200

Moreover, Table 9 compares INDM with LSGM in terms of the latent dimension. We compute the latent dimension of LSGM, according to their paper and released checkpoint. Contrary to the dimensional reduction property which is the crux of the auto-encoding structure, LSGM maps data into a latent space of a much higher dimension than the data dimension. LSGM is known to perform well, but having observed 15x higher latent dimension than the data dimension on CIFAR-10, the good performance was not gained for free. On the other hand, INDM always retains the same dimension to the data, while keeping the invertibility.

D.2 Diffusion Normalizing Flow (DiffFlow)

The Girsanov theorem [35] proves that the variational bound is derived by

$$D_{KL}(p_r \| p_{\boldsymbol{\theta}}) \leq \frac{1}{2}\int_0^T g^2(t)\mathbb{E}_{p_r(\mathbf{x}_0)}\mathbb{E}_{p_{0t}(\mathbf{x}_t|\mathbf{x}_0)}\left[\|\mathbf{s}_{\boldsymbol{\theta}}(\mathbf{x}_t,t) - \nabla_{\mathbf{x}_t}\log p_{0t}(\mathbf{x}_t|\mathbf{x}_0)\|_2^2\right]\mathrm{d}t + D_{KL}(p_T\|\pi). \tag{19}$$

When the forward diffusion is given as $\mathrm{d}\mathbf{x}_t = \mathbf{f}_{\boldsymbol{\phi}}(\mathbf{x}_t,t)\,\mathrm{d}t + g(t)\,\mathrm{d}\mathbf{w}_t$, where $\mathbf{f}_{\boldsymbol{\phi}}$ is an explicit parametrization of the drift term by a normalizing flow with parameters $\boldsymbol{\phi}$, then the transition probability, $p_{0t}(\mathbf{x}_t|\mathbf{x}_0)$, becomes intractable. Therefore, optimizing the continuous variational bound is not feasible. One might detour this issue by alternatively optimizing the continuous DDPM++ loss of

$$\int_0^T \tilde{\lambda}(t)\mathbb{E}_{p_r(\mathbf{x}_0)}\mathbb{E}_{\boldsymbol{\epsilon}\sim\mathcal{N}(0,\mathbf{I})}\left[\|\boldsymbol{\epsilon} - \hat{\boldsymbol{\epsilon}}_{\boldsymbol{\theta}}(\mathbf{x}_t,t)\|_2^2\right]\mathrm{d}t, \tag{20}$$

but the denoising score loss of Eq. (19) is not equivalent to the continuous DDPM++ loss of Eq. (20) when the transition probability is no longer a Gaussian distribution.

DiffFlow detours the intractability issue of the continuous loss of Eq. (19) by discretizing the nonlinear SDE in the Euler-Maruyama (EM) fashion [49]. We construct the discrete random variables that approximate the nonlinear SDE by the induction. If $\mathbf{x}_{t_0}^{\boldsymbol{\phi},\mathrm{EM}} := \mathbf{x}_0^{\boldsymbol{\phi}}$ and $\Delta t_i := t_i - t_{i-1}$, where $\{t_i\}_{t=0}^N$ are discretization timesteps with $t_0 = 0$ and $t_N = T$, then the solution of the nonlinear SDE that starts from $\mathbf{x}_{t_{i-1}}^{\boldsymbol{\phi},\mathrm{EM}}$ is

$$\mathbf{x}_{t_i}^{\boldsymbol{\phi}} - \mathbf{x}_{t_{i-1}}^{\boldsymbol{\phi},\mathrm{EM}} = \int_{t_{i-1}}^{t_i}\mathbf{f}_{\boldsymbol{\phi}}(\mathbf{x}_t^{\boldsymbol{\phi}},t)\,\mathrm{d}t + \int_{t_{i-1}}^{t_i} g(t)\,\mathrm{d}\mathbf{w}_t. \tag{21}$$

Here, the integral of the drift term is

$$\begin{aligned}\int_{t_{i-1}}^{t_i}\mathbf{f}_{\boldsymbol{\phi}}(\mathbf{x}_t^{\boldsymbol{\phi}},t)\,\mathrm{d}t &= \int_{t_{i-1}}^{t_i}\mathbf{f}_{\boldsymbol{\phi}}\big(\mathbf{x}_{t_{i-1}}^{\boldsymbol{\phi},\mathrm{EM}} + (\mathbf{x}_t^{\boldsymbol{\phi}} - \mathbf{x}_{t_{i-1}}^{\boldsymbol{\phi},\mathrm{EM}}), t_{i-1} + (t - t_{i-1})\big)\,\mathrm{d}t \\ &= \int_{t_{i-1}}^{t_i}\mathbf{f}_{\boldsymbol{\phi}}(\mathbf{x}_{t_{i-1}}^{\boldsymbol{\phi},\mathrm{EM}}, t_{i-1})\,\mathrm{d}t + O(\Delta t_i^{3/2}) \\ &= \mathbf{f}_{\boldsymbol{\phi}}(\mathbf{x}_{t_{i-1}}^{\boldsymbol{\phi},\mathrm{EM}}, t_{i-1})\Delta t_i + O(\Delta t_i^{3/2}),\end{aligned}$$

and the integral of the volatility term is

$$\int_{t_{i-1}}^{t_i} g(t)\,\mathrm{d}\mathbf{w}_t = g(t_{i-1})(\mathbf{w}_{t_i} - \mathbf{w}_{t_{i-1}}) + O(\Delta t_i^{3/2}) = g(t_{i-1})\boldsymbol{\epsilon}\sqrt{\Delta t_i} + O(\Delta t_i^{3/2}),$$

where $\boldsymbol{\epsilon} \sim \mathcal{N}(0,\mathbf{I})$. Therefore, DiffFlow defines the next discretized random variable, $\mathbf{x}_{t_i}^{\boldsymbol{\phi},\mathrm{EM}}$, to be

$$\mathbf{x}_{t_i}^{\boldsymbol{\phi}} = \mathbf{x}_{t_{i-1}}^{\boldsymbol{\phi},\mathrm{EM}} + \mathbf{f}_{\boldsymbol{\phi}}(\mathbf{x}_{t_{i-1}}^{\boldsymbol{\phi},\mathrm{EM}}, t_{i-1})\Delta t_i + g(t_{i-1})\boldsymbol{\epsilon}\sqrt{\Delta t_i} + O(\Delta t_i^{2/3})$$

$$
\begin{aligned}
&\approx \mathbf{x}_{t_{i-1}}^{\phi,\text{EM}} + \mathbf{f}_{\phi}(\mathbf{x}_{t_{i-1}}^{\phi,\text{EM}}, t_{i-1})\Delta t_i + g(t_{i-1})\boldsymbol{\epsilon}\sqrt{\Delta t_i} \\
&= \mathbf{x}_{t_i}^{\phi,\text{EM}},
\end{aligned}
$$

and this Euler-Maruyama random variable $\mathbf{x}_{t_i}^{\phi,\text{EM}}$ follows a Gaussian distribution of mean $\mathbf{x}_{t_{i-1}}^{\phi,\text{EM}} + \mathbf{f}_{\phi}(\mathbf{x}_{t_{i-1}}^{\phi,\text{EM}}, t_{i-1})\Delta t_i$ and variance $g^2(t_{i-1})\Delta t_i$. Note that this discretization approximates the nonlinear SDE with a finite Markov chain of $\{\mathbf{x}_{t_i}^{\text{EM}}\}_{i=0}^{N}$.

DiffFlow constructs the generative process as

$$
\mathbf{x}_{t_{i-1}}^{\boldsymbol{\theta}} = \mathbf{x}_{t_i}^{\boldsymbol{\theta}} - \left[\mathbf{f}_{\phi}(\mathbf{x}_{t_i}^{\phi}, t_i) - g^2(t_i)\mathbf{s}_{\boldsymbol{\theta}}(\mathbf{x}_{t_i}^{\phi}, t_i)\right]\Delta t_i + g(t_i)\boldsymbol{\epsilon}\sqrt{\Delta t_i}.
$$

Then, from the Jensen's inequality, the discrete DDPM loss satisfies

$$
D_{KL}(p_r \| p_{\phi,\boldsymbol{\theta}}) \leq \sum_{i=1}^{N-1} \mathbb{E}_{p_r(\mathbf{x}_{t_0}^{\text{EM}})} \mathbb{E}_{p_{\phi}(\mathbf{x}_{t_i}^{\text{EM}}, \mathbf{x}_{t_{i-1}}^{\text{EM}} | \mathbf{x}_{t_0}^{\text{EM}})} \left[D_{KL}(p_{\phi}(\mathbf{x}_{t_{i-1}}^{\text{EM}} | \mathbf{x}_{t_i}^{\text{EM}}, \mathbf{x}_{t_0}^{\text{EM}}) \| p_{\boldsymbol{\theta}}(\mathbf{x}_{t_{i-1}}^{\text{EM}} | \mathbf{x}_{t_i}^{\text{EM}})) \right]. \tag{22}
$$

While the true inference distribution on the continuous variables, $p_{\phi}(\mathbf{x}_{t_{i-1}} | \mathbf{x}_{t_i}, \mathbf{x}_{t_0})$, is not a Gaussian distribution due to terms related to $O(\Delta t_i^{3/2})$, the inference distribution on the *discretized* variables, $p_{\phi}(\mathbf{x}_{t_{i-1}}^{\text{EM}} | \mathbf{x}_{t_i}^{\text{EM}}, \mathbf{x}_{t_0}^{\text{EM}})$, becomes a Gaussian distribution by the Euler-Maruyama-style discretization. Therefore, Eq. (22) reduces to a tractable loss that does not need to compute the transition probability:

$$
\begin{aligned}
D_{KL}(p_r \| p_{\phi,\boldsymbol{\theta}}) &\leq \sum_{i=1}^{N-1} \mathbb{E}_{p_r(\mathbf{x}_{t_0}^{\text{EM}})} \mathbb{E}_{p_{\phi}(\mathbf{x}_{t_i}^{\text{EM}}, \mathbf{x}_{t_{i-1}}^{\text{EM}} | \mathbf{x}_{t_0}^{\text{EM}})} \left[D_{KL}(p_{\phi}(\mathbf{x}_{t_{i-1}}^{\text{EM}} | \mathbf{x}_{t_i}^{\text{EM}}, \mathbf{x}_{t_0}^{\text{EM}}) \| p_{\boldsymbol{\theta}}(\mathbf{x}_{t_{i-1}}^{\text{EM}} | \mathbf{x}_{t_i}^{\text{EM}})) \right] \\
&= \frac{1}{2} \sum_{i=1}^{N-1} \mathbb{E}_{p_r(\mathbf{x}_{t_0}^{\text{EM}})} \mathbb{E}_{p_{\phi}(\mathbf{x}_{t_i}^{\text{EM}}, \mathbf{x}_{t_{i-1}}^{\text{EM}} | \mathbf{x}_{t_0}^{\text{EM}})} \left[\frac{1}{g^2(t_i)\Delta t_i} \Big\| \mathbf{x}_{t_{i-1}}^{\text{EM}} - \mathbf{x}_{t_i}^{\text{EM}} \right. \\
&\qquad \left. + \left[\mathbf{f}_{\phi}(\mathbf{x}_{t_i}^{\text{EM}}, t_i) - g^2(t_i)\mathbf{s}_{\boldsymbol{\theta}}(\mathbf{x}_{t_i}^{\text{EM}}, t_i)\right]\Delta t_i \Big\|_2^2 \right] \\
&= \mathcal{L}_{\text{DiffFlow}}(\boldsymbol{\phi}, \boldsymbol{\theta})
\end{aligned} \tag{23}
$$

While Eq. (23) does not need to compute the transition probability, another issue of optimizing the variational bound originates from the expectation of $\mathbb{E}_{p_{\phi}(\mathbf{x}_{t_i}^{\text{EM}}, \mathbf{x}_{t_{i-1}}^{\text{EM}} | \mathbf{x}_{t_0}^{EM})}$. The empirical Monte-Carlo estimation is too expensive because a realization of $\mathbf{x}_{t_i}^{\text{EM}}$ needs i number of flow evaluations. In total, summing i over $i = 1$ to N requires $O(N^2)$ flow evaluations to estimate the discrete variational bound of Eq. (23). Therefore, DiffFlow exchanges the summation and the expectation to reduce the number of flow evaluations by

$$
\begin{aligned}
\mathcal{L}_{\text{DiffFlow}}(\boldsymbol{\phi}, \boldsymbol{\theta}) = \frac{1}{2} \mathbb{E}_{\{\mathbf{x}_{t_i}\}_{i=0}^{N-1} \sim p_{\phi}(\mathbf{x}_{t_0}, \ldots, \mathbf{x}_{t_{N-1}})} \Bigg[\sum_{i=1}^{N-1} \frac{1}{g^2(t_i)\Delta t_i} \Big\| \mathbf{x}_{t_{i-1}} - \mathbf{x}_{t_i} \\
+ \left[\mathbf{f}_{\phi}(\mathbf{x}_{t_i}, t_i) - g^2(t_i)\mathbf{s}_{\boldsymbol{\theta}}(\mathbf{x}_{t_i}, t_i)\right]\Delta t_i \Big\|_2^2 \Bigg].
\end{aligned} \tag{24}
$$

This reformulated Eq. (24) estimates $\mathcal{L}_{\text{DiffFlow}}$ with a single sample path from the Markov chain of $\{\mathbf{x}_{t_i}^{\text{EM}}\}_{t=1}^{N}$, so it requires $O(N)$ flow evaluations to estimate $\mathcal{L}_{\text{DiffFlow}}(\boldsymbol{\phi}, \boldsymbol{\theta})$. Therefore, DiffFlow takes $O(N)$ computational complexity in total for every optimization step.

There are five differences between DiffFlow and INDM. Basically, these differences arise from the different usage of the flow transformation between DiffFlow and INDM. First, INDM enables to train the continuous diffusion model without the sacrifice on training time, while DiffFlow is limited on the discrete diffusion model at the expense of slower training time. DiffFlow approximates the forward nonlinear SDE with a finite Markov chain. Suppose $\mathbf{x}_t^{\text{EM}}$ to be the continuous-time random variable defined by $\mathbf{x}_t^{\text{EM}} = \mathbf{x}_{t_{i-1}}^{\text{EM}} + \mathbf{f}_{\phi}(\mathbf{x}_{t_{i-1}}^{\text{EM}}, t_{i-1})(t - t_{i-1}) + g(t_{i-1})\boldsymbol{\epsilon}\sqrt{t - t_{i-1}}$ on time range of $t \in [t_{i-1}, t_i)$, then we have

$$
\mathbb{E}\left[\|\mathbf{x}_t - \mathbf{x}_t^{\text{EM}}\|_2\right] \leq C\sqrt{\Delta t_i}, \tag{25}
$$

where $C = C(T, K, \mathbb{E}[\|\mathbf{x}_0\|_2^2]) \geq O(K^2)$ is a constant with K being a Lipschits constant of

$$\|\mathbf{f}_{\boldsymbol{\phi}}(\mathbf{x}, t) - \mathbf{f}_{\boldsymbol{\phi}}(\mathbf{y}, t)\|_2 \leq K\|\mathbf{x} - \mathbf{y}\|_2$$

and

$$\|\mathbf{f}_{\boldsymbol{\phi}}(\mathbf{x}, t)\|_2 + |g(t)| \leq K(1 + \|\mathbf{x}\|_2)$$

for all $\mathbf{x}, \mathbf{y} \in \mathbb{R}^d$ and $t \in [t_{i-1}, t_i)$. Having that Δt_i is fixed a-priori, the upper bound in Inequality (25) could be arbitrarily large becuase it depends on K that represents the magnitude of nonlinearity of $\mathbf{f}_{\boldsymbol{\phi}}$. For instance, if $\mathbf{f}_{\boldsymbol{\phi}}(\mathbf{x}_t, t) = \mathbf{x}_t^2$, then there does not exist any $K > 0$ that satisfies above Lipschitz bounds. In such case, it is unable to guarantee the tightness of the discretized Markov chain to the continuous nonlinear SDE in the classical sense. Therefore, the Euler-Maruyama approximation of the nonlinear SDE should take N as many as possible if we want to regard the finite Markov chain as a discretized nonlinear SDE, which would eventually increase the training, evaluation, and sampling time.

Second, the computational complexity of INDM is $O(1)$ because the flow is evaluated only once at every optimization step. This is because the INDM loss is simply an addition of the flow loss and the linear diffusion loss. The training time of DiffFlow will be prohibitive as N increases.

Third, our INDM jointly models both drift and volatility terms nonlinearly, whereas DiffFlow nonlinearly models only the drift term. As illustrated in Figure 1 and 2-(c) in the main paper, nonlinearizing the volatility term brings a different diffusion to the overall process, compared to a diffusion that arises from a nonlinear drift. In particular, Figure 2-(c) depicts that the data-dependent volatility term yields an ellipsoidal covariance in the noise distribution, which was assumed to have a fixed diagonal covariance in previous research, as illustrated in Figure 6. In INDM, this covariance becomes the subject of matter to optimize.

DiffFlow, as its current form, cannot impose nonlinearity to the volatility term because the discretized Markov chain is not a Gaussian distribution, anymore. To clarify, suppose a SDE of $\mathrm{d}\mathbf{x}_t = \mathbf{f}_{\boldsymbol{\phi}}(\mathbf{x}_t, t)\,\mathrm{d}t + \mathbf{G}_{\boldsymbol{\phi}}(\mathbf{x}_t, t)\,\mathrm{d}\mathbf{w}_t$ (think of the green path of Figure 3 in the main paper) starts from a random variable $\mathbf{x}_{t_{i-1}}^{\text{EM}}$. The next discrete random variable of the Euler-Maruyama discretization is the approximate solution of this SDE at $t = t_i$, so let us approximate the right-hand-side of Eq. (26):

$$\mathbf{x}_{t_i} - \mathbf{x}_{t_{i-1}}^{\text{EM}} = \int_{t_{i-1}}^{t_i} \mathbf{f}_{\boldsymbol{\phi}}(\mathbf{x}_t, t)\,\mathrm{d}t + \int_{t_{i-1}}^{t_i} \mathbf{G}_{\boldsymbol{\phi}}(\mathbf{x}_t, t)\,\mathrm{d}\mathbf{w}_t. \tag{26}$$

The integral of the volatility term is

$$\int_{t_{i-1}}^{t_i} \mathbf{G}_{\boldsymbol{\phi}}(\mathbf{x}_t, t)\,\mathrm{d}\mathbf{w}_t = \int_{t_{i-1}}^{t_i} \mathbf{G}_{\boldsymbol{\phi}}\big(\mathbf{x}_{t_{i-1}}^{\text{EM}} + (\mathbf{x}_t - \mathbf{x}_{t_{i-1}}^{\text{EM}}), t_{i-1} + (t - t_{i-1})\big)\,\mathrm{d}\mathbf{w}_t$$

and since $\mathbf{x}_t - \mathbf{x}_{t_{i-1}}^{\text{EM}} = \mathbf{G}_{\boldsymbol{\phi}}(\mathbf{x}_{t_{i-1}}^{\text{EM}}, t_{i-1})(\mathbf{w}_t - \mathbf{w}_{t_{i-1}}) + O(\Delta t_i)$, we get

$$\begin{aligned}
&\int_{t_{i-1}}^{t_i} \mathbf{G}_{\boldsymbol{\phi}}(\mathbf{x}_t, t)\,\mathrm{d}\mathbf{w}_t \\
&\quad= \mathbf{G}_{\boldsymbol{\phi}}(\mathbf{x}_{t_{i-1}}^{\text{EM}}, t_{i-1})(\mathbf{w}_{t_i} - \mathbf{w}_{t_{i-1}}) \\
&\qquad+ \mathbf{G}_{\boldsymbol{\phi}}(\mathbf{x}_{t_{i-1}}^{\text{EM}}, t_{i-1}) \frac{\partial \mathbf{G}_{\boldsymbol{\phi}}(\mathbf{x}_t, t)}{\partial \mathbf{x}_t}\Big|_{\mathbf{x}_{t_{i-1}}^{\text{EM}}} \int_{t_{i-1}}^{t_i} \mathbf{w}_t - \mathbf{w}_{t_{i-1}}\,\mathrm{d}\mathbf{w}_t + O(\Delta t_i^2) \\
&\quad= \mathbf{G}_{\boldsymbol{\phi}}(\mathbf{x}_{t_{i-1}}^{\text{EM}}, t_{i-1})(\mathbf{w}_{t_i} - \mathbf{w}_{t_{i-1}}) \\
&\qquad+ \mathbf{G}_{\boldsymbol{\phi}}(\mathbf{x}_{t_{i-1}}^{\text{EM}}, t_{i-1}) \nabla_{\mathbf{x}_{t_{i-1}}^{\text{EM}}} \mathbf{G}_{\boldsymbol{\phi}}(\mathbf{x}_{t_{i-1}}^{\text{EM}}, t_{i-1}) \frac{1}{2}\big((\mathbf{w}_{t_i} - \mathbf{w}_{t_{i-1}})^2 - \Delta t_i\big) + O(\Delta t_i^2) \\
&\quad= \mathbf{G}_{\boldsymbol{\phi}}(\mathbf{x}_{t_{i-1}}^{\text{EM}}, t_{i-1}) \boldsymbol{\epsilon} \sqrt{\Delta t_i} \\
&\qquad+ \frac{1}{2} \mathbf{G}_{\boldsymbol{\phi}}(\mathbf{x}_{t_{i-1}}^{\text{EM}}, t_{i-1}) \nabla_{\mathbf{x}_{t_{i-1}}^{\text{EM}}} \mathbf{G}_{\boldsymbol{\phi}}(\mathbf{x}_{t_{i-1}}^{\text{EM}}, t_{i-1}) \big(\boldsymbol{\epsilon}^2 - 1\big) \Delta t_i + O(\Delta t_i^2),
\end{aligned}$$

where $\boldsymbol{\epsilon} \sim \mathcal{N}(0, \mathbf{I})$ and $\int_{t_{i-1}}^{t_i} \mathbf{w}_t - \mathbf{w}_{t_{i-1}}\,\mathrm{d}\mathbf{w}_t = \int_{t_{i-1}}^{t_i} \mathbf{w}_t\,\mathrm{d}\mathbf{w}_t - \mathbf{w}_{t_{i-1}}(\mathbf{w}_{t_i} - \mathbf{w}_{t_{i-1}}) = \int_{t_{i-1}}^{t_i} \frac{1}{2}\,\mathrm{d}(\mathbf{w}_t^2) - \int_{t_{i-1}}^{t_i} \frac{1}{2}\,\mathrm{d}t - \mathbf{w}_{t_{i-1}}(\mathbf{w}_{t_i} - \mathbf{w}_{t_{i-1}}) = \frac{1}{2}(\mathbf{w}_{t_i}^2 - \mathbf{w}_{t_{i-1}}^2 - \Delta t_i) - \mathbf{w}_{t_{i-1}}(\mathbf{w}_{t_i} - \mathbf{w}_{t_{i-1}}) =$

$\frac{1}{2}\big((\mathbf{w}_{t_i} - \mathbf{w}_{t_{i-1}})^2 - \Delta t_i\big)$ is according to the Ito's formula [17]. As $\mathbf{G}_{\boldsymbol{\phi}}(\mathbf{x}_t, t)$ now depends on $\mathbf{x}_t$, the term including $(\boldsymbol{\epsilon}^2 - 1)$ does not vanish. Therefore, $\mathbf{x}_{t_i}^{\text{EM}}$ is approximated by

$$\begin{aligned}
\mathbf{x}_{t_i} =& \mathbf{x}_{t_{i-1}}^{\text{EM}} + \mathbf{f}_{\boldsymbol{\phi}}(\mathbf{x}_{t_{i-1}}^{\text{EM}}, t_{i-1})\Delta t_i + \mathbf{G}_{\boldsymbol{\phi}}(\mathbf{x}_{t_{i-1}}^{\text{EM}}, t_{i-1})\boldsymbol{\epsilon}\sqrt{\Delta t_i} \\
&+ \frac{1}{2}\mathbf{G}_{\boldsymbol{\phi}}(\mathbf{x}_{t_{i-1}}^{\text{EM}}, t_{i-1})\nabla_{\mathbf{x}_{t_{i-1}}^{\text{EM}}}\mathbf{G}_{\boldsymbol{\phi}}(\mathbf{x}_{t_{i-1}}^{\text{EM}}, t_{i-1})\big(\boldsymbol{\epsilon}^2 - 1\big)\Delta t_i + O(\Delta t_i^{3/2}) \\
\approx& \mathbf{x}_{t_{i-1}}^{\text{EM}} + \mathbf{f}_{\boldsymbol{\phi}}(\mathbf{x}_{t_{i-1}}^{\text{EM}}, t_{i-1})\Delta t_i + \mathbf{G}(\mathbf{x}_{t_{i-1}}^{\text{EM}}, t_{i-1})\boldsymbol{\epsilon}\sqrt{\Delta t_i} \\
&+ \frac{1}{2}\mathbf{G}_{\boldsymbol{\phi}}(\mathbf{x}_{t_{i-1}}^{\text{EM}}, t_{i-1})\nabla_{\mathbf{x}_{t_{i-1}}^{\text{EM}}}\mathbf{G}_{\boldsymbol{\phi}}(\mathbf{x}_{t_{i-1}}^{\text{EM}}, t_{i-1})\big(\boldsymbol{\epsilon}^2 - 1\big)\Delta t_i \\
:=& \mathbf{x}_{t_i}^{\text{EM}}.
\end{aligned} \tag{27}$$

The order of the term $\frac{1}{2}\mathbf{G}_{\boldsymbol{\phi}}(\mathbf{x}_{t_{i-1}}^{\text{EM}}, t_{i-1})\nabla_{\mathbf{x}_{t_{i-1}}^{\text{EM}}}\mathbf{G}_{\boldsymbol{\phi}}(\mathbf{x}_{t_{i-1}}^{\text{EM}}, t_{i-1})\big(\boldsymbol{\epsilon}^2 - 1\big)\Delta t_i$ is $O(\Delta t_i)$, which is the same order of the term $\mathbf{f}_{\boldsymbol{\phi}}(\mathbf{x}_{t_{i-1}}^{\text{EM}}, t_{i-1})\Delta t_i$. Thus, this last term including $\boldsymbol{\epsilon}^2$ cannot be ignored in the approximation.

With this approximation, the discretized random variable, $\mathbf{x}_{t_i}^{\text{EM}}$, includes a term of $\boldsymbol{\epsilon}^2$, which is the square of the Brownian motion that does not follow a Gaussian distribution. Therefore, the variational bound of Eq. (22) is no longer reduced to a tractable loss, such as Eq. (23), and as a consequence, Eq. (22) is not optimizable even though the nonlinear SDE is discretized. Therefore, we have to ignore the last term, $\frac{1}{2}\mathbf{G}_{\boldsymbol{\phi}}\nabla\mathbf{G}_{\boldsymbol{\phi}}(\boldsymbol{\epsilon}^2 - 1)\Delta t_i$, to tractably optimize the variational bound, but such ingorance equals to the approximation of DiffFlow, which would incur a large approximation error if $\mathbf{G}_{\boldsymbol{\phi}}$ nonlinearly depends on $\mathbf{x}_t$. This leads DiffFlow limited on $\mathbf{G}_{\boldsymbol{\phi}}(\mathbf{x}_t, t) = g_{\boldsymbol{\phi}}(t)$, at its maximal capacity. This is contrastive to the result of INDM illustrated in Figure 6.

Fourth, as the generative process of DiffFlow starts from an easy-to-sample prior distribution, the flexibility of $\mathbf{f}_{\boldsymbol{\phi}}$ is severely restricted to constrain $p_T^{\boldsymbol{\phi}}(\mathbf{x}_T^{\boldsymbol{\phi}}) \approx \pi(\mathbf{x}_T^{\boldsymbol{\phi}})$. The feasible space of nonlinear $\mathbf{f}_{\boldsymbol{\phi}}$ that satisfies this constraint does not seem to be derived explicitly. Contrastive to DiffFlow, the data diffusion does not have to end at π in INDM. Instead, INDM assumes the linear diffusion on the latent variable, so the ending variable on the latent space, $\mathbf{z}_T^{\boldsymbol{\phi}}$, is already close to the prior distribution. Therefore, the space of admissible nonlinear drift in INDM, which is *explicitly* desribed in Eq. (10), should be larger than the space of DiffFlow. A lesson from this is that the explicit parametrization seems to be intuitive, but underneath the surface, not many properties could be uncovered explicitly, whereas the implicit parametrization using the invertible transformation enjoys its explicit derivations that enable to analyze concrete properties.

Fifth, DiffFlow estimates its loss of Eq. (24) using a single (or multiple) path to update the parameters with the reparametrization trick [50]. On the other hand, the discretized diffusion model estimates its loss with Eq. (23), where the sampling from $p_{0t}(\mathbf{x}_t|\mathbf{x}_0)$ is inexpensive because the transition probability is a Gaussian distribution. Therefore, the losses of Eqs. (24) and (23) coincide in the expectation sense, but they are estimated differently between DiffFlow and diffusion models with analytic transition probabilities. Taking $\frac{1}{g^2(t_i)\Delta t_i}\big\|\mathbf{x}_{t_{i-1}}^{\text{EM}} - \mathbf{x}_{t_i}^{\text{EM}} + \big[\mathbf{f}_{\boldsymbol{\phi}}(\mathbf{x}_{t_i}^{\text{EM}}, t_i) - g^2(t_i)\mathbf{s}_{\boldsymbol{\theta}}(\mathbf{x}_{t_i}^{\text{EM}}, t_i)\big]\Delta t_i\big\|_2^2$ as a random variable X_i, Eq. (23) is reduced to $\frac{1}{2}\sum\mathbb{E}[X_i]$, and Eq. (24) is reduced to $\frac{1}{2}\mathbb{E}_{\text{sample-path}}[\sum X_i]$. Therefore, the variance of the Monte-Carlo estimation of Eq. (23) becomes $\frac{1}{2}\sum\text{Var}(X_i)$, whereas the variance of the Monte-Carlo estimation of Eq. (24) becomes

$$\frac{1}{2}\text{Var}\Big(\sum X_i\Big) = \frac{1}{2}\Big[\sum\text{Var}(X_i) + 2\sum\text{Cov}(X_i, X_j)\Big],$$

where $\text{Cov}(X_i, X_j)$ represents the covariance of two random variables X_i and X_j. Table 10 represents the ratio of these two variances,

$$\text{Ratio} := \frac{\text{Var}(\sum X_i)}{\sum\text{Var}(X_i)} = \frac{\sum\text{Var}(X_i) + 2\sum\text{Cov}(X_i, X_j)}{\sum\text{Var}(X_i)} = 1 + 2\frac{\sum\text{Cov}(X_i, X_j)}{\sum\text{Var}(X_i)},$$

and it shows that the DiffFlow loss has prohibitively large variance as N increases, compared to the INDM loss, which computes its Monte-Carlo estimation in spirit of Eq. (23) with $N = \infty$.

Note that throughout our argument, we have omitted the prior and reconstruction terms on the variational bounds in this section.

Table 10: The variance ratio between the variances of the analytic transition probability-based estimation of Eq. (23) and the sample-based estimation of Eq. (24).

	Number of Random Variables (N)				
	1	10	100	1000	10000
Estimation Variance Ratio	1.00	1.02	2.08	16.68	76.08

D.3 Schrödinger Bridge Problem (SBP)

Schrödinger Bridge Problem (SBP) [14–16] has recently been highlighted in machine learning for its connection to the score-based diffusion model. Schrödinger Bridge Problem is a bi-constrained problem of

$$\min_{\boldsymbol{\rho}\in\mathcal{P}(p_r,\pi)} D_{KL}(\boldsymbol{\rho}\|\boldsymbol{\mu}),$$

where $\mathcal{P}(p_r,\pi)$ is a family of path measure with bi-constraints of p_r and π as its marginal distributions at $t=0$ and $t=T$, respectively, and $\boldsymbol{\mu}$ is a reference path measure that is governed by

$$\mathrm{d}\mathbf{x}_t = \mathbf{f}(\mathbf{x}_t,t)\,\mathrm{d}t + g(t)\,\mathrm{d}\mathbf{w}_t, \quad \mathbf{x}_0\sim p_r. \tag{28}$$

As the KL divergence becomes infinite if the diffusion coefficient of $\boldsymbol{\rho}$ is not equal to $g(t)$ (because quadratic variations of $\boldsymbol{\mu}$ and $\boldsymbol{\rho}$ becomes different), SBP is equivalently formulated as

$$\min_{\boldsymbol{\rho}\in\mathcal{P}(p_r,\pi)} D_{KL}(\boldsymbol{\rho}\|\boldsymbol{\mu}) = \min_{\boldsymbol{\rho}_{\mathbf{v}}\in\mathcal{P}(p_r,\pi)} D_{KL}(\boldsymbol{\rho}_{\mathbf{v}}\|\boldsymbol{\mu}),$$

where the path measure $\boldsymbol{\rho}_{\mathbf{v}}\in\mathcal{P}(p_r,\pi)$ follows the SDE of

$$\mathrm{d}\mathbf{x}_t = \left[\mathbf{f}(\mathbf{x}_t,t) + g^2(t)\mathbf{v}(\mathbf{x}_t,t)\right]\mathrm{d}t + g(t)\mathbf{w}_t. \tag{29}$$

From the Girsanov theorem and the Martingale property [51], we have

$$D_{KL}(\boldsymbol{\rho}_{\mathbf{v}}\|\boldsymbol{\mu}) = \frac{1}{2}\int_0^T g^2(t)\mathbb{E}_{\boldsymbol{\rho}_{\mathbf{v}}}[\|\mathbf{v}(\mathbf{x}_t,t)\|_2^2]\,\mathrm{d}t + D_{KL}(\pi\|p_T),$$

where p_T is the marginal distribution of $\boldsymbol{\mu}$ at $t=T$. If $\mathcal{V}(p_r,\pi)$ is the space of all vector fields $\mathbf{v}$ of which forward SDE with Eq. (29) satisfies the boundary conditions, then SBP is equivalent to

$$\min_{\boldsymbol{\nu}\in\mathcal{P}(p_r,\pi)} D_{KL}(\boldsymbol{\nu}\|\boldsymbol{\mu}) = \min_{\mathbf{v}\in\mathcal{V}(p_r,\pi)} \frac{1}{2}\int_0^T g^2(t)\mathbb{E}_{\boldsymbol{\rho}_{\mathbf{v}}}[\|\mathbf{v}(\mathbf{x}_t,t)\|_2^2]\,\mathrm{d}t, \tag{30}$$

where $\boldsymbol{\rho}_{\mathbf{v}}$ is the associated path measure of Eq. (29). Eq. (30) interprets the solution of SBP as the least energy (weighted by g^2) of the auxiliary vector field ($\mathbf{v}$) among admissible space of vector fields ($\mathcal{V}(p_r,\pi)$). Hence, if $\boldsymbol{\mu}\in\mathcal{P}(p_r,\pi)$, then the trivial vector field, $\mathbf{v}\equiv 0$, is the solution of SBP. When the reference SDE of Eq. (28) is one of the family of linear SDEs, such as VESDE or VPSDE, then $\boldsymbol{\mu}\notin\mathcal{P}(p_r,\pi)$, so the trivial vector field is not the solution of SBP, anymore. Instead, $\boldsymbol{\mu}$'s ending variable is close enough to π (e.g., $D_{KL}(p_T\|\pi)\approx 10^{-5}$ in bpd scale [8]), so the closest path measure in $\mathcal{V}(p_r,\pi)$ to $\boldsymbol{\mu}$ is nearly identical to a trivial vector field, $\mathbf{v}^*\approx 0$, and the nonlinearity of SBP is limited.

Chen et al. [16] connects the optimal solution of SBP with PDEs. At the optimal point, if we denote by $\boldsymbol{\rho}^* = \arg\min_{\boldsymbol{\rho}\in\mathcal{P}(p_r,\pi)} D_{KL}(\boldsymbol{\rho}\|\boldsymbol{\mu})$, then this *optimal* diffusion process follows a forward diffusion SDE [16] of

$$\mathrm{d}\mathbf{x}_t = \left[\mathbf{f}(\mathbf{x}_t,t) + g^2(t)\nabla_{\mathbf{x}_t}\log\Psi(\mathbf{x}_t,t)\right]\mathrm{d}t + g(t)\,\mathrm{d}\mathbf{w}_t, \quad \mathbf{x}_0\sim p_r,$$

with the corresponding reverse diffusion as

$$\mathrm{d}\mathbf{x}_t = \left[\mathbf{f}(\mathbf{x}_t,t) - g^2(t)\nabla_{\mathbf{x}_t}\log\hat{\Psi}(\mathbf{x}_t,t)\right]\mathrm{d}\bar{t} + g(t)\,\mathrm{d}\bar{\mathbf{w}}_t, \quad \mathbf{x}_T\sim\pi,$$

where $\Psi(\mathbf{x}_t,t)$ and $\hat{\Psi}(\mathbf{x}_t,t)$ are the solutions of a system of PDEs [21]:

$$\begin{aligned}\frac{\partial\Psi}{\partial t} &= -\nabla_{\mathbf{x}_t}\Psi^T\mathbf{f} - \frac{1}{2}\mathrm{tr}(g^2\nabla^2_{\mathbf{x}_t}\Psi)\\ \frac{\partial\hat{\Psi}}{\partial t} &= -\mathrm{div}(\hat{\Psi}\mathbf{f}) + \frac{1}{2}\mathrm{tr}(g^2\nabla^2_{\mathbf{x}_t}\hat{\Psi}),\end{aligned} \tag{31}$$

such that $\Psi(\mathbf{x}_0, 0)\hat{\Psi}(\mathbf{x}_0, 0) = p_r(\mathbf{x}_0)$ and $\Psi(\mathbf{x}_T, T)\hat{\Psi}(\mathbf{x}_T, T) = \pi(\mathbf{x}_T)$. With Ψ and $\hat{\Psi}$, the forward diffusion SDE ends exactly at π, and the corresponding reverse SDE ends at p_r. Therefore, SBP is equivalent to solve the system of PDEs given by Eq. (31).

Chen et al. [16] solves the system of coupled PDEs with Eq. (31) using a theory of forward-backward SDEs, which requires a deep understanding of PDE theory. SB-FBSDE [16] uses the fact that the solution $(\Psi, \hat{\Psi})$ of Hopf-Cole transform in Eq. (31) is derived from the solution of the forward-backward SDEs of

$$\begin{cases} \mathrm{d}\mathbf{x}_t = \left[\mathbf{f}(\mathbf{x}_t, t) + g(t)\mathbf{z}_t(\mathbf{x}_t, t)\right] \mathrm{d}t + g(t)\,\mathrm{d}\mathbf{w}_t \\ \mathrm{d}\mathbf{y}_t = \frac{1}{2}(\mathbf{z}_t^T \mathbf{z}_t)(\mathbf{x}_t, t)\,\mathrm{d}t + \mathbf{z}_t^T(\mathbf{x}_t, t)\,\mathrm{d}\mathbf{w}_t \\ \mathrm{d}\hat{\mathbf{y}}_t = \left[\frac{1}{2}(\hat{\mathbf{z}}_t^T \hat{\mathbf{z}}_t)(\mathbf{x}_t, t) + \mathrm{div}\big(g(t)\hat{\mathbf{z}}_t(\mathbf{x}_t, t) - \mathbf{f}(\mathbf{x}_t, t)\big) + (\hat{\mathbf{z}}_t^T \mathbf{z}_t)(\mathbf{x}_t, t)\right] \mathrm{d}t + \hat{\mathbf{z}}_t^T(\mathbf{x}_t, t)\,\mathrm{d}\mathbf{w}_t, \end{cases} \tag{32}$$

where the boundary conditions are given by $\mathbf{x}(0) = \mathbf{x}_0$ and $\mathbf{y}_T + \hat{\mathbf{y}}_T = \log \pi(\mathbf{x}_T)$. The solution of the above system of forward-backward SDEs satisfies $\mathbf{z}_t(\mathbf{x}_t, t) = g(t)\nabla \log \Psi(\mathbf{x}_t, t)$ and $\hat{\mathbf{z}}_t(\mathbf{x}_t, t) = g(t)\nabla \log \hat{\Psi}(\mathbf{x}_t, t)$, where $(\Psi, \hat{\Psi})$ is the solution of Eq. (31). SB-FBSDE parametrizes $(\mathbf{z}_t, \hat{\mathbf{z}}_t)$ as $\boldsymbol{\theta}$ and $\boldsymbol{\phi}$, and it estimates the solution $(\mathbf{z}_t, \hat{\mathbf{z}}_t)$ of Eq. (32) from MLE training of the log-likelihood $\log p_{\boldsymbol{\phi},\boldsymbol{\theta}}(\mathbf{x}_0)$.

Other than the PDE-driven approach [16], SBP has been traditionally solved via Iterative Proportional Fitting (IPF) [52]. Concretely, suppose

$$\mathrm{d}\mathbf{x}_t^{\boldsymbol{\phi}} = \left[\mathbf{f}(\mathbf{x}_t^{\boldsymbol{\phi}}, t) + g^2(t)\mathbf{s}_{\boldsymbol{\phi}}(\mathbf{x}_t^{\boldsymbol{\phi}}, t)\right] \mathrm{d}t + g(t)\,\mathrm{d}\mathbf{w}_t, \quad \mathbf{x}_0^{\boldsymbol{\phi}} \sim p_r, \tag{33}$$

is a forward diffusion with a parametrized vector field of $\mathbf{s}_{\boldsymbol{\phi}}$, and

$$\mathrm{d}\mathbf{x}_t^{\boldsymbol{\theta}} = \left[\mathbf{f}(\mathbf{x}_t^{\boldsymbol{\theta}}, t) - g^2(t)\mathbf{s}_{\boldsymbol{\theta}}(\mathbf{x}_t^{\boldsymbol{\theta}}, t)\right] \mathrm{d}\bar{t} + g^2(t)\bar{\mathbf{w}}_t, \quad \mathbf{x}_T^{\boldsymbol{\theta}} \sim \pi,$$

is a generative diffusion with a parametrized vector field of $\mathbf{s}_{\boldsymbol{\theta}}$. Then, IPF get its optimal vector fields by alternatively solving below half-bridge problems

$$\boldsymbol{\nu}_{\boldsymbol{\phi}_n} = \underset{\boldsymbol{\nu}_{\boldsymbol{\phi}} \in \mathcal{P}(p_r, \cdot)}{\arg\min}\, D_{KL}(\boldsymbol{\nu}_{\boldsymbol{\phi}} \| \boldsymbol{\nu}_{\boldsymbol{\theta}_{n-1}}), \tag{34}$$

$$\boldsymbol{\nu}_{\boldsymbol{\theta}_n} = \underset{\boldsymbol{\nu}_{\boldsymbol{\theta}} \in \mathcal{P}(\cdot, \pi)}{\arg\min}\, D_{KL}(\boldsymbol{\nu}_{\boldsymbol{\theta}} \| \boldsymbol{\nu}_{\boldsymbol{\phi}_n}), \tag{35}$$

where the convergence of $\boldsymbol{\nu}_{\boldsymbol{\phi}^n} \to \boldsymbol{\nu}_{\boldsymbol{\phi}^*}$ and $\boldsymbol{\mu}_{\boldsymbol{\theta}^n} \to \boldsymbol{\nu}_{\boldsymbol{\theta}^*}$ is guaranteed in De Bortoli et al. [15]. Here, analogously, $\mathcal{P}(\cdot, \pi)$ is a family of path measure with π as its marginal distribution at $t = T$. Notably, each of the half-bridge problem is a diffusion problem with the KL divergence replaced with the reverse KL divergence. Since SBP learns the forward SDE, sampling particle paths is expensive as it requires to solve an SDE numerically, so the training of IPF is slow.

E Correction of Density Estimation Metrics of Diffusion Models with Time Truncation

E.1 Equivalent Reverse SDEs

Throughout Section E, the diffusion process is assumed to follow a SDE of $\mathrm{d}\mathbf{x}_t = \mathbf{f}(\mathbf{x}_t, t)\,\mathrm{d}t + g(t)\,\mathrm{d}\mathbf{w}_t$ because the below argument is generally applicable for any continuous diffusion models. For INDM, we apply the below argument on the latent space, which has a linear drift term. Let $\mathrm{d}\mathbf{x}_t = \left[\mathbf{f}(\mathbf{x}_t, t) - \frac{1+\lambda^2}{2} g^2(t)\nabla_{\mathbf{x}_t} \log p_t^\lambda(\mathbf{x}_t)\right] \mathrm{d}\bar{t} + \lambda g(t)\bar{\mathbf{w}}_t$ be the reverse SDEs starting from p_T, where p_t^λ is the probability law of the solution at t. Then, the reverse Kolmogorov equation (or Fokker-Planck equation) becomes

$$\begin{aligned} \frac{\partial p_t^\lambda(\mathbf{x}_t, t)}{\partial t} = &- \sum_{i=1}^d \frac{\partial}{\partial x_i} \left(\left[f_i(\mathbf{x}_t, t) - \frac{1+\lambda^2}{2} g^2(t) \big(\nabla_{\mathbf{x}_t} \log p_t^\lambda(\mathbf{x}_t, t)\big)_i \right] p_t^\lambda(\mathbf{x}_t, t) \right) \\ &- \frac{\lambda^2 g^2(t)}{2} \sum_{i=1}^d \frac{\partial^2}{\partial x_i^2} \left[p_t^\lambda(\mathbf{x}_t, t) \right] \end{aligned}$$

$$
\begin{aligned}
&= -\sum_{i=1}^{d} \frac{\partial}{\partial x_i} \left(f_i(\mathbf{x}_t, t) p_t^{\lambda}(\mathbf{x}_t, t) - \frac{1+\lambda^2}{2} g^2(t) \frac{\partial p_t^{\lambda}(\mathbf{x}_t, t)}{\partial x_i} \right) \\
&\quad - \frac{\lambda^2 g^2(t)}{2} \sum_{i=1}^{d} \frac{\partial^2}{\partial x_i^2} \left[p_t^{\lambda}(\mathbf{x}_t, t) \right] \\
&= -\sum_{i=1}^{d} \frac{\partial}{\partial x_i} \left[f_i(\mathbf{x}_t, t) p_t^{\lambda}(\mathbf{x}_t, t) \right] + \frac{1}{2} g^2(t) \sum_{i=1}^{d} \frac{\partial^2}{\partial x_i^2} \left[p_t^{\lambda}(\mathbf{x}_t, t) \right],
\end{aligned}
$$

which is independent of λ. Therefore, it satisfies $p_t^{\lambda} = p_t^{\lambda'}$ for any $\lambda \neq \lambda'$.

For any $\lambda \in [0, 1]$, the generative SDE is constructed by plugging $\mathbf{s}_{\boldsymbol{\theta}}(\mathbf{x}_t, t)$ in place of $\nabla_{\mathbf{x}_t} \log p_t^{\lambda}(\mathbf{x}_t)$ in the reverse SDE as $\mathrm{d}\mathbf{x}_t = \left[\mathbf{f}(\mathbf{x}_t, t) - \frac{1+\lambda^2}{2} g^2(t) \mathbf{s}_{\boldsymbol{\theta}}(\mathbf{x}_t, t) \right] \mathrm{d}\bar{t} + \lambda g(t) \bar{\mathbf{w}}_t$. Suppose we denote $p_t^{\lambda, \boldsymbol{\theta}}$ as the marginal distribution of the model at t. Then, the generative SDEs with different λ have distinctive marginal distributions: $p_t^{\lambda, \boldsymbol{\theta}} \neq p_t^{\lambda', \boldsymbol{\theta}}$ for $\lambda \neq \lambda'$.

E.2 Log-Likelihood for Diffusion Models with Time Truncation

Due to the unbounded score loss illustrated in [27], a diffusion model truncates the diffusion time to be $[\epsilon, 1]$ for small enough $\epsilon > 0$. However, since the small range of diffusion time contributes significant portion of the log-likelihood [27], the effect of truncation should be counted both on training and evaluation. To describe, as we have no knowledge on the score estimation at $t \in [0, \epsilon)$, we have estimate the data log-likelihood by using the variational inferecence:

$$
\begin{aligned}
\log p_0^{\lambda, \boldsymbol{\theta}}(\mathbf{x}_0) &= \log \int p_0^{\lambda, \boldsymbol{\theta}}(\mathbf{x}_0, \mathbf{x}_\epsilon) \, \mathrm{d}\mathbf{x}_\epsilon \\
&\geq \int p_{0\epsilon}(\mathbf{x}_\epsilon | \mathbf{x}_0) \log \frac{p_\epsilon^{\lambda, \boldsymbol{\theta}}(\mathbf{x}_\epsilon) p_{\epsilon 0}^{\boldsymbol{\theta}}(\mathbf{x}_0 | \mathbf{x}_\epsilon)}{p_{0\epsilon}(\mathbf{x}_\epsilon | \mathbf{x}_0)} \, \mathrm{d}\mathbf{x}_\epsilon \\
&= \mathbb{E}_{p_{0\epsilon}(\mathbf{x}_\epsilon | \mathbf{x}_0)} \left[\log p_\epsilon^{\lambda, \boldsymbol{\theta}}(\mathbf{x}_\epsilon) \right] + \mathbb{E}_{p_{0\epsilon}(\mathbf{x}_\epsilon | \mathbf{x}_0)} \left[\log \frac{p_{\epsilon 0}^{\boldsymbol{\theta}}(\mathbf{x}_0 | \mathbf{x}_\epsilon)}{p_{0\epsilon}(\mathbf{x}_\epsilon | \mathbf{x}_0)} \right],
\end{aligned}
$$

where $p_\epsilon^{\lambda, \boldsymbol{\theta}}$ is the generative distribution perturbed by ϵ, and $p_{\epsilon 0}^{\boldsymbol{\theta}}(\mathbf{x}_0 | \mathbf{x}_\epsilon)$ is the reconstruction transition probability given $\mathbf{x}_\epsilon$. Then, we have

$$
\begin{aligned}
\mathbb{E}_{p_r(\mathbf{x}_0)} [-\log p_0^{\lambda, \boldsymbol{\theta}}(\mathbf{x}_0)] &\leq \mathbb{E}_{\mathbf{x}_\epsilon} \left[-\log p_\epsilon^{\lambda, \boldsymbol{\theta}}(\mathbf{x}_\epsilon) \right] - \mathbb{E}_{\mathbf{x}_0, \mathbf{x}_\epsilon} \left[\log \frac{p_{\epsilon 0}^{\boldsymbol{\theta}}(\mathbf{x}_0 | \mathbf{x}_\epsilon)}{p_{0\epsilon}(\mathbf{x}_\epsilon | \mathbf{x}_0)} \right] \\
&= D_{KL}(p_\epsilon \| p_\epsilon^{\lambda, \boldsymbol{\theta}}) - \mathbb{E}_{\mathbf{x}_0, \mathbf{x}_\epsilon} \left[\log \frac{p_{\epsilon 0}^{\boldsymbol{\theta}}(\mathbf{x}_0 | \mathbf{x}_\epsilon)}{p_{0\epsilon}(\mathbf{x}_\epsilon | \mathbf{x}_0)} \right] + \mathcal{H}(p_\epsilon),
\end{aligned}
$$

which is equivalent to

$$
\begin{aligned}
D_{KL}(p_r \| p_0^{\lambda, \boldsymbol{\theta}}) &\leq D_{KL}(p_\epsilon \| p_\epsilon^{\lambda, \boldsymbol{\theta}}) - \mathbb{E}_{\mathbf{x}_0, \mathbf{x}_\epsilon} \left[\log \frac{p_{\epsilon 0}^{\boldsymbol{\theta}}(\mathbf{x}_0 | \mathbf{x}_\epsilon)}{p_{0\epsilon}(\mathbf{x}_\epsilon | \mathbf{x}_0)} \right] + \mathcal{H}(p_\epsilon) - \mathcal{H}(p_r) \\
&= D_{KL}(p_\epsilon \| p_\epsilon^{\lambda, \boldsymbol{\theta}}) + D_{KL}\big(p_r(\mathbf{x}_0) p_{0\epsilon}(\mathbf{x}_\epsilon | \mathbf{x}_0) \| p_\epsilon(\mathbf{x}_\epsilon) p_{\epsilon 0}^{\boldsymbol{\theta}}(\mathbf{x}_0 | \mathbf{x}_\epsilon) \big).
\end{aligned}
$$

E.3 NELBO Correction

Suppose $\boldsymbol{\mu}_\epsilon$ is the path measure of $\mathrm{d}\mathbf{x}_t = \mathbf{f}(\mathbf{x}_t, t) \, \mathrm{d}t + g(t) \, \mathrm{d}\mathbf{w}_t$ on $[\epsilon, T]$, and $\boldsymbol{\nu}_{\boldsymbol{\theta}, \epsilon}^{\lambda}$ is the path measure of $\mathrm{d}\mathbf{x}_t = \left[\mathbf{f}(\mathbf{x}_t, t) - \frac{1+\lambda^2}{2} g^2(t) \nabla_{\mathbf{x}_t} \log p_t^{\lambda}(\mathbf{x}_t) \right] \mathrm{d}\bar{t} + \lambda g(t) \bar{\mathbf{w}}_t$ on $[\epsilon, T]$. Then, the continuous variational bound on the truncated diffusion model becomes

$$
\begin{aligned}
\mathbb{E}_{p_r(\mathbf{x}_0)} \left[-\log p_0^{\lambda, \boldsymbol{\theta}}(\mathbf{x}_0) \right] &\leq D_{KL}(p_\epsilon \| p_\epsilon^{\lambda, \boldsymbol{\theta}}) - \mathbb{E}_{\mathbf{x}_0, \mathbf{x}_\epsilon} \left[\log \frac{p_{\epsilon 0}^{\boldsymbol{\theta}}(\mathbf{x}_0 | \mathbf{x}_\epsilon)}{p_{0\epsilon}(\mathbf{x}_\epsilon | \mathbf{x}_0)} \right] + \mathcal{H}(p_\epsilon) \\
&\leq D_{KL}(\boldsymbol{\mu}_\epsilon \| \boldsymbol{\nu}_{\boldsymbol{\theta}, \epsilon}^{\lambda}) - \mathbb{E}_{\mathbf{x}_0, \mathbf{x}_\epsilon} \left[\log \frac{p_{\epsilon 0}^{\boldsymbol{\theta}}(\mathbf{x}_0 | \mathbf{x}_\epsilon)}{p_{0\epsilon}(\mathbf{x}_\epsilon | \mathbf{x}_0)} \right] + \mathcal{H}(p_\epsilon) \\
&= \frac{1}{2} \frac{(1+\lambda^2)^2}{4\lambda^2} \int_\epsilon^T g^2(t) \mathbb{E}_{\mathbf{x}_t} \left[\| \mathbf{s}_{\boldsymbol{\theta}}(\mathbf{x}_t, t) - \log p_t(\mathbf{x}_t) \|_2^2 \right] \mathrm{d}t - \mathbb{E}_{\mathbf{x}_T} \left[\log \pi(\mathbf{x}_T) \right]
\end{aligned}
$$

$$
\begin{aligned}
&-\mathbb{E}_{\mathbf{x}_0,\mathbf{x}_\epsilon}\left[\log \frac{p^{\boldsymbol{\theta}}_{\epsilon 0}(\mathbf{x}_0|\mathbf{x}_\epsilon)}{p_{0\epsilon}(\mathbf{x}_\epsilon|\mathbf{x}_0)}\right] + \mathcal{H}(p_\epsilon) - \mathcal{H}(p_T) \\
&= \frac{1}{2}\int_\epsilon^T \mathbb{E}_{\mathbf{x}_0,\mathbf{x}_t}\Bigg[\frac{(1+\lambda^2)^2}{4\lambda^2} g^2(t)\|\log p_{0t}(\mathbf{x}_t|\mathbf{x}_0) - \mathbf{s}_{\boldsymbol{\theta}}(\mathbf{x}_t,t)\|_2^2 - g^2(t)\|\nabla_{\mathbf{x}_t}\log p_{0t}(\mathbf{x}_t|\mathbf{x}_0)\|_2^2 \\
&\qquad -2\nabla_{\mathbf{x}_t}\cdot \mathbf{f}(\mathbf{x}_t,t)\Bigg]\,\mathrm{d}t - \mathbb{E}_{\mathbf{x}_T}\big[\log \pi(\mathbf{x}_T)\big] - \mathbb{E}_{\mathbf{x}_0,\mathbf{x}_\epsilon}\left[\log \frac{p^{\boldsymbol{\theta}}_{\epsilon 0}(\mathbf{x}_0|\mathbf{x}_\epsilon)}{p_{0\epsilon}(\mathbf{x}_\epsilon|\mathbf{x}_0)}\right],
\end{aligned}
$$

where $\mathcal{H}(p_\epsilon) - \mathcal{H}(p_T)$ is derived to be $-\frac{1}{2}\int_\epsilon^T \mathbb{E}\big[g^2\|\nabla \log p_{0t}\|_2^2 + 2\nabla\cdot\mathbf{f}\big]\,\mathrm{d}t$ by Theorem 4 of Song et al. [11]. The residual term, $\mathbb{E}_{p_r(\mathbf{x}_0)p_{0\epsilon}(\mathbf{x}_\epsilon|\mathbf{x}_0)}\big[\log \frac{p^{\boldsymbol{\theta}}_{\epsilon 0}(\mathbf{x}_0|\mathbf{x}_\epsilon)}{p_{0\epsilon}(\mathbf{x}_\epsilon|\mathbf{x}_0)}\big]$, has been ignored both on training and evaluation in previous research. Therefore, we report the *correct* NELBO (denoted by *w/ residual* in the main paper) by counting the residual term $\mathbb{E}_{p_r(\mathbf{x}_0)p_{0\epsilon}(\mathbf{x}_\epsilon|\mathbf{x}_0)}\big[\log \frac{p^{\boldsymbol{\theta}}_{\epsilon 0}(\mathbf{x}_0|\mathbf{x}_\epsilon)}{p_{0\epsilon}(\mathbf{x}_\epsilon|\mathbf{x}_0)}\big]$ into account. Note that $\frac{(1+\lambda^2)^2}{4\lambda^2}$ is minimized when $\lambda = 1$, so our reported NELBO is based on the generative SDE at $\lambda = 1$.

E.4 NLL Correction

NLL of the generative SDE can be computed through the Feynman-Kac formula [12] by

$$
p^{\lambda}_{\boldsymbol{\theta},\epsilon}(\mathbf{x}_\epsilon) = \mathbb{E}_{\{\mathbf{x}_t\}_{t>\epsilon}|\mathbf{x}_\epsilon}\left[\pi(\mathbf{x}_T)\exp\left(-\int_\epsilon^T \mathrm{tr}\Big(\nabla_{\mathbf{x}_t}\Big[\mathbf{f}(\mathbf{x}_t,t) - \frac{1+\lambda^2}{2}g^2(t)\mathbf{s}_{\boldsymbol{\theta}}(\mathbf{x}_t,t)\Big]\Big)\,\mathrm{d}t\right)\right]. \tag{36}
$$

However, the expectation is intractable because there are infinitely-many sample paths. Fortunately, the sample variance diminishes as $\lambda \to 0$, and the generative SDE collapses to a generative ODE when $\lambda = 0$ [1], i.e., the generative SDE of $\lambda = 0$ becomes

$$
\mathrm{d}\mathbf{x}_t = \left[\mathbf{f}(\mathbf{x}_t,t) - \frac{1}{2}g^2(t)\mathbf{s}_{\boldsymbol{\theta}}(\mathbf{x}_t,t)\right]\mathrm{d}\bar{t},
$$

which corresponds to the generative ODE of forward time as

$$
\mathrm{d}\mathbf{x}_t = \left[\mathbf{f}(\mathbf{x}_t,t) - \frac{1}{2}g^2(t)\mathbf{s}_{\boldsymbol{\theta}}(\mathbf{x}_t,t)\right]\mathrm{d}t. \tag{37}
$$

Then, the sample path becomes deterministic, and the expectation in Eq. (36) is degenerated as the single sample path of ODE with Eq. (37) starting $\mathbf{x}_\epsilon$. The instantaneous change-of-variable formula [1], which is a collapsed Feynman-Kac formula in Eq. (36), guarantees that there is a corresponding ODE of Eq. (37) as

$$
\frac{\mathrm{d}\log p^{0,\boldsymbol{\theta}}_t(\mathbf{y}_t)}{\mathrm{d}t} = -\mathrm{tr}\Big(\nabla_{\mathbf{y}_t}\Big[\mathbf{f}(\mathbf{y}_t,t) - \frac{1}{2}g^2(t)\mathbf{s}_{\boldsymbol{\theta}}(\mathbf{y}_t,t)\Big]\Big). \tag{38}
$$

From the fact that the reverse SDEs have the identical marginal distributions described in Section E.1, we approximate the model log-likelihood at $\lambda = 1$ by the log-likelihood at $\lambda = 0$ at the expense of slight difference between the model distributions of different λs. When computing the model log-likelihood at $\lambda = 0$, we integrate the ODE of Eq. (38) over $[\epsilon, 1]$ using an ODE solver, such as the Runge-Kutta 45 method [25].

There are minor subtleties in computing the log-likelihood at $\lambda = 0$ that significantly affects to bpd evaluation. To the best of our knowledge, all the current practice on continuous diffusion models computes bpd by integrating

$$
\frac{\mathrm{d}\log p^{0,\boldsymbol{\theta}}_t(\mathbf{y}_t)}{\mathrm{d}t} = -\mathrm{tr}\Big(\nabla_{\mathbf{y}_t}\Big[\mathbf{f}(\mathbf{y}_t,t) - \frac{1}{2}g^2(t)\mathbf{s}_{\boldsymbol{\theta}}(\mathbf{y}_t,t)\Big]\Big),
$$

on $t \in [\epsilon, T]$, where $\{\mathbf{y}_t\}_{t=\epsilon}^T$ is a sample path starting from $\mathbf{y}_\epsilon := \mathbf{x}_0$. This is equivalent of computing $\log p^{0,\boldsymbol{\theta}}_\epsilon(\mathbf{x}_0)$. However, starting from $\mathbf{x}_0$ incurs large discrepancy on the NLL output, compared to starting from instead of $\mathbf{x}_\epsilon$. Since the integration is on $[\epsilon, 1]$, the starting variable should follow $\mathbf{x}_\epsilon$, which is a slightly perturbed variable.

Table 11: The difference of the integration with different initial points of $\mathbf{x}_\epsilon$ and $\mathbf{x}_0$ on DDPM++ (VP, NLL). The difference increases by ϵ.

	ϵ			
	10^{-2}	10^{-3}	10^{-4}	10^{-5}
$\mathbb{E}_{\mathbf{x}_\epsilon}\left[-\log p_\epsilon^{\boldsymbol{\theta}}(\mathbf{x}_\epsilon)\right] - \mathbb{E}_{\mathbf{x}_0}\left[-\log p_\epsilon^{\boldsymbol{\theta}}(\mathbf{x}_0)\right]$	1.13	0.73	0.24	0.05

To fix this subtlety, we solve the below alternative differential equation of

$$\frac{\mathrm{d}\log p_t^{0,\boldsymbol{\theta}}}{\mathrm{d}t} = -\mathrm{tr}\left(\nabla_{\mathbf{y}_t}\left[\mathbf{f}(\mathbf{y}_t,t) - \frac{1}{2}g^2(t)\mathbf{s}_{\boldsymbol{\theta}}(\mathbf{y}_t,t)\right]\right), \tag{39}$$

on $t \in [\epsilon, T]$, where $\{\mathbf{y}_t^0\}_{t=\epsilon}^T$ is a sample path starting from $\mathbf{y}_\epsilon := \mathbf{x}_\epsilon$. By replacing the initial value to $\mathbf{x}_\epsilon$ from $\mathbf{x}_0$, we could correctly compute $\log p_\epsilon^{\boldsymbol{\theta}}(\mathbf{x}_\epsilon)$. Table 11 presents the difference of $\mathbb{E}_{\mathbf{x}_\epsilon}\left[-\log p_\epsilon^{0,\boldsymbol{\theta}}(\mathbf{x}_\epsilon)\right] - \mathbb{E}_{\mathbf{x}_0}\left[-\log p_\epsilon^{0,\boldsymbol{\theta}}(\mathbf{x}_0)\right]$ with various ϵ. We report the *correct* NLL as

$$\mathbb{E}_{\mathbf{x}_\epsilon}\left[-\log p_\epsilon^{0,\boldsymbol{\theta}}(\mathbf{x}_\epsilon)\right] - \mathbb{E}_{\mathbf{x}_0,\mathbf{x}_\epsilon}\left[\log \frac{p_{\epsilon 0}^{\boldsymbol{\theta}}(\mathbf{x}_0|\mathbf{x}_\epsilon)}{p_{0\epsilon}(\mathbf{x}_\epsilon|\mathbf{x}_0)}\right],$$

where $\log p_\epsilon^{0,\boldsymbol{\theta}}(\mathbf{x}_\epsilon)$ is computed based on the initial point of $\mathbf{x}_\epsilon$ when $\lambda = 0$.

E.5 Calculating the Residual Term

This section calculates the residual term, $\mathbb{E}_{p_r(\mathbf{x}_0)p_{0\epsilon}(\mathbf{x}_\epsilon|\mathbf{x}_0)}\left[\log \frac{p_{\epsilon 0}^{\boldsymbol{\theta}}(\mathbf{x}_0|\mathbf{x}_\epsilon)}{p_{0\epsilon}(\mathbf{x}_\epsilon|\mathbf{x}_0)}\right]$. The transition probability of $p_{0\epsilon}(\mathbf{x}_\epsilon|\mathbf{x}_0)$ is the Gaussian distribution of $\mathcal{N}(\mathbf{x}_\epsilon; \mu(\epsilon)\mathbf{x}_0, \sigma^2(\epsilon)\mathbf{I})$ if $\mathbf{f}(\mathbf{x}_t,t) = -\frac{1}{2}\beta(t)\mathbf{x}_t$ with

$$\mu(\epsilon) = e^{-\frac{1}{2}\int_0^\epsilon \beta(s)\,\mathrm{d}s} \text{ and } \sigma^2(\epsilon) = \left(\frac{g^2(t)}{\beta(t)} - \frac{g^2(0)}{\beta(0)} + 1 - e^{-\int_0^t \beta(s)\,\mathrm{d}s}\right),$$

see Appendix A.1 of Kim et al. [27] for detailed computation. On the other hand, the generative distribution of $p_{\boldsymbol{\theta},\epsilon 0}(\mathbf{x}_0|\mathbf{x}_\epsilon)$ is assumed to be a Gaussian distribution of $\mathcal{N}\big(\mathbf{x}_0; \boldsymbol{\mu}_{\boldsymbol{\theta},\epsilon 0}(\mathbf{x}_\epsilon), \sigma_{\boldsymbol{\theta},\epsilon 0}^2\mathbf{I}\big)$, where $\boldsymbol{\mu}_{\boldsymbol{\theta},\epsilon 0}(\mathbf{x}_\epsilon) = \frac{1}{\mu(\epsilon)}\big(\mathbf{x}_\epsilon + \sigma^2(\epsilon)\mathbf{s}_{\boldsymbol{\theta}}(\mathbf{x}_\epsilon,\epsilon)\big)$ [28]. Then, we have

$$\begin{aligned}
&\mathbb{E}_{p_{0\epsilon}(\mathbf{x}_\epsilon|\mathbf{x}_0)}\left[\log \frac{p_{\epsilon 0}^{\boldsymbol{\theta}}(\mathbf{x}_0|\mathbf{x}_\epsilon)}{p_{0\epsilon}(\mathbf{x}_\epsilon|\mathbf{x}_0)}\right] \\
&\quad = \log \mu(\epsilon) - \frac{1}{2\sigma_{\boldsymbol{\theta},\epsilon 0}^2(\epsilon)}\mathbb{E}_{p_{0\epsilon}(\mathbf{x}_\epsilon|\mathbf{x}_0)}\left[\left\|\mathbf{x}_0 - \frac{1}{\mu(\epsilon)}\Big(\mathbf{x}_t + \sigma^2(\epsilon)\mathbf{s}_{\boldsymbol{\theta}}(\mathbf{x}_\epsilon,\epsilon)\Big)\right\|_2^2\right] + \frac{1}{2}.
\end{aligned}$$

We could approximate the variance of $p_{\epsilon 0}^{\boldsymbol{\theta}}(\mathbf{x}_0|\mathbf{x}_\epsilon)$ to be the variance of $p_{\epsilon 0}(\mathbf{x}_0|\mathbf{x}_\epsilon)$, if $p_{\epsilon 0}(\mathbf{x}_0|\mathbf{x}_\epsilon)$ is derived as a closed-form. For that, let us assume $\mathbf{x}_0 \sim \mathcal{N}(0,\sigma^2)$. Then,

$$\begin{aligned}
p(\mathbf{x}_0,\mathbf{x}_\epsilon) &= p(\mathbf{x}_0)p_{0\epsilon}(\mathbf{x}_\epsilon|\mathbf{x}_0) \\
&\propto \exp\left(-\frac{\|\mathbf{x}_0\|_2^2}{2\sigma^2} - \frac{\|\mathbf{x}_\epsilon - \mu(\epsilon)\mathbf{x}_0\|_2^2}{2\sigma^2(\epsilon)}\right) \\
&= \exp\left(-\frac{1}{2}\left(\frac{1}{\sigma^2} + \frac{\mu^2(\epsilon)}{\sigma^2(\epsilon)}\right)\left\|\mathbf{x}_0 - \frac{\mu(\epsilon)\sigma^2}{\sigma^2(\epsilon) + \mu^2(\epsilon)\sigma^2}\mathbf{x}_\epsilon\right\|_2^2 + O(\|\mathbf{x}_\epsilon\|_2^2)\right).
\end{aligned}$$

Therefore, $p_{\epsilon 0}(\mathbf{x}_0|\mathbf{x}_\epsilon) = \mathcal{N}\big(\mathbf{x}_0 \big| \frac{\mu(\epsilon)\sigma^2}{\sigma^2(\epsilon)+\mu^2(\epsilon)\sigma^2}\mathbf{x}_\epsilon, 1/(\frac{1}{\sigma^2} + \frac{\mu^2(\epsilon)}{\sigma^2(\epsilon)})\big)$. When σ is sufficiently large compared to $\frac{\sigma^2(\epsilon)}{\mu^2(\epsilon)}$, the variance of $p_{\epsilon 0}(\mathbf{x}_0|\mathbf{x}_\epsilon)$ is approximately $\frac{\sigma^2(\epsilon)}{\mu^2(\epsilon)}$. Now, if $\mathbf{x}_0 \sim p_r$, then the variance of $\mathbf{x}_0$ is large enough compared to $\frac{\sigma^2(\epsilon)}{\mu^2(\epsilon)}$, so we could approximate $\sigma_{\boldsymbol{\theta},\epsilon 0}^2(\epsilon)$ to be $\frac{\sigma^2(\epsilon)}{\mu^2(\epsilon)}$. Note that DDPM [8] assumes the variance to be $\sigma^2(\epsilon)$. We compute the residual term with $\frac{\sigma^2(\epsilon)}{\mu^2(\epsilon)}$ variance for both VESDE and VPSDE. Note that this residual term is inspired from the released code of Song et al. [11].

Table 12: Despite of our implementation is built deeply based on Song et al. [1], our pytorch implementation and the jax implementation of Song et al. [11] differs in their final performances.

SDE	Model	NLL		NELBO		Gap		FID
		after	before	w/ residual	w/o residual	after	before	ODE
VP	DDPM++ (NLL, reported) [11]	-	2.95	-	3.08	-	0.13	6.03
	DDPM++ (NLL, ours)	3.03	2.97	3.13	3.11	0.10	0.14	6.70
	INDM (NLL)	2.98	2.95	2.98	2.97	0.00	0.02	6.01

F Experimental Details and Additional Results

F.1 Model Architecture

Diffusion Model We implement two diffusion models as backbone: NCSN++ (VE) [1] and DDPM++ (VP) [1], where two backbones are one of the best performers in CIFAR-10 dataset. In our setting, NCSN++ assumes the score network with parametrization of $\mathbf{s}_{\boldsymbol{\theta}}(\mathbf{z}_t, \log \sigma^2(t))$, where $\sigma^2(t) = \sigma_{min}^2(\frac{\sigma_{max}}{\sigma_{min}})^{2t}$ is the variance of the transition probability $p_{0t}(\mathbf{z}_t|\mathbf{z}_0)$ with VESDE. As introduced in Song et al. [1], we use the Gaussian Fourier embeddings [53] to model the high frequency details across the temporal embedding. DDPM++ models the score network with parametrization of $\epsilon_{\boldsymbol{\theta}}(\mathbf{z}_t, t)$, which targets to estimate $-\sigma(t)\nabla_{\mathbf{z}_t} \log p_t(\mathbf{z}_t)$. We use the Transformer sinusoidal temporal embedding [54].

We use the U-Net [55] architecture for the score networks on both NCSN++ and DDPM++ based on [8]. We stack U-Net resblocks of up-and-down convolutions with skip connections that give input information to the output layer. Also, we follow Ho et al. [8] by applying the global attention at the resolution of 16×16. We use four U-Net resblocks with four feature map resolutions (32×32 to 4×4). On CIFAR-10, we use four and eight resblocks for shallow and deep settings, respectively. The performances of shallow and deep models turn out to be insignificant, so we use four resblocks on CelebA. We provide the identical diffusion model structures to compare the baseline linear diffusion model and the INDM model in a fair setting.

Flow Model We build a normalizing flow model as follows. Ma et al. [24] uses the autoencoding structure of decouple the global information and the local representation. The compression encoder extracts the global information, and the invertible decoder is a conditional flow conditioned by the encoded latent representation. Ma et al. [24] utilizes a shallow network for the compressive encoder, and it applies Glow [56] for the invertible decoder. We empirically find that resnet-based flow network outperforms the Glow-based flow, so we replace Glow to ResFlow [23].

For the ResFlow, we drop three components from the original paper: 1) the activation normalization [56], 2) the batch normalization [57], and 3) the fully connected layers. For the activation function, we use the sine function [58] on quantitative comparisons in Section 7, and we use swish function [59] on qualitative analysis in otherwise sections including Section 6. With the sine activation, the training becomes more stable, and the FID performance is significantly improved while maintaining the NLL performance. For the multi-GPU training, we use the Neumann log-determinant gradient estimator, instead of the memory-efficient estimator [23].

F.2 Experimental details

With the batch size of 128, we train the diffusion model with Exponential Moving Average (EMA) [28] rate of 0.9999, and we do not use EMA on our flow model. Using EMA on the flow model is advantageous on NLL at the expense of FID, and we build our model with emphasis on FID. We train the model by two step. The pre-training stage trains the diffusion model about five days with a flow model fixed as an identity function on four P40 GPUs with 96Gb GPU memory for all experiments. After the pre-training, we train both flow and diffusion networks about five days. In this stage, we apply the learning rate scheduling to boost the FID score. We initiate the learning rate after the sample generation performance is saturated. For the diffusion model, we drop the learning rate from 2×10^{-4} to 10^{-5}. For the flow model, we drop the learning rate from 10^{-3} to 10^{-5} for VPSDE and 5×10^{-5} to 10^{-5} for VESDE.

VESDE and VPSDE have different training details. We apply INDM on VESDE with $\sigma_{min} = 10^{-2}$. Throughout the experiments, VESDE has $\sigma_{max} = 50$ on CIFAR-10 and $\sigma_{max} = 90$ on CelebA. On the other hand, VPSDE assumes $\beta(t) = \beta_{min} + (\beta_{max} - \beta_{min})t$ with $\beta_{min} = 0.1$ and $\beta_{max} = 20$. Both VESDE and VPSDE truncate the diffusion time on $[\epsilon, T]$ in order to stabilize the diffusion model [27], where $\epsilon = 10^{-5}$ and $T = 1$.

With all hyperparameters identical to Song et al. [11], however, we could not achieve the reported performance. Table 12 compares the reported performance and the model performance trained on out implementation, of which structure is heavily based on the released code of [1]. Due to the discrepancy between the reported and the regenerated performances, we compare our INDM to the regenerated performance as default to investigate the effect of nonlinear diffusion in a fair setting. Throughout the training, we used 4× NVIDIA RTX 3090.

F.2.1 Variance Reduction

Flow Training When we train the flow network with $\mathcal{L}\big(\{\mathbf{x}_t\}_{t=0}^T, g^2; \{\boldsymbol{\phi}, \boldsymbol{\theta}\}\big)$, this NELBO contains the integration of

$$\mathcal{L}\big(\{\mathbf{z}_t\}_{t=0}^T, g^2; \boldsymbol{\theta}\big) = \frac{1}{2}\int_0^T g^2(t)\mathbb{E}_{\mathbf{z}_0,\mathbf{z}_t}\left[\|\mathbf{s}_{\boldsymbol{\theta}}(\mathbf{z}_t, t)\right] \mathrm{d}t,$$

up to a constant. Suppose $\mathcal{L}_t\big(\{\mathbf{z}_t\}_{t=0}^T; \boldsymbol{\theta}\big)$ to be $\frac{1}{2}\mathbb{E}_{\mathbf{z}_0,\mathbf{z}_t}[\|\mathbf{s}_{\boldsymbol{\theta}}(\mathbf{z}_t, t) - \nabla_{\mathbf{z}_t}\log p_{0t}(\mathbf{z}_t|\mathbf{x}_0)\|_2^2]$. Previous works on diffusion models [60, 12, 11, 27] show that the estimation variance is largely reduced with the importance sampling, which could improve the model performance [11], and we apply this importance sampling throughout the experiments for NLL setting. Concretely, the importance sampling chooses an importance weight that is proportional to $\frac{g^2(t)}{\sigma^2(t)}$, and estimates the integration by $\mathcal{L}\big(\{\mathbf{z}_t\}_{t=0}^T, g^2; \boldsymbol{\theta}\big) = \int_0^T g^2(t)\mathcal{L}_t\big(\{\mathbf{z}_t\}_{t=0}^T; \boldsymbol{\theta}\big)\,\mathrm{d}t \approx \sum_{n=1}^N \sigma^2(t_n)\mathcal{L}_{t_n}\big(\{\mathbf{z}_t\}_{t=0}^T; \boldsymbol{\theta}\big)$, where t_n is sampled from the importance distribution.

For VESDE, it satisfies $\beta(t) = 0$ and $g(t) = \sigma_{min}(\frac{\sigma_{max}}{\sigma_{min}})^t\sqrt{2\log(\frac{\sigma_{max}}{\sigma_{min}})}$. The transition probability becomes $p_{-\infty t}(\mathbf{z}_t|\mathbf{z}_{-\infty}) = \mathcal{N}(\mathbf{z}_t; \mathbf{z}_{-\infty}, \sigma^2(t))$, where $\sigma^2(t) = \int_{-\infty}^t g^2(s)\,\mathrm{d}s = \sigma_{min}^2\big(\frac{\sigma_{max}}{\sigma_{min}}\big)^{2t}$. Since $\sigma^2(t)$ is proportional to $g^2(t)$ in VESDE, the importance weight follows the uniform distribution, and the importance sampling is equivalent with choosing the uniform t. This is why there is no experimetal setting of VE with NLL.

On the other hand, VPSDE satisfies $\beta(t) = \beta_{min} + (\beta_{max} - \beta_{min})t$ with $g(t) = \sqrt{\beta(t)}$. Then, the transition probability becomes $p_{0t}(\mathbf{z}_t|\mathbf{z}_0) = \mathcal{N}(\mathbf{z}_t; \mu(t)\mathbf{z}_t, \sigma^2(t)\mathbf{I})$, where $\mu(t) = e^{-\frac{1}{2}\int_0^t \beta(s)\,\mathrm{d}s}$ and $\sigma^2(t) = 1 - e^{-\int_0^t \beta(s)\,\mathrm{d}s}$. Thus, VPSDE has the importance weight of $\frac{g^2(t)}{\sigma^2(t)} = \frac{\beta(t)}{1-e^{-\int_0^t \beta(s)\,\mathrm{d}s}}$.

The Monte-Carlo sample from this importance weight is the solution of the inverse Cumulative Distribution Function (CDF) of the importance distribution as

$$\begin{aligned} & t = F^{-1}(u) \\ \iff & u = F(t) = \frac{1}{Z}\int_\epsilon^t \frac{g^2(s)}{\sigma^2(s)}\,\mathrm{d}s = \frac{1}{Z}\big(\mathcal{F}(t) - \mathcal{F}(\epsilon)\big), \end{aligned} \tag{40}$$

where u is a uniform sample from $[0, 1]$, $\mathcal{F}(t)$ is the antiderivative of the importance weight given by $\mathcal{F}(t) = \log\left(1 - e^{-0.5t^2(\beta_{max}-\beta_{min})-t\beta_{min}}\right) + 0.5t^2(\beta_{max} - \beta_{min}) + t\beta_{min}$, and Z is the normalizing constant given by

$$\begin{aligned} Z = & \int_\epsilon^T \frac{g^2(t)}{\sigma^2(t)}\,\mathrm{d}t \\ = & \Big[\log\left(1 - e^{-0.5t^2(\beta_{max}-\beta_{min})-t\beta_{min}}\right) + 0.5t^2(\beta_{max} - \beta_{min}) + t\beta_{min}\Big]_\epsilon^T \\ = & \log\left(1 - e^{-0.5T^2(\beta_{max}-\beta_{min})-T\beta_{min}}\right) - \log\left(1 - e^{-0.5\epsilon^2(\beta_{max}-\beta_{min})-\epsilon\beta_{min}}\right) \\ & + 0.5(T^2 - \epsilon^2)(\beta_{max} - \beta_{min}) + (T - \epsilon)\beta_{min} \\ \approx & 23.86 \end{aligned}$$

Table 13: Ablation study on the stopping sampling time trained on DDPM++ (VP) in CIFAR-10.

Model	FID ($t_{min} = 10^{-3}$)	FID ($t_{min} = 10^{-4}$)	FID ($t_{min} = 10^{-5}$)
INDM (deep, VP, NLL)	5.94	5.74	5.71

Table 14: Ablation study on the SNR trained on NCSN++ (VE) in CIFAR-10. The performances are FID-5k scores.

Model	Signal-to-Natio Ratio (SNR)				
	0.13	0.14	0.15	0.16	0.17
INDM (VE, FID)	7.24	7.12	7.20	7.25	7.34

for $T = 1$ and $\epsilon = 10^{-5}$. The solution for the inverse CDF in Eq. (40) becomes

$$
\begin{aligned}
& e^{\int_0^t \beta(s)\,\mathrm{d}s} = 1 + \exp\left(Zu + \mathcal{F}(\epsilon)\right) \\
\iff & \int_0^t \beta(s)\,\mathrm{d}s = \frac{1}{2}(\beta_{max} - \beta_{min})t^2 + \beta_{min}t = \log\left(1 + \exp\left(Zu + \mathcal{F}(\epsilon)\right)\right) \\
\iff & t = \frac{-\beta_{min} + \sqrt{\beta_{min}^2 + 2(\beta_{max} - \beta_{min})\log\left(1 + \exp\left(Zu + \mathcal{F}(\epsilon)\right)\right)}}{\beta_{max} - \beta_{min}}.
\end{aligned}
$$

The variation of the Monte-Carlo diffusion time depends on the uniform sample of u.

$$
\begin{aligned}
& \int_0^t \beta(s)\,\mathrm{d}s = \log\left(\frac{1 - \sigma_{min}^2}{1 - \sigma_{min}^2\left(\frac{\sigma_{max}}{\sigma_{min}}\right)^t}\right) = \log\left(1 + \exp\left(Zu + \mathcal{F}(\epsilon)\right)\right) \\
\iff & 1 - \sigma_{min}^2\left(\frac{\sigma_{max}}{\sigma_{min}}\right)^t = \frac{1 - \sigma_{min}^2}{1 + e^{Zu + \mathcal{F}(\epsilon)}} \\
\iff & \sigma_{min}^2\left(\frac{\sigma_{max}^2}{\sigma_{min}^2}\right)^t = \frac{e^{Zu + \mathcal{F}(\epsilon)} + \sigma_{min}^2}{1 + e^{Zu + \mathcal{F}(\epsilon)}} \\
\iff & t\log\frac{\sigma_{max}^2}{\sigma_{min}^2} = \log\left(e^{Zu + \mathcal{F}(\epsilon)} + \sigma_{min}^2\right) - \log\left(1 + e^{Zu + \mathcal{F}(\epsilon)}\right) - \log\sigma_{min}^2.
\end{aligned}
$$

F.2.2 Sampling Tricks to Improve FID

For ODE sampler, we use Runge Kutta 45 method [61] for the ODE solver. Since the score network was not trained beneath the truncation time, i.e., $\mathbf{s}_{\boldsymbol{\theta}}(\mathbf{z}_t, t)$ has not been trained on $t \in [0, \epsilon)$, keep denoising up to the zero diffusion time would harm the sample fidelity. If t_{min} is the stopping diffusion time of the ODE, one predictor step from t_{min} to 0 is applied to the noised sample, $\mathbf{z}_{t_{min}}$, in order to eliminate the residual noise in $\mathbf{z}_{t_{min}}$ to $\mathbf{z}_0$ [62]. Table 13 searches the optimal stopping diffusion time, and it shows that the truncation time (10^{-5}) turns out to be the optimal stopping time. Throughout the paper, we report the FID (ODE) performance of our INDM with the training truncation time (10^{-5}). For VESDE, the ODE sampler fails to generate realistic images, so we do not report sample generation performance.

In PC sampler, for the predictor, we use the Reverse Diffusion Predictor for VESDE and the Euler-Maruyama Predictor for VPSDE. For the corrector, we use the Langevin dynamics [63] for VESDE, and we do not use any corrector for VPSDE. We use 1) Signal-to-Noise Ratio (SNR) scheduling, 2) temperature scheduling, 3) stopping time scheduling, and 4) data-adaptive prior than a fixed prior to improve FID. First, Table 14 presents that the optimal SNR is 0.14, which is slightly different from the optimal SNR of 0.16 in the linear diffusion [1]. We use SNR of 0.14 as default in our PC sampling.

Figure 16: Ablation study for the flow temperature.

Table 15: Ablation study on the temperature for PC sampler trained on DDPM++ (VP) in CIFAR-10. The performances are FID scores. Contrary to Kingma and Dhariwal [56], the temperature bigger than 1 works the best.

Model	Temperature					
	1	1.03	1.04	1.05	1.1	1.2
INDM (VP, FID)	2.92	2.91	2.90	2.90	2.91	3.09

Table 16: Ablation study on the final denoising step trained on VESDE in CIFAR-10. The performances are FID scores.

Model	FID ($\mathbf{x}_{\epsilon}$)	FID ($\mathbf{x}_{-0.25}$)	FID ($\mathbf{x}_{-0.5}$)	FID ($\mathbf{x}_{-0.75}$)	FID ($\mathbf{x}_{-1}$)	FID ($\mathbf{x}_{-1.5}$)	FID ($\mathbf{x}_{-\infty}$)
NCSN++ (VE, FID)	11.7	8.40	40.8	65.7	85.8	118	2.46
INDM (VE, FID)	2.40	2.33	2.31	2.29	2.29	2.34	2.37
INDM (VE, deep, FID)	2.35	2.29	2.28	2.29	2.29	2.36	2.33

Second, as introduced in Kingma and Dhariwal [56], we scale the generated latent, $\mathbf{z}_0^{\boldsymbol{\theta}}$, by multiplying the temperature. Table 15 presents that the optimal temperature for VPSDE is $1.04 \sim 1.05$ in terms of FID on INDM (VP, FID) setting. We use the temperature of 1 for the remaining settings except INDM (VP, FID). With temperature τ, the normalizing flow puts its latent input scaled by τ to the flow network. In Figure 16, the image color with a higher temperature tends to be brighter, and we find that the optimal temperature depends on the experimental settings.

Third, the stopping time scheduling is a method that manipulate the final denoising step. To attain the variance of VESDE as $\sigma^2(t) = \sigma_{min}^2(\frac{\sigma_{max}^2}{\sigma_{min}^2})^{2t}$, we should start the diffusion process of $\mathrm{d}\mathbf{z}_t = \sigma^2(t)\,\mathrm{d}\mathbf{w}_t$ at $t = -\infty$ because

$$\sigma^2(t) = \int_{t_0}^{t} g^2(s)\,\mathrm{d}s = \sigma_{min}^2\left(\frac{\sigma_{max}^2}{\sigma_{min}^2}\right)^{2t} \tag{41}$$

implies $t_0 = -\infty$. If the generative SDE is $\mathrm{d}\mathbf{z}_t = g^2(t)\mathbf{s}_{\boldsymbol{\theta}}(\mathbf{z}_t, t)\,\mathrm{d}\bar{t} + \sigma^2(t)\,\mathrm{d}\bar{\mathbf{w}}_t$, then the Euler-Maruyama discretization is

$$\mathbf{z}_{t_i} \leftarrow \mathbf{z}_{t_{i+1}} + g^2(t_{i+1})(t_i - t_{i+1})\mathbf{s}_{\boldsymbol{\theta}}(\mathbf{z}_{t_{i+1}}, t_{i+1}) + \sqrt{\sigma(t_{i+1})^2 - \sigma(t_i)^2}\boldsymbol{\epsilon}, \tag{42}$$

where $\boldsymbol{\epsilon} \sim \mathcal{N}(0, \mathbf{I})$. However, since the initial time of VESDE is $t = -\infty$, denoising the noised sample with the Euler-Maruyama discretization would incur arbitrary large error at the final step that denoises from $t = \epsilon$ to $t = -\infty$. Therefore, Song et al. [1] suggested the reverse diffusion predictor that denoises by

$$\mathbf{z}_{\sigma^{-1}(\sigma_i)} \leftarrow \mathbf{z}_{\sigma^{-1}(\sigma_{i+1})} + (\sigma_{i+1}^2 - \sigma_i^2)\mathbf{s}_{\boldsymbol{\theta}}(\mathbf{z}_{\sigma^{-1}(\sigma_{i+1})}, \sigma_{i+1}) + \sqrt{\sigma_{i+1}^2 - \sigma_i^2}\boldsymbol{\epsilon}, \tag{43}$$

which is equivalent to the Euler-Maruyama discretization if $t_i - t_{i+1}$ is small enough (because $\Delta\sigma^2(t) \approx g^2(t)\Delta t$ by Eq. (41)). The difference of Eqs. (42) and (43) is minor as long as we denoise on the range of $[\epsilon, T]$, but only Eq. (43) enables to denoise from $t = \epsilon$ to $t = -\infty$.

However, it turns out that the direction of the score network is not aligned to the direction of the data score near $t \approx 0$, so $\mathbf{s}_{\boldsymbol{\theta}}(\mathbf{z}_{\epsilon}, \sigma_{min})$ would not be accurate enough to the perturbed data score. Therefore, the final denoising step of

$$\mathbf{z}_{-\infty} \leftarrow \mathbf{z}_{\epsilon} + \sigma_{min}^2\mathbf{s}_{\boldsymbol{\theta}}(\mathbf{z}_{\epsilon}, \sigma_{min}) + \sigma_{min}\boldsymbol{\epsilon},$$

might not be mostly effective. This leads us to try the final step as

$$\mathbf{z}_{\epsilon-\delta} = \mathbf{z}_{\epsilon} + \frac{1}{2}\Big(\sigma^2(\epsilon) - \sigma^2(\epsilon - \delta)\Big)\mathbf{s}_{\boldsymbol{\theta}}(\mathbf{z}_{\epsilon}, \sigma_{min}),$$

for various $\delta \geq 0$. After the denoising up to $\mathbf{z}_{\epsilon-\delta}$, we apply the inverse of the flow network to obtain $\mathbf{x}_{\epsilon-\delta} = \mathbf{h}_{\boldsymbol{\phi}}^{-1}(\mathbf{z}_{\epsilon-\delta})$, and Table 16 presents that there is a sweet spot ($\mathbf{x}_{-0.5} \sim \mathbf{x}_{-0.75}$) that works the best in terms of FID. We report the line searched FID performance for each of VESDE setting.

Lastly, we use $p_T^{\boldsymbol{\phi}}$ instead of π to sample from INDM (VE). This data-adaptive prior is particularly beneficial on the experiment of VESDE. In INDM (VE), the data-adaptive prior reduces FID-5k

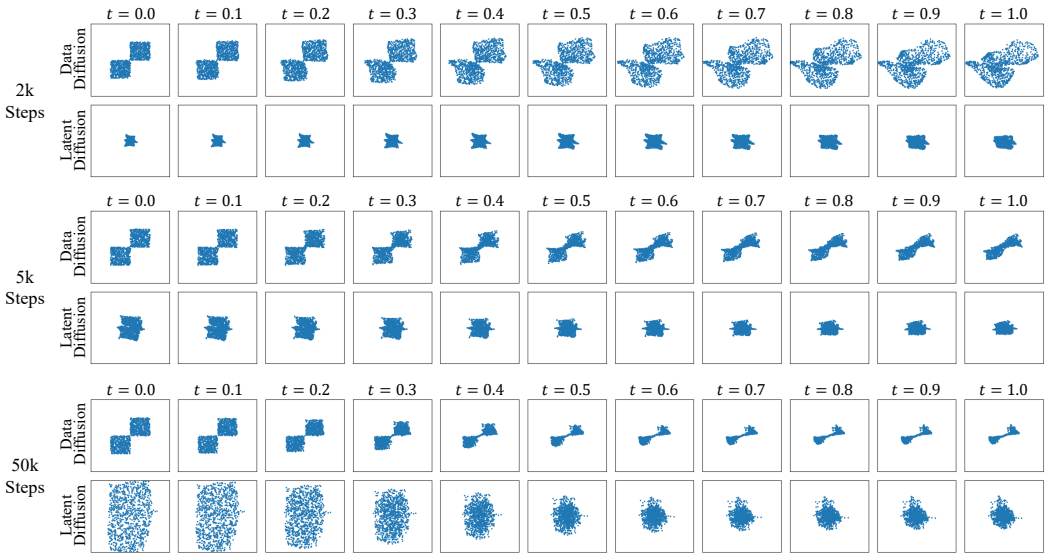

Figure 17: Comparison of data and latent diffusions by training steps of Checkerboard.

from 8.14 to 7.52, so we use this technique by default throughout out performance report. In INDM (VP), this technique is not effective, and we use the vanilla prior distribution. The reason why the data-adaptive prior is effective in VESDE is because the discrepancy of VESDE between p_T^{ϕ} and π is significantly larger than VPSDE, see Figure 5 of Chen et al. [16].

We compute FID [18] for CIFAR-10 based on the statistics released by Song et al. [1][2], which used the modified Inception V1 network[3] in order to compare INDM to the baselines [1, 11] in a fair setting. On the other hand, for the CelebA dataset, we compute the clean-FID [64] that provides consistently antialiased performance.

F.2.3 Interpolation Task

For the interpolation task, we provide the line-by-line algorithm in Algorithm 2. We train with the likelihood weighting as default for our experiment on the dataset interpolation. The interpolation loss of $\mathcal{L}_{int}$ consumes 0.2Gb of GPU memory, and the INDM loss of $\mathcal{L}_{INDM}$ takes 2.5Gb of GPU memory in the EMNIST-MNIST experiment.

Algorithm 2 Data Interpolation of INDM

1: **repeat**
2: Compute $\mathcal{L}_{INDM} = \mathcal{L}(\{\mathbf{x}_t\}_{t=0}^T, g^2; \{\boldsymbol{\phi}, \boldsymbol{\theta}\})$ for $\mathbf{x}_0 \sim p_r^{(1)}$
3: Compute $\mathcal{L}_{int} = \mathbb{E}_{p_r^{(2)}}[-\log p_{\boldsymbol{\phi}}(\mathbf{y})]$ for $\mathbf{y} \sim p_r^{(2)}$
4: Compute $\mathcal{L}_{tot} = \mathcal{L}_{INDM} + \mathcal{L}_{int}$
5: Update $\boldsymbol{\phi} \leftarrow \boldsymbol{\phi} - \frac{\partial \mathcal{L}_{tot}}{\partial \boldsymbol{\phi}}$
6: Update $\boldsymbol{\theta} \leftarrow \boldsymbol{\theta} - \frac{\partial \mathcal{L}_{tot}}{\partial \boldsymbol{\theta}}$
7: **until** converged

F.3 Effect of Pre-training

We find that training INDM with a pre-trained score network of linear diffusion models improves FID. Table 17 conducts the ablation study on the number of pre-training steps. We

Table 17: Ablation study on pre-training.

# Pre-training Steps	100k	200k	300k	400k	500k
NLL	3.00	2.99	2.99	2.99	2.98
FID	7.39	7.31	6.80	6.65	6.22

[2] https://github.com/yang-song/score_sde_pytorch
[3] https://tfhub.dev/tensorflow/tfgan/eval/inception/1

Table 18: Elapsed time per a training step by discretization.

Model	Complexity	$N = 100$	$N = 1,000$	$N = \infty$
DDPM	$O(1)$	0.27	0.27	0.27
SBP (w/o experience memory)	$O(N)$	2.83	23.3	∞
SBP (w/ experience memory)	$O(N)$	0.52	2.39	∞
DiffFlow	$O(N)$	18.45	180.88	∞
INDM	$O(1)$	1.69	1.69	1.69

Table 19: Total training time in a single GPU days.

Model	Total Training Time (GPU Days)	Training Steps	GPU Spec	#GPUs	NLL	FID
DDPM++	5	500k	P40	1	3.03	6.70
LSGM	44	450k	RTX 3090	8	2.87	6.89
SBP	3	260k	RTX 3090	-	2.98	3.18
DiffFlow	32	100k	RTX 2080	8	3.04	14.14
INDM (including pre-training time)	25	700k	P40	4	2.98	6.01
INDM (w/o pre-training)	60	600k	P40	4	2.98	8.49

pre-train the score network with DDPM++ (VP, NLL) for five variations of pre-training steps (100k/200k/300k/400k/500k), and we train flow+score networks for 350k steps further with NLL setting ($\lambda = g^2$). Table 17 empirically demonstrates that it is better to search the nonlinearity of the data process near the linear process. For this clear empirical advantage of pre-training, we report the quantitative performances in Section 7 with pre-training.

F.4 Training Time

Table 18 presents the elapsed time per a training step by the number of discretization on CIFAR-10. In contrast to INDM which is invariant on the choice of N, the training time of SBP and DiffFlow is not scalable for their $O(N)$ complexities. The training time is measured under the identical computing resource (1x NVIDIA RTX 3090/Intel I7 3.8GHz) and the same batch size (32) to compare INDM with baselines in a fair setting.

Table 19 compares INDM with baselines with respect to a single GPU-time for the total training time on CIFAR-10. The remaining columns including training steps, GPU Spec, NLL, and FID are reported for the reference. For DiffFlow, we present the reported GPU days in the paper. For LSGM and SBP, we estimate the elapsed time with the released training configuration in their papers and GitHub repositories. For DDPM++ and INDM, we report the elapsed time from our own experiments. From the table, the overall training time of INDM/DiffFlow/LSGM remains at a similar scale. SBP is the fastest algorithm because of the experience replay memory technique. Note that a completely fair comparison between algorithms is infeasible because the training setup (e.g. #GPUs, training steps, network size ...) varies by algorithms. Also, P40 is strictly slower than RTX series GPUs.

F.5 Visualization of Latent

F.5.1 Visualization of 2d Latent Manifold

Figure 17 illustrates the data and latent manifolds of the 2d checkerboard dataset by training steps. The data manifold has the singularity at the origin, but this singularity disappears in the latent manifold after the training.

F.5.2 Visualization of High-dimensional Latent Vector on Benchmark Datasets

Figure 18 illustrates the samples from (a) the data space and (b) the latent space. To visualize the latent vectors, we normalize the latent value into the $[0, 1]^d$ space.

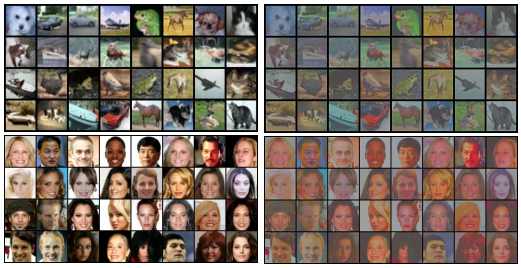

(a) Samples from $\mathbf{x}_0^{\phi,\theta}$ (b) Samples from $\mathbf{z}_0^{\theta}$

Figure 18: Samples from the data space and latent space on CIFAR-10 and CelebA.

F.6 Nonlinear Diffusion Coefficient

INDM trains the volatility term, $\mathbf{G}_{\phi}$, which was fixed across previous research, except LSGM. The exact form of $\mathbf{G}_{\phi}$ in LSGM, however, is not derivable, so we exclude comparing LSGM in this section. As stated in Section 3, the noise distribution of a diffusion process is $\mathcal{N}(0, \mathbf{G}(\mathbf{x}_t, t)\mathbf{G}^T(\mathbf{x}_t, t))$, which is anisotropic by the input data, $\mathbf{x}_t$, and time, t. The influence of diffusion time on this covariance matrix is illustrated in Figure 19-(a). It presents the box plot of the eigenvalue distribution of the (normalized) covariance, $\mathbf{G}_{\phi}(\mathbf{x}_t, t)\mathbf{G}_{\phi}^T(\mathbf{x}_t, t)/g^2(t)$, on CIFAR-10, from $t = 0$ to $t = T$. All the eigenvalues of previous research collapse to one as they share the isotropic covariance matrix, $g^2(t)\mathbf{I}$. On the other hand, the eigenvalues of INDM is dispersive throughout the diffusion time. As the distribution becomes more dispersive, the covariance matrix becomes more unisotropic, and Figure 19-(a) implies that the learnt diffusion process is under a highly nonlinear noise perturbation in a range of large diffusion time. The covariance matrix also depends on the input data, and Figure 19-(b) illustrates the eigenvalue distribution of the covariance at distinctive data instances of $\mathbf{x}_t$ at $t = 0$. The eigenvalue distribution varies by instance, implying that data is diffused inhomogeneously by its location.

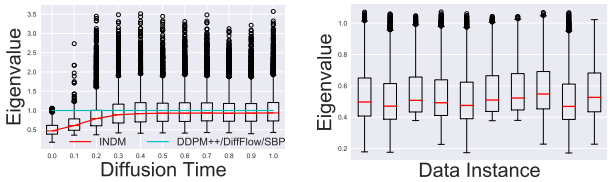

(a) Eigenvalue by t (b) Eigenvalue by $\mathbf{x}_t$

Figure 19: Eigenvalue of $\mathbf{G}\mathbf{G}^T/g^2$ on CIFAR-10.

F.7 Relative Energy

Each flow network parameter constructs a different latent trajectory, so training the flow network has the effect of shifting the diffusion bridge. To check if learning the flow network is helpful for the transportation cost or not, recall the Benamou-Brenier formula [65, 66], which is a dual formulation of the Wasserstein distance [66, 67] that the optimal transportation cost is the least kinetic energy out of all admissible transportation plans: $W_2^2(p, q) = \inf_{\{p_t, \mathbf{v}_t\}_t} \Big\{ \mathcal{K}(\{p_t, \mathbf{v}_t\}_t); \underbrace{\frac{\partial p_t}{\partial t} + \mathrm{div}(p_t \mathbf{v}_t) = 0}_{\text{continuity equation}}, \underbrace{p_0 = p, p_T = q}_{\text{boundary conditions}} \Big\}$, where $\mathcal{K}(\{p_t, \mathbf{v}_t\}_t) := \int_0^T \int p_t(\mathbf{x}) \|\mathbf{v}_t(\mathbf{x})\|_2^2 \, \mathrm{d}\mathbf{x} \, \mathrm{d}t / T$ is the kinetic energy of the transportation. The continuity equation (that guarantees the conservation of mass along time transition [68]) and the boundary conditions determine the set of admissible trajectories, and the forward diffusion constructs an admissible trajectory. We *quantify* how much a trajectory is close to the optimal transport as the *relative* energy, given by $R(\phi) = \frac{\mathcal{K}(\{p_t^{\phi}, \mathbf{v}_t^{\phi}\}_t)}{W_2^2(p_0^{\phi}, p_T^{\phi})}$. Table 20 shows that INDM's latent diffusion is more close to the optimal transport than DDPM++ on CIFAR-10.

Table 20: *Relative* Energy.

Model	*Relative* Energy
DDPM++	1.60
INDM	1.23

F.8 Full Quantitative Tables

Tables 21, 22, and 23 gives the full details of the quantitative comparisons to baseline models.

F.9 Random samples

Figures 20 and 21 show the non cherry-picked random samples from INDM (VE, FID) on CIFAR-10 and INDM (VP, FID) on CelebA, respectively.

G Proofs of Theorems and Propositions

Theorem 1. *Suppose that $p_{\phi,\theta}(\mathbf{x}_0)$ is the likelihood of a generative random variable $\mathbf{x}_0^{\phi,\theta}$. Then, the negative log-likelihood is bounded by*

$$\mathbb{E}_{p_r(\mathbf{x}_0)}\big[-\log p_{\phi,\theta}(\mathbf{x}_0)\big] \leq \mathcal{L}\big(\{\mathbf{x}_t\}_{t=0}^T, g^2; \{\phi, \theta\}\big),$$

where

$$\mathcal{L}\big(\{\mathbf{x}_t\}_{t=0}^T, g^2; \{\boldsymbol{\phi}, \boldsymbol{\theta}\}\big) = -\mathbb{E}_{p_r(\mathbf{x}_0)}\big[\log\big|\det\big(\nabla_{\mathbf{x}_0}\mathbf{h}_{\boldsymbol{\phi}}\big)\big|\big] + \mathcal{L}\big(\{\mathbf{z}_t\}_{t=0}^T, g^2; \boldsymbol{\theta}\big) - \mathbb{E}_{\mathbf{z}_T}\big[\log \pi(\mathbf{z}_T)\big] + \frac{d}{2}\int_0^T \beta(t) - \frac{g^2(t)}{\sigma^2(t)}\,\mathrm{d}t,$$

with $\mathcal{L}\big(\{\mathbf{z}_t\}_{t=0}^T, g^2; \boldsymbol{\theta}\big) := \frac{1}{2}\int_0^T g^2(t)\mathbb{E}_{\mathbf{z}_0,\mathbf{z}_t}\big[\|\mathbf{s}_{\boldsymbol{\theta}}(\mathbf{z}_t, t) - \nabla_{\mathbf{z}_t}\log p_{0t}(\mathbf{z}_t|\mathbf{z}_0)\|_2^2\big]\,\mathrm{d}t$. *Here,* $p_{0t}(\mathbf{z}_t|\mathbf{z}_0)$ *is the transition probability of the forward linear diffusion process on latent space.*

Proof of Theorem 1. From the change of variable, the transformation of $\mathbf{z}_0 = \mathbf{h}_{\boldsymbol{\phi}}(\mathbf{x}_0)$ induces

$$p_r(\mathbf{x}_0) = \frac{p_0(\mathbf{z}_0)}{\Big|\det\Big(\frac{\partial \mathbf{h}_{\boldsymbol{\phi}}}{\partial \mathbf{x}_0}\Big)\Big|^{-1}},$$

and thus the entropy of the data distribution becomes

$$\begin{aligned}
\mathcal{H}(p_r) &= -\int p_r(\mathbf{x}_0)\log p_r(\mathbf{x}_0)\,\mathrm{d}\mathbf{x}_0 \\
&= -\int p_0(\mathbf{z}_0)\log\frac{p_0(\mathbf{z}_0)}{\Big|\det\Big(\frac{\partial \mathbf{h}_{\boldsymbol{\phi}}}{\partial \mathbf{x}_0}\Big)\Big|^{-1}}\,\mathrm{d}\mathbf{z}_0 \\
&= -\int p_r(\mathbf{x}_0)\log\Big|\det\Big(\frac{\partial \mathbf{h}_{\boldsymbol{\phi}}}{\partial \mathbf{x}_0}\Big)\Big|\,\mathrm{d}\mathbf{x}_0 - \int p_0(\mathbf{z}_0)\log p_0(\mathbf{z}_0)\,\mathrm{d}\mathbf{z}_0 \\
&= -\mathbb{E}_{p_r(\mathbf{x}_0)}\Big[\log\Big|\det\Big(\frac{\partial \mathbf{h}_{\boldsymbol{\phi}}}{\partial \mathbf{x}_0}\Big)\Big|\Big] - \int p_0(\mathbf{z}_0)\log p_0(\mathbf{z}_0)\,\mathrm{d}\mathbf{z}_0 \\
&= -\mathbb{E}_{p_r(\mathbf{x}_0)}\Big[\log\Big|\det\Big(\frac{\partial \mathbf{h}_{\boldsymbol{\phi}}}{\partial \mathbf{x}_0}\Big)\Big|\Big] + \mathcal{H}(p_0).
\end{aligned}$$

From Theorem 4 of Song et al. [11], the entropy at $t = 0$ equals to

$$\mathcal{H}(p_0) = \mathcal{H}(p_T) - \frac{1}{2}\int_0^T \mathbb{E}_{p_t(\mathbf{z}_t)}\big[2\nabla_{\mathbf{z}_t}\cdot\mathbf{f}(\mathbf{z}_t, t) + g^2(t)\|\nabla_{\mathbf{z}_t}\log p_t(\mathbf{z}_t)\|_2^2\big]\,\mathrm{d}t,$$

where $\mathbf{f}(\mathbf{z}_t, t)$ is a drift term of the diffusion for $\mathbf{z}_t$ and p_t is the probability distribution of $\mathbf{z}_t$. Therefore, the negative log-likelihood becomes

$$\begin{aligned}
-\mathbb{E}_{p_r(\mathbf{x}_0)}\big[\log p_{\boldsymbol{\phi},\boldsymbol{\theta}}(\mathbf{x}_0)\big] &= D_{KL}(p_r\|p_{\boldsymbol{\phi},\boldsymbol{\theta}}) + \mathcal{H}(p_r) \\
&\le D_{KL}(\boldsymbol{\mu}_{\boldsymbol{\phi}}(\{\mathbf{x}_t\})\|\boldsymbol{\nu}_{\boldsymbol{\phi},\boldsymbol{\theta}}(\{\mathbf{x}_t\})) + \mathcal{H}(p_r) \\
&= D_{KL}(\boldsymbol{\mu}_{\boldsymbol{\phi}}(\{\mathbf{x}_t\})\|\boldsymbol{\nu}_{\boldsymbol{\phi},\boldsymbol{\theta}}(\{\mathbf{x}_t\})) - \mathbb{E}_{p_r(\mathbf{x}_0)}\Big[\log\Big|\det\Big(\frac{\partial \mathbf{h}_{\boldsymbol{\phi}}}{\partial \mathbf{x}_0}\Big)\Big|\Big] + \mathcal{H}(p_0) \\
&= D_{KL}(\boldsymbol{\mu}_{\boldsymbol{\phi}}(\{\mathbf{z}_t\})\|\boldsymbol{\nu}_{\boldsymbol{\theta}}(\{\mathbf{z}_t\})) - \mathbb{E}_{p_r(\mathbf{x}_0)}\Big[\log\Big|\det\Big(\frac{\partial \mathbf{h}_{\boldsymbol{\phi}}}{\partial \mathbf{x}_0}\Big)\Big|\Big] + \mathcal{H}(p_T) \\
&\quad -\frac{1}{2}\int_0^T \mathbb{E}_{\mathbf{z}_t^{\boldsymbol{\phi}}}\big[-d\beta(t) + g^2(t)\|\nabla_{\mathbf{z}_t}\log p_t(\mathbf{z}_t)\|_2^2\big]\,\mathrm{d}t.
\end{aligned}$$

Now, from Theorem 1 of [11], the KL-divergence between the path measures becomes

$$D_{KL}(\boldsymbol{\mu}_{\boldsymbol{\phi}}(\{\mathbf{z}_t\})\|\boldsymbol{\nu}_{\boldsymbol{\theta}}(\{\mathbf{z}_t\})) = D_{KL}(p_T(\mathbf{z}_T)\|\pi(\mathbf{z}_T)) \tag{44}$$

$$+ \frac{1}{2}\int_0^T g^2(t)\mathbb{E}_{p_t(\mathbf{z}_t)}\big[\|\mathbf{s}_{\boldsymbol{\theta}}(\mathbf{z}_t, t) - \nabla_{\mathbf{z}_t}\log p_t(\mathbf{z}_t)\|_2^2\big]\,\mathrm{d}t, \tag{45}$$

so if we plug in this into the negative log-likelihood, we yield the following:

$$\begin{aligned}
&-\mathbb{E}_{p_r(\mathbf{x}_0)}\big[\log p_{\boldsymbol{\phi},\boldsymbol{\theta}}(\mathbf{x}_0)\big] \\
&\quad\le -\mathbb{E}_{p_r(\mathbf{x}_0)}\Big[\log\Big|\det\Big(\frac{\partial \mathbf{h}_{\boldsymbol{\phi}}}{\partial \mathbf{x}_0}\Big)\Big|\Big] + \frac{1}{2}\int_0^T g^2(t)\mathbb{E}_{\mathbf{z}_t}\big[\|\mathbf{s}_{\boldsymbol{\theta}}(\mathbf{z}_t, t) - \nabla_{\mathbf{z}_t}\log p_t(\mathbf{z}_t)\|_2^2\big]\,\mathrm{d}t
\end{aligned}$$

$$
\begin{aligned}
&+D_{KL}(p_T\|\pi)+\mathcal{H}(p_T)-\frac{1}{2}\int_0^T \mathbb{E}_{\mathbf{z}_t}\big[-d\beta(t)+g^2(t)\|\nabla_{\mathbf{z}_t}\log p_t(\mathbf{z}_t)\|_2^2\big]\,\mathrm{d}t\\
=&-\mathbb{E}_{p_r(\mathbf{x}_0)}\Big[\log\Big|\det\Big(\frac{\partial \mathbf{h}_{\boldsymbol{\phi}}}{\partial \mathbf{x}_0}\Big)\Big|\Big]-\mathbb{E}_{\mathbf{z}_T}\big[\log\pi(\mathbf{z}_T)\big]+\frac{d}{2}\int_0^T\beta(t)\,\mathrm{d}t\\
&+\frac{1}{2}\int_0^T g^2(t)\mathbb{E}_{\mathbf{z}_t}\big[\|\mathbf{s}_{\boldsymbol{\theta}}(\mathbf{z}_t,t)-\nabla_{\mathbf{z}_t}\log p_t(\mathbf{z}_t)\|_2^2-\|\nabla_{\mathbf{z}_t}\log p_t(\mathbf{z}_t)\|_2^2\big]\,\mathrm{d}t
\end{aligned}
$$

Also, we have

$$
\begin{aligned}
\mathbb{E}_{\mathbf{z}_t}\big[\mathbf{s}_{\boldsymbol{\theta}}(\mathbf{z}_t,t)\cdot\nabla_{\mathbf{z}_t}\log p_t(\mathbf{z}_t)\big]&=\int p_t(\mathbf{z}_t)\mathbf{s}_{\boldsymbol{\theta}}(\mathbf{z}_t,t)\cdot\nabla_{\mathbf{z}_t}\log p_t(\mathbf{z}_t)\,\mathrm{d}\mathbf{z}_t\\
&=\int \mathbf{s}_{\boldsymbol{\theta}}(\mathbf{z}_t,t)\cdot\nabla_{\mathbf{z}_t}p_t(\mathbf{z}_t)\,\mathrm{d}\mathbf{z}_t\\
&=\int \mathbf{s}_{\boldsymbol{\theta}}(\mathbf{z}_t,t)\cdot\int p_0(\mathbf{z}_0)\nabla_{\mathbf{z}_t}p_{0t}(\mathbf{z}_t|\mathbf{z}_0)\,\mathrm{d}\mathbf{z}_0\,\mathrm{d}\mathbf{z}_t\\
&=\mathbb{E}_{\mathbf{z}_0}\mathbb{E}_{\mathbf{z}_t|\mathbf{z}_0}\big[\mathbf{s}_{\boldsymbol{\theta}}(\mathbf{z}_t,t)\cdot\nabla_{\mathbf{z}_t}\log p_{0t}(\mathbf{z}_t|\mathbf{z}_0)\big]
\end{aligned}
$$

Therefore,

$$
\begin{aligned}
&\frac{1}{2}\int_0^T g^2(t)\mathbb{E}_{\mathbf{z}_t}\big[\|\mathbf{s}_{\boldsymbol{\theta}}(\mathbf{z}_t,t)-\nabla_{\mathbf{z}_t}\log p_t(\mathbf{z}_t)\|_2^2-\|\nabla_{\mathbf{z}_t}\log p_t(\mathbf{z}_t)\|_2^2\big]\\
&=\int_0^T g^2(t)\mathbb{E}_{\mathbf{z}_t}\Big[\frac{1}{2}\|\mathbf{s}_{\boldsymbol{\theta}}(\mathbf{z}_t,t)\|_2^2-\mathbf{s}_{\boldsymbol{\theta}}(\mathbf{z}_t,t)\cdot\nabla_{\mathbf{z}_t}\log p_t(\mathbf{z}_t)\Big]\\
&=\int_0^T g^2(t)\mathbb{E}_{\mathbf{z}_0}\mathbb{E}_{\mathbf{z}_t|\mathbf{z}_0}\Big[\frac{1}{2}\|\mathbf{s}_{\boldsymbol{\theta}}(\mathbf{z}_t,t)\|_2^2-\mathbf{s}_{\boldsymbol{\theta}}(\mathbf{z}_t,t)\cdot\nabla_{\mathbf{z}_t}\log p_{0t}(\mathbf{z}_t|\mathbf{z}_0)\Big]\\
&=\frac{1}{2}\int_0^T g^2(t)\mathbb{E}_{\mathbf{z}_0}\mathbb{E}_{\mathbf{z}_t|\mathbf{z}_0}\Big[\|\mathbf{s}_{\boldsymbol{\theta}}(\mathbf{z}_t,t)-\nabla_{\mathbf{z}_t}\log p_{0t}(\mathbf{z}_t|\mathbf{z}_0)\|_2^2-\|\nabla_{\mathbf{z}_t}\log p_{0t}(\mathbf{z}_t|\mathbf{z}_0)\|_2^2\Big].
\end{aligned}
$$

Now, since $p_{0t}(\mathbf{z}_t|\mathbf{z}_0)=\mathcal{N}(\mathbf{z}_t;\mu(t)\mathbf{z}_t,\sigma^2(t)\mathbf{I})$ for $\mu(t)$ and $\sigma^2(t)$ determined by $\beta(t)$ and $g(t)$, we have

$$
\mathbb{E}_{\mathbf{z}_t|\mathbf{z}_0}\big[\|\nabla_{\mathbf{z}_t}\log p_{0t}(\mathbf{z}_t|\mathbf{z}_0)\|_2^2\big]=\mathbb{E}_{\mathbf{z}_t|\mathbf{z}_0}\Big[\Big\|\frac{\mathbf{z}_t-\mu(t)\mathbf{z}_0}{\sigma^2(t)}\Big\|_2^2\Big]=\mathbb{E}_{\mathcal{N}(\mathbf{z};0,\mathbf{I})}\Big[\frac{\|\mathbf{z}\|_2^2}{\sigma^2(t)}\Big]=\frac{d}{\sigma^2(t)},
$$

and we have the desired result. □

Proposition 1. *Suppose $q_t^{\boldsymbol{\theta}}$ is the marginal distribution of $\nu_{\boldsymbol{\theta}}$ at t. The variational gap is*

$$
\begin{aligned}
\mathrm{Gap}\big(\boldsymbol{\mu}_{\boldsymbol{\phi}}(\{\mathbf{x}_t\}),\boldsymbol{\nu}_{\boldsymbol{\phi},\boldsymbol{\theta}}(\{\mathbf{x}_t\})\big)&:=D_{KL}\big(\boldsymbol{\mu}_{\boldsymbol{\phi}}(\{\mathbf{x}_t\})\|\boldsymbol{\nu}_{\boldsymbol{\phi},\boldsymbol{\theta}}(\{\mathbf{x}_t\})\big)-D_{KL}\big(p_0^{\boldsymbol{\phi}}(\mathbf{x}_0)\|q_0^{\boldsymbol{\theta}}(\mathbf{x}_0)\big)\\
&=\frac{1}{2}\int_0^T g^2(t)\mathbb{E}_{p_t^{\boldsymbol{\phi}}(\mathbf{z}_t)}\big[\underbrace{\|\nabla\log q_t^{\boldsymbol{\theta}}(\mathbf{z}_t)-\mathbf{s}_{\boldsymbol{\theta}}(\mathbf{z}_t,t)\|_2^2}_{\textit{Score-only error}}\big]\,\mathrm{d}t.
\end{aligned}
$$

Proof of Proposition 1. Suppose $q_t^{\boldsymbol{\theta}}$ is a marginal distribution of the path measure of the generative SDE given by

$$
\mathrm{d}\mathbf{z}_t=\big[\mathbf{f}(\mathbf{z}_t,t)-g^2(t)\mathbf{s}_{\boldsymbol{\theta}}(\mathbf{z}_t,t)\big]\,\mathrm{d}\bar{t}+g(t)\,\mathrm{d}\bar{\mathbf{w}}_t. \tag{46}
$$

The Fokker-Planck equation of the above generative SDE satisfies

$$
\begin{aligned}
\frac{\partial q_t^{\boldsymbol{\theta}}}{\partial t}(\mathbf{z}_t)=&-\sum_{i=1}^d\frac{\partial}{\partial z_i}\Big(\big[f_i(\mathbf{z}_t,t)-g^2(t)\big(\mathbf{s}_{\boldsymbol{\theta}}(\mathbf{z}_t,t)\big)_i\big]\,q_t^{\boldsymbol{\theta}}(\mathbf{z}_t)\Big)-\frac{g^2(t)}{2}\sum_{i=1}^d\frac{\partial^2}{\partial z_i^2}\big[q_t^{\boldsymbol{\theta}}(\mathbf{z}_t)\big]\\
=&\mathrm{div}\left(\Big(-\mathbf{f}(\mathbf{z}_t,t)+g^2(t)\mathbf{s}_{\boldsymbol{\theta}}(\mathbf{z}_t,t)-\frac{g^2(t)}{2}\nabla\log q_t^{\boldsymbol{\theta}}(\mathbf{z}_t)\Big)q_t^{\boldsymbol{\theta}}(\mathbf{z}_t)\right).
\end{aligned} \tag{47}
$$

On the other hand, if $p_t^{\boldsymbol{\phi}}$ is the marginal distribution of the path measure of the forward SDE given by

$$\mathrm{d}\mathbf{z}_t = \mathbf{f}(\mathbf{z}_t, t)\,\mathrm{d}t + g(t)\,\mathrm{d}\mathbf{w}_t,$$

then the corresponding Fokker-Planck equation becomes

$$\frac{\partial p_t^{\boldsymbol{\phi}}}{\partial t}(\mathbf{z}_t) = \operatorname{div}\left(\left(-\mathbf{f}(\mathbf{z}_t, t) + \frac{g^2(t)}{2}\nabla \log p_t^{\boldsymbol{\phi}}(\mathbf{z}_t, t)\right)p_t^{\boldsymbol{\phi}}(\mathbf{z}_t)\right). \tag{48}$$

Combining Eq. (47) with Eq. (48) and using the integration by parts, the derivative of the KL divergence becomes

$$\begin{aligned}
\frac{\partial D_{KL}(p_t^{\boldsymbol{\phi}} \| q_t^{\boldsymbol{\theta}})}{\partial t} &= \frac{\partial}{\partial t}\int p_t^{\boldsymbol{\phi}}(\mathbf{z}_t)\log\frac{p_t^{\boldsymbol{\phi}}(\mathbf{z}_t)}{q_t^{\boldsymbol{\theta}}(\mathbf{z}_t)}\,\mathrm{d}\mathbf{z}_t \\
&= \int \frac{\partial p_t^{\boldsymbol{\phi}}}{\partial t}(\mathbf{z}_t)\log\frac{p_t^{\boldsymbol{\phi}}(\mathbf{z}_t)}{q_t^{\boldsymbol{\theta}}(\mathbf{z}_t)}\,\mathrm{d}\mathbf{z}_t - \int \frac{\partial q_t^{\boldsymbol{\theta}}}{\partial t}(\mathbf{z}_t)\frac{p_t^{\boldsymbol{\phi}}(\mathbf{z}_t)}{q_t^{\boldsymbol{\theta}}(\mathbf{z}_t)}\,\mathrm{d}\mathbf{z}_t \\
&= -\int p_t^{\boldsymbol{\phi}}(\mathbf{z}_t)\left(-\mathbf{f}(\mathbf{z}_t, t) + \frac{g^2(t)}{2}\nabla\log p_t^{\boldsymbol{\phi}}(\mathbf{z}_t)\right)^T \nabla\log\frac{p_t^{\boldsymbol{\phi}}(\mathbf{z}_t)}{q_t^{\boldsymbol{\theta}}(\mathbf{z}_t)}\,\mathrm{d}\mathbf{z}_t \\
&\quad + \int p_t^{\boldsymbol{\phi}}(\mathbf{z}_t)\left(-\mathbf{f}(\mathbf{z}_t, t) + g^2(t)\mathbf{s}_{\boldsymbol{\theta}}(\mathbf{z}_t, t) - \frac{g^2(t)}{2}\nabla\log q_t^{\boldsymbol{\theta}}(\mathbf{z}_t)\right)^T \nabla\log\frac{p_t^{\boldsymbol{\phi}}(\mathbf{z}_t)}{q_t^{\boldsymbol{\theta}}(\mathbf{z}_t)}\,\mathrm{d}\mathbf{z}_t \\
&= \frac{g^2(t)}{2}\int p_t^{\boldsymbol{\phi}}(\mathbf{z}_t)\left(\nabla\log\frac{p_t^{\boldsymbol{\phi}}(\mathbf{z}_t)}{q_t^{\boldsymbol{\theta}}(\mathbf{z}_t)}\right)^T\left(2\mathbf{s}_{\boldsymbol{\theta}}(\mathbf{z}_t, t) - \nabla\log p_t^{\boldsymbol{\phi}}(\mathbf{z}_t) - \nabla\log q_t^{\boldsymbol{\theta}}(\mathbf{z}_t)\right)\mathrm{d}\mathbf{z}_t.
\end{aligned}$$

Integrating the above derivative, we get the KL divergence of

$$\begin{aligned}
D_{KL}\big(p_0^{\boldsymbol{\phi}}(\mathbf{z}_0)\|q_0^{\boldsymbol{\theta}}(\mathbf{z}_0)\big) &= -\int_0^T \frac{\partial D_{KL}(p_t^{\boldsymbol{\phi}}\|q_t^{\boldsymbol{\theta}})}{\partial t}\,\mathrm{d}t + D_{KL}(p_T^{\boldsymbol{\phi}}\|q_T^{\boldsymbol{\theta}}) \\
&= \int_0^T \frac{g^2(t)}{2}\mathbb{E}_{\mathbf{z}_t^{\boldsymbol{\phi}}}\left[(\nabla\log p_t^{\boldsymbol{\phi}} - \nabla\log q_t^{\boldsymbol{\theta}})^T(\nabla\log p_t^{\boldsymbol{\phi}} + \nabla\log q_t^{\boldsymbol{\theta}} - 2\mathbf{s}_{\boldsymbol{\theta}})\right]\mathrm{d}t + D_{KL}(p_T^{\boldsymbol{\phi}}\|q_T^{\boldsymbol{\theta}}).
\end{aligned} \tag{49}$$

Also, from Eq. (44), we have

$$\begin{aligned}
D_{KL}\big(\boldsymbol{\mu}_{\boldsymbol{\phi}}(\{\mathbf{x}_t\})\|\boldsymbol{\nu}_{\boldsymbol{\phi},\boldsymbol{\theta}}(\{\mathbf{x}_t\})\big) &= D_{KL}\big(\boldsymbol{\mu}_{\boldsymbol{\phi}}(\{\mathbf{z}_t\})\|\boldsymbol{\nu}_{\boldsymbol{\theta}}(\{\mathbf{z}_t\})\big) \\
&= \int_0^T \frac{g^2(t)}{2}\mathbb{E}_{p_t^{\boldsymbol{\phi}}(\mathbf{z}_t)}\left[\|\nabla\log p_t^{\boldsymbol{\phi}}(\mathbf{z}_t) - \mathbf{s}_{\boldsymbol{\theta}}(\mathbf{z}_t, t)\|_2^2\right]\mathrm{d}t + D_{KL}(p_T^{\boldsymbol{\phi}}\|q_T^{\boldsymbol{\theta}}).
\end{aligned} \tag{50}$$

By subtracting Eq. (49) from Eq. (50), we get the desired result:

$$\begin{aligned}
&\mathrm{Gap}(\boldsymbol{\mu}_{\boldsymbol{\phi}}, \boldsymbol{\nu}_{\boldsymbol{\phi},\boldsymbol{\theta}}) = D_{KL}\big(\boldsymbol{\mu}_{\boldsymbol{\phi}}(\{\mathbf{x}_t\})\|\boldsymbol{\nu}_{\boldsymbol{\phi},\boldsymbol{\theta}}(\{\mathbf{x}_t\})\big) - D_{KL}\big(p_r(\mathbf{x}_0)\|p_{\boldsymbol{\phi},\boldsymbol{\theta}}(\mathbf{x}_0)\big) \\
&= D_{KL}\big(\boldsymbol{\mu}_{\boldsymbol{\phi}}(\{\mathbf{z}_t\})\|\boldsymbol{\nu}_{\boldsymbol{\theta}}(\{\mathbf{z}_t\})\big) - D_{KL}\big(p_0^{\boldsymbol{\phi}}(\mathbf{z}_0)\|q_0^{\boldsymbol{\theta}}(\mathbf{z}_0)\big) \\
&= \int \frac{g^2(t)}{2}\mathbb{E}_{\mathbf{z}_t^{\boldsymbol{\phi}}}\left[\|\nabla\log p_t^{\boldsymbol{\phi}} - \mathbf{s}_{\boldsymbol{\theta}}\|_2^2 - (\nabla\log p_t^{\boldsymbol{\phi}} - \nabla\log q_t^{\boldsymbol{\theta}})^T(\nabla\log p_t^{\boldsymbol{\phi}} + \nabla\log q_t^{\boldsymbol{\theta}} - 2\mathbf{s}_{\boldsymbol{\theta}})\right]\mathrm{d}t \\
&= \int \frac{g^2(t)}{2}\mathbb{E}_{p_t^{\boldsymbol{\phi}}(\mathbf{z}_t)}\left[\|\nabla\log q_t^{\boldsymbol{\theta}} - \mathbf{s}_{\boldsymbol{\theta}}\|_2^2\right]\mathrm{d}t.
\end{aligned}$$

□

Theorem 2. $\mathrm{Gap}(\boldsymbol{\mu}_{\boldsymbol{\phi}}, \boldsymbol{\nu}_{\boldsymbol{\phi},\boldsymbol{\theta}}) = 0$ *if and only if* $\mathbf{s}_{\boldsymbol{\theta}} \in \mathbf{S}_{sol}$.

Proof of Theorem 2. ($\Rightarrow$) Suppose the variational gap is zero. Then, as the support of $p_t^{\boldsymbol{\phi}}$ is the whole space of $\mathbb{R}^d$, Theorem 1 implies that $\mathbf{s}_{\boldsymbol{\theta}}(\mathbf{z}_t, t) = \nabla\log q_t^{\boldsymbol{\theta}}(\mathbf{z}_t)$ almost everywhere, for any $t > 0$. To check if $\mathbf{s}_{\boldsymbol{\theta}}(\mathbf{z}_0, 0) = \nabla\log q_0^{\boldsymbol{\theta}}(\mathbf{z}_0)$ at $t = 0$, suppose $\mathbf{s}_{\boldsymbol{\theta}}(\mathbf{z}_0, 0) \neq \nabla\log q_0^{\boldsymbol{\theta}}(\mathbf{z}_0)$ on a set of positive measure. Then, from the continuity of $\mathbf{s}_{\boldsymbol{\theta}}$ and $\nabla\log q_t^{\boldsymbol{\theta}}$, we have $\mathbf{s}_{\boldsymbol{\theta}}(\mathbf{z}_s, s) \neq \nabla\log q_s^{\boldsymbol{\theta}}(\mathbf{z}_s)$

on $s < t_0$ for some t_0. Therefore, for any $t \in [0, T]$, we conclude that $\mathbf{s}_{\boldsymbol{\theta}}(\mathbf{z}_t, t) = \nabla \log q_t^{\boldsymbol{\theta}}(\mathbf{z}_t)$ almost everywhere and Eq. (46) becomes

$$\mathrm{d}\mathbf{z}_t = \left[\mathbf{f}(\mathbf{z}_t, t) - g^2(t)\nabla \log q_t^{\boldsymbol{\theta}}(\mathbf{z}_t)\right] \mathrm{d}\bar{t} + g(t)\, \mathrm{d}\bar{\mathbf{w}}_t. \tag{51}$$

As the Fokker-Planck equation of the SDE of Eq. (51) becomes

$$\frac{\partial q_t^{\boldsymbol{\theta}}}{\partial t}(\mathbf{z}_t) = \mathrm{div}\left(\left(-\mathbf{f}(\mathbf{z}_t, t) + \frac{g^2(t)}{2}\nabla \log q_t^{\boldsymbol{\theta}}(\mathbf{z}_t)\right) q_t^{\boldsymbol{\theta}}(\mathbf{z}_t)\right),$$

which coincide with the Fokker-Planck equation of the forward SDE of $\mathrm{d}\mathbf{z}_t = \mathbf{f}(\mathbf{z}_t, t)\,\mathrm{d}t + g(t)\,\mathrm{d}\mathbf{w}_t$, we conclude $\mathbf{s}_{\boldsymbol{\theta}} \in \mathbf{S}_{sol}$ by definition.

($\Leftarrow$) holds from Lemma 2. □

Theorem 3. *For any fixed $\mathbf{s}_{\bar{\boldsymbol{\theta}}} \in \mathbf{S}_{sol}$, if $\boldsymbol{\phi}^* \in \arg\min_{\boldsymbol{\phi}} D_{KL}(\boldsymbol{\mu}_{\boldsymbol{\phi}} \| \boldsymbol{\nu}_{\boldsymbol{\phi},\bar{\boldsymbol{\theta}}})$, then $\mathbf{s}_{\boldsymbol{\phi}^*}(\mathbf{z}_t, t) = \nabla \log p_t^{\boldsymbol{\phi}^*}(\mathbf{z}_t) = \mathbf{s}_{\bar{\boldsymbol{\theta}}}(\mathbf{z}_t, t)$, and $D_{KL}(\boldsymbol{\mu}_{\boldsymbol{\phi}^*} \| \boldsymbol{\nu}_{\boldsymbol{\phi}^*,\bar{\boldsymbol{\theta}}}) = D_{KL}(p_r \| p_{\boldsymbol{\phi}^*,\bar{\boldsymbol{\theta}}}) = Gap(\boldsymbol{\mu}_{\boldsymbol{\phi}^*}, \boldsymbol{\nu}_{\boldsymbol{\phi}^*,\bar{\boldsymbol{\theta}}}) = 0$.*

Proof of Theorem 3. If $\mathbf{s}_{\bar{\boldsymbol{\theta}}} \in \mathbf{S}_{sol}$, there exists q_0 such that $\mathbf{s}_{\bar{\boldsymbol{\theta}}}(\mathbf{z}_t, t) = \nabla \log q_t(\mathbf{z}_t)$, where $\mathbf{z}_t \sim q_t$ is governed by $\mathrm{d}\mathbf{z}_t = \mathbf{f}(\mathbf{z}_t, t)\,\mathrm{d}t + g(t)\,\mathrm{d}\mathbf{w}_t$ that starts from $\mathbf{z}_0 \sim q_0$. This implies that the generative path measure of $\boldsymbol{\nu}_{\boldsymbol{\phi},\bar{\boldsymbol{\theta}}}$ coincides with some forward path measure. On the other hand, the forward latent diffusion is also governed by $\mathrm{d}\mathbf{z}_t = \mathbf{f}(\mathbf{z}_t, t)\,\mathrm{d}t + g(t)\,\mathrm{d}\mathbf{w}_t$ that starts from $\mathbf{z}_0 \sim p_0^{\boldsymbol{\phi}}$. Therefore, if $p_0^{\boldsymbol{\phi}} = q_0$ almost everywhere, then the generative path measure of $\boldsymbol{\nu}_{\boldsymbol{\phi},\bar{\boldsymbol{\theta}}}$ coincides with the forward path measure of $\boldsymbol{\mu}_{\boldsymbol{\phi}}$, and it holds that $D_{KL}(\boldsymbol{\mu}_{\boldsymbol{\phi}} \| \boldsymbol{\nu}_{\boldsymbol{\phi},\bar{\boldsymbol{\theta}}}) = \int_0^T \frac{g^2(t)}{2}\mathbb{E}[\|\nabla \log p_t^{\boldsymbol{\phi}} - \nabla \log q_t\|_2^2]\,\mathrm{d}t + D_{KL}(p_T^{\boldsymbol{\phi}} \| q_T) = 0$. If $p_0^{\boldsymbol{\phi}} \neq q_0$ on a set of positive measure A, then $D_{KL}(\boldsymbol{\mu}_{\boldsymbol{\phi}} \| \boldsymbol{\nu}_{\boldsymbol{\phi},\bar{\boldsymbol{\theta}}}) = \int_0^T \frac{g^2(t)}{2}\mathbb{E}[\|\nabla \log p_t^{\boldsymbol{\phi}} - \nabla \log q_t\|_2^2]\,\mathrm{d}t + D_{KL}(p_T^{\boldsymbol{\phi}} \| q_T)$ is strictly positive because $\|\nabla \log p_t^{\boldsymbol{\phi}} - \nabla \log q_t\|_2^2 > 0$ on A, for any t. This leads that if $\boldsymbol{\phi}^* \in \arg\min_{\boldsymbol{\phi}} D_{KL}(\boldsymbol{\mu}_{\boldsymbol{\phi}} \| \boldsymbol{\nu}_{\boldsymbol{\phi},\bar{\boldsymbol{\theta}}})$, then $D_{KL}(\boldsymbol{\mu}_{\boldsymbol{\phi}^*} \| \boldsymbol{\nu}_{\boldsymbol{\phi}^*,\bar{\boldsymbol{\theta}}}) = 0$, and $p_0^{\boldsymbol{\phi}^*} = q_0$ almost everywhere. Therefore, we get the desired result because $0 = D_{KL}(\boldsymbol{\mu}_{\boldsymbol{\phi}^*} \| \boldsymbol{\nu}_{\boldsymbol{\phi}^*,\bar{\boldsymbol{\theta}}}) \geq D_{KL}(p_r \| p_{\boldsymbol{\phi}^*,\bar{\boldsymbol{\theta}}}) \geq 0$. □

Proposition 2. *$\mathbf{s}_{\boldsymbol{\theta}} \in \mathbf{S}_{div}$ if and only if $\nabla_{\mathbf{z}_t}\mathbf{s}_{\boldsymbol{\theta}}(\mathbf{z}_t, t)$ is symmetric.*

Proof of Proposition 2. If $\nabla_{\mathbf{z}_t}\mathbf{s}_{\boldsymbol{\theta}}(\mathbf{z}_t, t)$ is symmetric, then $\mathbf{s}_{\boldsymbol{\theta}}(\mathbf{z}_t, t)$ is a 1-form, and $\mathbf{s}_{\boldsymbol{\theta}} \in \mathbf{S}_{div}$. If $\mathbf{s}_{\boldsymbol{\theta}} \in \mathbf{S}_{div}$, then there exists p_t such that $\mathbf{s}_{\boldsymbol{\theta}}(\mathbf{z}_t, t) = \nabla \log p_t(\mathbf{z}_t)$. Thus, $\nabla \mathbf{s}_{\boldsymbol{\theta}} = \nabla^2 \log p_t$, which is symmetric. □

Proposition 3. *A matrix $A \in \mathbb{R}^{d\times d}$ is symmetric if and only if $\mathbb{E}_{\boldsymbol{\epsilon}_1,\boldsymbol{\epsilon}_2\sim\mathcal{N}(0,\mathbf{I})}\left[(\boldsymbol{\epsilon}_2^T(A - A^T)\boldsymbol{\epsilon}_1)^2\right] = 0$.*

Proof of Proposition 3. As

$$\mathbb{E}_{\boldsymbol{\epsilon}_1,\boldsymbol{\epsilon}_2\sim\mathcal{N}(0,\mathbf{I})}\left[(\boldsymbol{\epsilon}_2^T A\boldsymbol{\epsilon}_1 - \boldsymbol{\epsilon}_1^T A\boldsymbol{\epsilon}_2)^2\right] = \mathbb{E}_{\boldsymbol{\epsilon}_1,\boldsymbol{\epsilon}_2\sim\mathcal{N}(0,\mathbf{I})}\left[(\boldsymbol{\epsilon}_2^T(A - A^T)\boldsymbol{\epsilon}_1)^2\right],$$

A is symmetric if and only if $\mathbb{E}_{\boldsymbol{\epsilon}_1,\boldsymbol{\epsilon}_2\sim\mathcal{N}(0,\mathbf{I})}\left[(\boldsymbol{\epsilon}_2^T A\boldsymbol{\epsilon}_1 - \boldsymbol{\epsilon}_1^T A\boldsymbol{\epsilon}_2)^2\right] = 0$. □

Proposition 4. *Let $\boldsymbol{\epsilon}_1$ and $\boldsymbol{\epsilon}_2$ be vectors of d independent samples from a random variable U with mean zero. Then*

$$\mathbb{E}_{\boldsymbol{\epsilon}_1,\boldsymbol{\epsilon}_2}[(\boldsymbol{\epsilon}_2^T(A - A^T)\boldsymbol{\epsilon}_1)^2] = \mathbb{E}_U[U^2]^2\|A - A^T\|_F^2$$

and

$$\begin{aligned}
Var\Big(\big(\boldsymbol{\epsilon}_2^T(A - A^T)\boldsymbol{\epsilon}_1\big)^2\Big) &= Var(U^2)\Big(Var(U^2) + 2\big(Var(U) + \mathbb{E}_U[U]^2\big)^2\Big)\sum_{a,b}(\Delta A)_{ab}^4 \\
&+ 2\big(Var(U) + \mathbb{E}_U[U]^2\big)^2\Big(3Var(U^2) + 2\big(Var(U) + \mathbb{E}_U[U]^2\big)^2\Big)\sum_a\sum_{b\neq d}(\Delta A)_{ab}^2(\Delta A)_{ad}^2 \\
&+ 2\big(Var(U) + \mathbb{E}_U[U]^2\big)^4\Big(\sum_{a\neq c}\sum_{b\neq d}(\Delta A)_{ab}^2(\Delta A)_{cd}^2 \\
&\qquad + 3\sum_{a\neq c}\sum_{b\neq d}(\Delta A)_{ab}(\Delta A)_{ad}(\Delta A)_{cb}(\Delta A)_{cd}\Big),
\end{aligned}$$

where $(\Delta A)_{ab} := A_{ab} - A_{ba}$.

Proof of Proposition 4.

$$
\begin{aligned}
\mathbb{E}_{\boldsymbol{\epsilon}_1,\boldsymbol{\epsilon}_2}\Big[\big(\boldsymbol{\epsilon}_2^T(A-A^T)\boldsymbol{\epsilon}_1\big)^2\Big] =& \mathbb{E}_{\boldsymbol{\epsilon}_1,\boldsymbol{\epsilon}_2}\Big[\big(\sum_{i,j}\epsilon_{1,i}\epsilon_{2,j}(A_{ij}-A_{ji})^2\big)^2\Big] \\
=& \mathbb{E}_{\boldsymbol{\epsilon}_1,\boldsymbol{\epsilon}_2}\Big[\sum_{i,j,r,s}\epsilon_{1,i}\epsilon_{2,j}\epsilon_{1,r}\epsilon_{2,s}(A_{ij}-A_{ji})(A_{rs}-A_{sr})\Big] \\
=& \mathbb{E}_{\boldsymbol{\epsilon}_1,\boldsymbol{\epsilon}_2}\Big[\sum_{i,j}\epsilon_{1,i}^2\epsilon_{2,j}^2(A_{ij}-A_{ji})^2\Big] \\
=& \mathbb{E}_U[U^2]^2\sum_{i,j}(A_{ij}-A_{ji})^2 \\
=& \mathbb{E}_U[U^2]^2\|A-A^T\|_F^2.
\end{aligned}
$$

Also, if $B := A - A^T$, then

$$
\begin{aligned}
&\mathbb{E}_{\boldsymbol{\epsilon}_1,\boldsymbol{\epsilon}_2}\Big[\big(\boldsymbol{\epsilon}_2^T(A-A^T)\boldsymbol{\epsilon}_1\big)^4\Big] \\
&= \mathbb{E}_{\boldsymbol{\epsilon}_1,\boldsymbol{\epsilon}_2}\Big[\sum_{a,b,c,d,e,f,g,h}\epsilon_{1,a}\epsilon_{2,b}\epsilon_{1,c}\epsilon_{2,d}\epsilon_{1,e}\epsilon_{2,f}\epsilon_{1,g}\epsilon_{2,h}B_{ab}B_{cd}B_{ef}B_{gh}\Big] \\
&= \mathbb{E}_{\boldsymbol{\epsilon}_1,\boldsymbol{\epsilon}_2}\Big[\sum_{b,d,f,h}\epsilon_{2,b}\epsilon_{2,d}\epsilon_{2,f}\epsilon_{2,h}\sum_{a,c}\epsilon_{1,a}\epsilon_{1,c}\sum_{e,g}\epsilon_{1,e}\epsilon_{1,g}B_{ab}B_{cd}B_{ef}B_{gh}\Big] \\
&= \mathbb{E}_{\boldsymbol{\epsilon}_1,\boldsymbol{\epsilon}_2}\Big[\sum_{b,d,f,h}\epsilon_{2,b}\epsilon_{2,d}\epsilon_{2,f}\epsilon_{2,h}\sum_{a}\epsilon_{1,a}^2\sum_{e,g}\epsilon_{1,e}\epsilon_{1,g}B_{ab}B_{ad}B_{ef}B_{gh}\Big] \\
&\quad+\mathbb{E}_{\boldsymbol{\epsilon}_1,\boldsymbol{\epsilon}_2}\Big[\sum_{b,d,f,h}\epsilon_{2,b}\epsilon_{2,d}\epsilon_{2,f}\epsilon_{2,h}\sum_{a\neq c}\epsilon_{1,a}\epsilon_{1,c}\sum_{e,g}\epsilon_{1,e}\epsilon_{1,g}B_{ab}B_{cd}B_{ef}B_{gh}\Big] \\
&= \mathbb{E}_{\boldsymbol{\epsilon}_1,\boldsymbol{\epsilon}_2}\Big[\sum_{b,d,f,h}\epsilon_{2,b}\epsilon_{2,d}\epsilon_{2,f}\epsilon_{2,h}\sum_{a}\epsilon_{1,a}^2\sum_{e}\epsilon_{1,e}^2B_{ab}B_{ad}B_{ef}B_{eh}\Big] \\
&\quad+\mathbb{E}_{\boldsymbol{\epsilon}_1,\boldsymbol{\epsilon}_2}\Big[\sum_{b,d,f,h}\epsilon_{2,b}\epsilon_{2,d}\epsilon_{2,f}\epsilon_{2,h}\sum_{a\neq c}\epsilon_{1,a}^2\epsilon_{1,c}^2B_{ab}B_{cd}(B_{af}B_{ch}+B_{cf}B_{ah})\Big] \\
&= \mathbb{E}_{\boldsymbol{\epsilon}_1,\boldsymbol{\epsilon}_2}\Big[\sum_{b,d,f,h}\epsilon_{2,b}\epsilon_{2,d}\epsilon_{2,f}\epsilon_{2,h}\sum_{a}\epsilon_{1,a}^4B_{ab}B_{ad}B_{af}B_{ah}\Big] \\
&\quad+3\mathbb{E}_{\boldsymbol{\epsilon}_1,\boldsymbol{\epsilon}_2}\Big[\sum_{b,d,f,h}\epsilon_{2,b}\epsilon_{2,d}\epsilon_{2,f}\epsilon_{2,h}\sum_{a\neq c}\epsilon_{1,a}^2\epsilon_{1,c}^2B_{ab}B_{af}B_{cd}B_{ch}\Big] \\
&= \mathbb{E}_U[U^4]\sum_{a}\mathbb{E}_{\boldsymbol{\epsilon}_2}\Big[\sum_{b,d,f,h}\epsilon_{2,b}\epsilon_{2,d}\epsilon_{2,f}\epsilon_{2,h}B_{ab}B_{ad}B_{af}B_{ah}\Big] \\
&\quad+3\mathbb{E}_U[U^2]^2\sum_{a\neq c}\mathbb{E}_{\boldsymbol{\epsilon}_2}\Big[\sum_{b,d,f,h}\epsilon_{2,b}\epsilon_{2,d}\epsilon_{2,f}\epsilon_{2,h}B_{ab}B_{af}B_{cd}B_{ch}\Big] \\
&= \mathbb{E}_U[U^4]\sum_{a}\mathbb{E}_{\boldsymbol{\epsilon}_2}\Big[\sum_{b}\epsilon_{2,b}^4B_{ab}^4+3\sum_{b\neq d}\epsilon_{2,b}^2\epsilon_{2,d}^2B_{ab}^2B_{ad}^2\Big] \\
&\quad+3\mathbb{E}_U[U^2]^2\sum_{a\neq c}\mathbb{E}_{\boldsymbol{\epsilon}_2}\Big[\sum_{b}\epsilon_{2,b}^4B_{ab}^2B_{cb}^2+\sum_{b\neq d}\epsilon_{2,b}^2\epsilon_{2,d}^2(B_{ab}^2B_{cd}^2+2B_{ab}B_{ad}B_{cb}B_{cd})\Big] \\
&= \mathbb{E}_U[U^4]^2\sum_{a,b}B_{ab}^4+3\mathbb{E}_U[U^2]^2\mathbb{E}_U[U^4]\Big[\Big(\sum_{a}\sum_{b\neq d}B_{ab}^2B_{ad}^2+\sum_{b}\sum_{a\neq c}B_{ab}^2B_{cb}^2\Big)\Big] \\
&\quad+3\mathbb{E}_U[U^2]^4\sum_{a\neq c}\sum_{b\neq d}\Big(B_{ab}^2B_{cd}^2+2B_{ab}B_{ad}B_{cb}B_{cd}\Big) \\
&= \mathbb{E}_U[U^4]^2\sum_{a,b}B_{ab}^4+6\mathbb{E}_U[U^2]^2\mathbb{E}_U[U^4]\Big[\sum_{a}\sum_{b\neq d}B_{ab}^2B_{ad}^2\Big]
\end{aligned}
$$

$$+3\mathbb{E}_U[U^2]^4 \sum_{a\neq c}\sum_{b\neq d}\Big(B_{ab}^2B_{cd}^2 + 2B_{ab}B_{ad}B_{cb}B_{cd}\Big)$$

Also,

$$\begin{aligned}
\mathbb{E}_{\boldsymbol{\epsilon}_1,\boldsymbol{\epsilon}_2}\left[\left(\boldsymbol{\epsilon}_2^T(A-A^T)\boldsymbol{\epsilon}_1\right)^2\right]^2 &= \Big(\mathbb{E}_U[U^2]^2\sum_{i,j}B_{ij}^2\Big)^2 \\
&= \mathbb{E}_U[U^2]^4\sum_{i,j,r,s}B_{ij}^2B_{rs}^2 \\
&= \mathbb{E}_U[U^2]^4\Big(\sum_{i,j}\sum_{s}B_{ij}^2B_{is}^2 + \sum_{j,s}\sum_{i\neq r}B_{ij}^2B_{rs}^2\Big) \\
&= \mathbb{E}_U[U^2]^4\Big(\sum_{i,j}\sum_{s}B_{ij}^2B_{is}^2 + \sum_{j}\sum_{i\neq r}B_{ij}^2B_{rj}^2 + \sum_{i\neq r}\sum_{j\neq s}B_{ij}^2B_{rs}^2\Big) \\
&= \mathbb{E}_U[U^2]^4\Big(\sum_{i,j}B_{ij}^4 + \sum_{i}\sum_{j\neq s}B_{ij}^2B_{is}^2 + \sum_{j}\sum_{i\neq r}B_{ij}^2B_{rj}^2 + \sum_{i\neq r}\sum_{j\neq s}B_{ij}^2B_{rs}^2\Big)
\end{aligned}$$

Therefore,

$$\begin{aligned}
\mathrm{Var}\left(\left(\boldsymbol{\epsilon}_2^T(A-A^T)\boldsymbol{\epsilon}_1\right)^2\right) &= \mathbb{E}_{\boldsymbol{\epsilon}_1,\boldsymbol{\epsilon}_2}\left[\left(\boldsymbol{\epsilon}_2^T(A-A^T)\boldsymbol{\epsilon}_1\right)^4\right] - \mathbb{E}_{\boldsymbol{\epsilon}_1,\boldsymbol{\epsilon}_2}\left[\left(\boldsymbol{\epsilon}_2^T(A-A^T)\boldsymbol{\epsilon}_1\right)^2\right]^2 \\
&= \Big(\mathbb{E}_U[U^4]^2 - \mathbb{E}_U[U^2]^4\Big)\sum_{a,b}B_{ab}^4 + 2\mathbb{E}_U[U^2]^2\Big(3\mathbb{E}_U[U^4] - \mathbb{E}_U[U^2]^2\Big)\sum_{a}\sum_{b\neq d}B_{ab}^2B_{ad}^2 \\
&\quad +2\mathbb{E}_U[U^2]^4\Big(\sum_{a\neq c}\sum_{b\neq d}B_{ab}^2B_{cd}^2 + 3\sum_{a\neq c}\sum_{b\neq d}B_{ab}B_{ad}B_{cb}B_{cd}\Big) \\
&= \mathrm{Var}(U^2)\Big(\mathrm{Var}(U^2) + 2\big(\mathrm{Var}(U) + \mathbb{E}_U[U]^2\big)^2\Big)\sum_{a,b}B_{ab}^4 \\
&\quad +2\big(\mathrm{Var}(U) + \mathbb{E}_U[U]^2\big)^2\Big(3\mathrm{Var}(U^2) + 2\big(\mathrm{Var}(U) + \mathbb{E}_U[U]^2\big)^2\Big)\sum_{a}\sum_{b\neq d}B_{ab}^2B_{ad}^2 \\
&\quad +2\big(\mathrm{Var}(U) + \mathbb{E}_U[U]^2\big)^4\Big(\sum_{a\neq c}\sum_{b\neq d}B_{ab}^2B_{cd}^2 + 3\sum_{a\neq c}\sum_{b\neq d}B_{ab}B_{ad}B_{cb}B_{cd}\Big)
\end{aligned}$$

□

Proposition 5. *Let U be the discrete random variable which takes the values $1, -1$ each with probability $1/2$. Then $(\boldsymbol{\epsilon}_2^T(A-A^T)\boldsymbol{\epsilon}_1)^2$ is the unbiased estimator of $\|A-A^T\|_F^2$. Moreover, U is the unique random variable amongst zero-mean random variables for which the estimator is an unbiased estimator, and attains a minimum variance.*

Proof of Proposition 5. A random variable U^2 has strictly positive variance if U^2 attains more than two values on a nonzero measure. To make $\mathrm{Var}(U^2) = 0$, the random variable should be a discrete variable which takes the values 1, -1 each with probability 1/2. □

Theorem 4 (De Bortoli et al. [15] and Guth et al. [22])**.** *Assume that there exists $M \geq 0$ such that for any $t \in [0,T]$ and $\mathbf{z} \in \mathbb{R}^d$, the score estimation is close enough to the forward score by M, $\|\mathbf{s}_{\boldsymbol{\theta}}(\mathbf{x},t) - \nabla \log p_t^{\boldsymbol{\phi}}(\mathbf{x})\| \leq M$, with $\mathbf{s}_{\boldsymbol{\theta}} \in C([0,T]\times\mathbb{R}^d,\mathbb{R}^d)$. Assume that $\nabla \log p_t^{\boldsymbol{\phi}}(\mathbf{z})$ is C^2 in both t and $\mathbf{z}$, and that $\sup_{\mathbf{z},t}\|\nabla^2 \log p_t^{\boldsymbol{\phi}}(\mathbf{z})\| \leq K$ and $\|\frac{\partial}{\partial t}\nabla \log p_t^{\boldsymbol{\phi}}(\mathbf{z})\| \leq Me^{-\alpha t}\|\mathbf{z}\|$ for some $K, M, \alpha > 0$. Suppose $(\mathbf{h}_{\boldsymbol{\phi}}^{-1})_{\#}$ s a push-forward map. Then $\|p_r - (\mathbf{h}_{\boldsymbol{\phi}}^{-1})_{\#}p_{0,N}^{\boldsymbol{\theta}}\|_{TV} \leq E_{pri}(\boldsymbol{\phi}) + E_{dis}(\boldsymbol{\phi}) + E_{est}(\boldsymbol{\phi},\boldsymbol{\theta})$, where $E_{pri}(\boldsymbol{\phi}) = \sqrt{2}e^{-T}D_{KL}(p_T^{\boldsymbol{\phi}}\|\pi)^{1/2}$ is the error originating from the prior mismatch; $E_{dis}(\boldsymbol{\phi}) = 6\sqrt{\delta}(1 + \mathbb{E}_{p_0^{\boldsymbol{\phi}}(\mathbf{z})}[\|\mathbf{z}\|^4]^{1/4})(1 + K + M(1 + \frac{1}{\sqrt{2\alpha}}))$ is the discretization error with $\delta = \frac{\max \gamma_k{}^2}{\min \gamma_k}$; $E_{est}(\boldsymbol{\phi},\boldsymbol{\theta}) = 2TM^2$ is the score estimation error.*

Remark 5. Although the proof is based on the standard form of the Ornstein-Uhlenbeck process, the direct extension of the theorem holds for generic VPSDE if there exists $\bar{\beta} > 0$ such that $\frac{1}{\bar{\beta}} \leq \beta(t) \leq \bar{\beta}$. See De Bortoli [69].

Lemma 4 (Lemma S11 of De Bortoli et al. [15]). *Let $(\mathsf{E}, \mathcal{E})$ and $(\mathsf{F}, \mathcal{F})$ be two measurable spaces and $K : \mathsf{E} \times \mathcal{F} \to [0, 1]$ be a Markov kernel. Then for any $\mu_0, \mu_1 \in \mathcal{P}(\mathsf{E})$ we have*

$$\|\mu_0 K - \mu_1 K\|_{TV} \leq \|\mu_0 - \mu_1\|_{TV}.$$

In addition, for any $\varphi : \mathsf{E} \to \mathsf{F}$ measurable we get that

$$\|\varphi_\# \mu_0 - \varphi_\# \mu_1\|_{TV} \leq \|\mu_0 - \mu_1\|_{TV},$$

with equality if φ is injective.

Proof of Theorem 4. For any $k \in \{1, ..., N\}$, denote R_k the Markov kernel such that for any $\mathbf{z} \in \mathbb{R}^d$, $\mathsf{A} \in \mathcal{B}(\mathbb{R}^d)$ and $k \in \{0, ..., N-1\}$ we have

$$R^{\boldsymbol{\theta}}_{k+1}(\mathbf{z}, \mathsf{A}) = (4\pi\gamma_{k+1})^{-d/2} \int_{\mathsf{A}} \exp\left[- \frac{\|\tilde{\mathbf{z}} - \mathcal{T}^{\boldsymbol{\theta}}_{k+1}(\mathbf{z})\|^2}{4\gamma_{k+1}} \right] \mathrm{d}\tilde{\mathbf{z}},$$

where for any $\mathbf{z} \in \mathbb{R}^d$, $\mathcal{T}^{\boldsymbol{\theta}}_{k+1}(\mathbf{z}) = \mathbf{z} + \gamma_{k+1}\{\mathbf{z} + 2\mathbf{s}_{\boldsymbol{\theta}}(\mathbf{z}, t_k)\}$, where $t_k = \sum_l^{k-1} \gamma_l$. Define $Q^{\boldsymbol{\theta}}_N = \prod_{l=1}^N R^{\boldsymbol{\theta}}_l$. Analogously, let us define

$$R^{\boldsymbol{\phi}}_{k+1}(\mathbf{z}, \mathsf{A}) = (4\pi\gamma_{k+1})^{-d/2} \int_{\mathsf{A}} \exp\left[- \frac{\|\tilde{\mathbf{z}} - \mathcal{T}^{\boldsymbol{\phi}}_{k+1}(\mathbf{z})\|^2}{4\gamma_{k+1}} \right] \mathrm{d}\tilde{\mathbf{z}},$$

for $\mathcal{T}^{\boldsymbol{\phi}}_{k+1}(\mathbf{z}) = \mathbf{z} + \gamma_{k+1}\{\mathbf{z} + 2\nabla \log p^{\boldsymbol{\phi}}_t(\mathbf{z}, t_k)\}$ and $Q^{\boldsymbol{\phi}}_N = \prod_{l=1}^N R^{\boldsymbol{\phi}}_l$.

Suppose $\mathbb{P}_{T|0}$ is the transition kernel from time zero to T and $\mathbb{P}^R$ is the reverse-time measure, i.e., for any $\mathsf{A} \in \mathcal{B}(\mathcal{C})$ we have $\mathbb{P}^R(\mathsf{A}) = \mathbb{P}(\mathsf{A}^R)$ with $\mathsf{A}^R = \{t \mapsto \omega(T - t) : \omega \in \mathsf{A}\}$. Then,

$$p^{\boldsymbol{\phi}}_0 \mathbb{P}_{T|0} \mathbb{P}^R{}_{T|0}(\mathsf{A}) = \mathbb{P}_T \mathbb{P}^R{}_{T|0}(\mathsf{A}) = \mathbb{P}^R{}_0 \mathbb{P}^R{}_{T|0}(\mathsf{A}) = \mathbb{P}^R{}_T(\mathsf{A}) = p^{\boldsymbol{\phi}}_0(\mathsf{A}). \tag{52}$$

Combining Eq. (52) with Lemma 4, we have

$$\begin{aligned}
\|p^{\boldsymbol{\phi}}_0 - p^{\boldsymbol{\theta}}_{0,N}\|_{TV} &= \|p^{\boldsymbol{\phi}}_0 \mathbb{P}_{T|0} \mathbb{P}^R{}_{T|0} - \pi Q^{\boldsymbol{\theta}}_N\|_{TV} \\
&\leq \|p^{\boldsymbol{\phi}}_0 \mathbb{P}_{T|0} \mathbb{P}^R{}_{T|0} - \pi \mathbb{P}^R{}_{T|0}\|_{TV} + \|\pi \mathbb{P}^R{}_{T|0} - \pi Q^{\boldsymbol{\phi}}_N\|_{TV} + \|\pi Q^{\boldsymbol{\phi}}_N - \pi Q^{\boldsymbol{\theta}}_N\|_{TV} \\
&\leq \underbrace{\|p^{\boldsymbol{\phi}}_0 \mathbb{P}_{T|0} - \pi\|_{TV}}_{E_{pri}} + \underbrace{\|\pi \mathbb{P}^R{}_{T|0} - \pi Q^{\boldsymbol{\phi}}_N\|_{TV}}_{E_{dis}} + \underbrace{\|\pi Q^{\boldsymbol{\phi}}_N - \pi Q^{\boldsymbol{\theta}}_N\|_{TV}}_{E_{est}}.
\end{aligned}$$

The first two terms, $E_{pri}(\boldsymbol{\phi}) + E_{dis}(\boldsymbol{\phi})$, are those terms derived in Theorem 2 of Guth et al. [22]. By Lemma S13 of De Bortoli et al. [15], the last term, $E_{est}(\boldsymbol{\phi}, \boldsymbol{\theta})$, is bounded by

$$\|\pi Q^{\boldsymbol{\phi}}_N - \pi Q^{\boldsymbol{\theta}}_N\|^2_{TV} \leq \frac{1}{2} \int_0^T \mathbb{E}\big[\|b_{\boldsymbol{\phi}}(\{\mathbf{z}_t\}^T_{t=0}, t) - b_{\boldsymbol{\theta}}(\{\mathbf{z}_t\}^T_{t=0}, t)\|^2\big] \, \mathrm{d}t,$$

where $b_{\boldsymbol{\phi}}(\{\mathbf{z}_t\}^T_{t=0}, t) = \sum_{k=0}^{N-1} 1_{[t_k, t_{k+1})}(t)\{\mathbf{z}_{t_k} + 2\log p^{\boldsymbol{\phi}}_t(\mathbf{z}_{t_k})\}$ and $b_{\boldsymbol{\theta}}(\{\mathbf{z}_t\}^T_{t=0}, t) = \sum_{k=0}^{N-1} 1_{[t_k, t_{k+1})}(t)\{\mathbf{z}_{t_k} + 2\mathbf{s}_{\boldsymbol{\theta}}(\mathbf{z}_{t_k}, t_k)\}$ are the drift terms of piecewise generative processes, given by

$$\mathrm{d}\mathbf{z}_t = \Big[- \mathbf{z}_t - 2\nabla \log p^{\boldsymbol{\phi}}_{t_k}(\mathbf{z}_{t_k}) \Big] \, \mathrm{d}\bar{t} + g(t) \, \mathrm{d}\bar{\mathbf{w}}_t$$

and

$$\mathrm{d}\mathbf{z}_t = \Big[- \mathbf{z}_t - 2\mathbf{s}_{\boldsymbol{\theta}}(\mathbf{z}_{t_k}, t_k) \Big] \, \mathrm{d}\bar{t} + g(t) \, \mathrm{d}\bar{\mathbf{w}}_t$$

defined each of the interval $[t_k, t_{k+1}]$ for $k = 0, ..., N-1$, respectively. Therefore, $E_{est}(\boldsymbol{\phi}, \boldsymbol{\theta})$ is bounded by

$$\begin{aligned}
E_{est}(\boldsymbol{\phi}, \boldsymbol{\theta}) &\leq \frac{1}{2} \int_0^T \mathbb{E}\big[\|b_{\boldsymbol{\phi}}(\{\mathbf{z}_t\}^T_{t=0}, t) - b_{\boldsymbol{\theta}}(\{\mathbf{z}_t\}^T_{t=0}, t)\|^2\big] \, \mathrm{d}t \\
&= 2 \sum_{k=0}^{N-1} \int_{t_k}^{t_{k+1}} \mathbb{E}\big[\|\nabla \log p^{\boldsymbol{\phi}}_{t_k}(\mathbf{z}_{t_k}) - \mathbf{s}_{\boldsymbol{\theta}}(\mathbf{z}_{t_k}, t_k)\|^2\big] \, \mathrm{d}t
\end{aligned}$$

Table 21: Performance comparison to linear/nonlinear diffusion models on CIFAR-10. We report both before/after correction of density estimation performances. We report the baseline performances of linear diffusions by training our PyTorch implementation based on Song et al. [1, 11] with identical hyperparameters and networks on both linear/nonlinear diffusions in order to quantify the effect of nonlinearity in a fair setting. Boldface numbers represent the best performance in a column, and underlined numbers represent the second best.

SDE	Model	Nonlinear Data Diffusion	# Params	NLL (↓) after correction	NLL (↓) before correction	NELBO (↓) w/ residual (after)	NELBO (↓) w/o residual (before)	Gap (↓) (=NELBO-NLL) after	Gap (↓) (=NELBO-NLL) before	FID (↓) ODE	FID (↓) PC
VE	NCSN++ (FID)	✗	63M	4.86	3.66	4.89	4.45	0.03	0.79	-	2.38
	INDM (FID)	✓	76M	3.22	3.13	3.28	3.24	0.06	0.11	-	2.29
	NCSN++ (deep, FID)	✗	108M	4.85	3.45	4.86	4.43	0.01	0.98	-	**2.20**
	INDM (deep, FID)	✓	118M	3.13	3.03	3.14	3.10	0.01	0.07	-	2.28
VP	DDPM++ (FID)	✗	62M	3.21	3.16	3.34	3.32	0.13	0.16	3.90	2.89
	INDM (FID)	✓	75M	3.17	3.11	3.23	3.18	0.06	0.07	**3.61**	2.90
	DDPM++ (deep, FID)	✗	108M	3.19	3.13	3.32	3.29	0.13	0.16	3.69	2.64
	INDM (deep, FID)	✓	121M	3.09	3.02	3.13	3.08	0.04	0.06	3.67	3.15
	DDPM++ (NLL)	✗	62M	3.03	2.97	3.13	3.11	0.10	0.14	6.70	5.17
	INDM (NLL)	✓	75M	2.98	2.95	2.98	2.97	**0.00**	**0.02**	6.01	5.30
	INDM (NLL, ST)	✓	75M	3.01	2.98	3.02	3.01	0.01	0.03	3.88	3.25
	DDPM++ (deep, NLL)	✗	108M	3.01	2.95	3.11	3.09	0.10	0.14	6.43	4.88
	INDM (deep, NLL)	✓	121M	**2.97**	**2.94**	**2.97**	**2.96**	**0.00**	**0.02**	5.71	4.79

Table 22: Performance comparison on CIFAR-10.

Class	SDE	Type	Model	NLL (↓) after correction	NLL (↓) before correction	NELBO (↓) w/ residual (after)	NELBO (↓) w/o residual (before)	Gap (↓) (=NELBO-NLL) after	Gap (↓) (=NELBO-NLL) before	FID (↓) ODE	FID (↓) PC
GAN			StyleGAN2 + ADA [70]	-	-	-	-	-	-	2.92	
			StyleFormer [32]	-	-	-	-	-	-	2.82	
			SNGAN + DGflow [71]	-	-	-	-	-	-	9.62	
			TransGAN [72]	-	-	-	-	-	-	9.26	
Autoregressive			PixcelCNN [73]	3.14	-	-	-	-	-	65.9	
			PixcelRNN [73]	3.00	-	-	-	-	-	-	
			Sparse Transformer [74]	2.80	-	-	-	-	-	-	
Flow			Glow [56]	3.35	-	-	-	-	-	48.9	
			Residual Flow [23]	3.28	-	-	-	-	-	46.4	
			Flow++ [26]	3.28	-	-	-	-	-	46.4	
			Wolf [24]	3.27	-	-	-	-	-	37.5	
			VFlow [75]	2.98	-	-	-	-	-	-	
			DenseFlow-74-10 [4]	2.98	-	-	-	-	-	34.9	
VAE			NVAE [6]	-	-	2.91	-	-	-	23.5	
			Very Deep VAE [76]	-	-	2.87	-	-	-	-	
			δ-VAE [77]	-	-	2.83	-	-	-	-	
			DCVAE [78]	-	-	-	-	-	-	17.9	
			CR-NVAE [31]	-	-	-	-	-	-	2.51	
Diffusion	Linear		DDPM [8]	-	-	3.75	-	-	-	3.17	
			NCSNv2 [7]	-	-	-	-	-	-	10.87	
			DDIM [79]	-	-	-	-	-	-	4.04	
			IDDPM [60]	3.37	-	-	-	-	-	2.90	
			VDM [28]	**2.65**	-	-	-	-	-	7.41	
			NCSN++ (FID) [1]	4.85	3.45	4.86	4.43	0.01	0.98	-	**2.20**
			DDPM++ (FID) [1]	3.19	3.13	3.32	3.29	0.13	0.16	3.69	2.64
			DDPM++ (NLL) [11]	3.01	2.95	3.11	3.09	0.10	0.14	6.43	4.88
			CLD-SGM [20]	-	-	-	3.31	-	-	2.25	-
	Nonlinear	SBP	SB-FBSDE [16]	-	2.98	-	-	-	-	-	3.18
		VAE -based	LSGM (FID) [9]	-	-	3.45	3.43	-	-	**2.10**	-
			LSGM (NLL)-269M	-	-	-	2.97	-	-	6.15	-
			LSGM (NLL)	-	-	**2.87**	**2.87**	-	-	6.89	-
			LSGM (balanced)-109M	-	-	-	2.96	-	-	4.60	-
			LSGM (balanced)	-	-	2.98	2.95	-	-	2.17	-
		Flow -based	DiffFlow (FID) [13]	-	-	3.04	-	-	-	-	14.14
			INDM (FID)	3.13	3.03	3.14	3.10	0.01	0.07	-	2.28
			INDM (NLL)	2.97	**2.94**	2.97	2.96	**0.00**	**0.02**	5.71	4.79
			INDM (ST)	3.01	2.98	3.02	3.01	0.01	0.03	3.88	3.25

$$\leq 2TM^2.$$

Now, from Lemma 4 and the invertibility of the flow transformation, we have

$$\|p_r - (\mathbf{h}_{\boldsymbol{\phi}}^{-1})_{\#} \circ p_{0,N}^{\boldsymbol{\theta}}\|_{TV} = \|(\mathbf{h}_{\boldsymbol{\phi}})_{\#} \circ p_r - p_{0,N}^{\boldsymbol{\theta}}\|_{TV} = \|p_0^{\boldsymbol{\phi}} - p_{0,N}^{\boldsymbol{\theta}}\|_{TV},$$

which completes the proof. □

Table 23: Performance comparison on CelebA 64×64.

Model	NLL (↓)		NELBO (↓)		Gap (↓)		FID (↓)	
	after	before	w/ res-	w/o res-	after	before	ODE	PC
UNCSN++ [27]	-	**1.93**	-	-	-	-	-	**1.92**
DDGM [29]	-	-	-	-	-	-	-	2.92
Efficient-VDVAE [30]	-	**1.83**	-	-				
CR-NVAE [31]	-	-	1.86	-	-	-	-	-
DenseFlow-74-10 [4]	1.99	-	-	-	-	-	-	-
StyleFormer [32]	-	-	-	-	-	-	3.66	
NCSN++ (VE)	3.41	2.37	3.42	3.96	0.01	1.59	-	3.95
INDM (VE, FID)	2.31	1.95	2.33	2.17	0.02	0.22	-	2.54
DDPM++ (VP, FID)	2.14	2.07	2.21	2.22	0.06	0.14	2.32	3.03
INDM (VP, FID)	2.27	2.13	2.31	2.20	0.04	0.07	**1.75**	2.32
DDPM++ (VP, NLL)	2.00	1.93	2.09	2.09	0.09	0.16	3.95	5.31
INDM (VP, NLL)	2.05	1.97	2.05	2.00	0.00	0.03	3.06	5.14

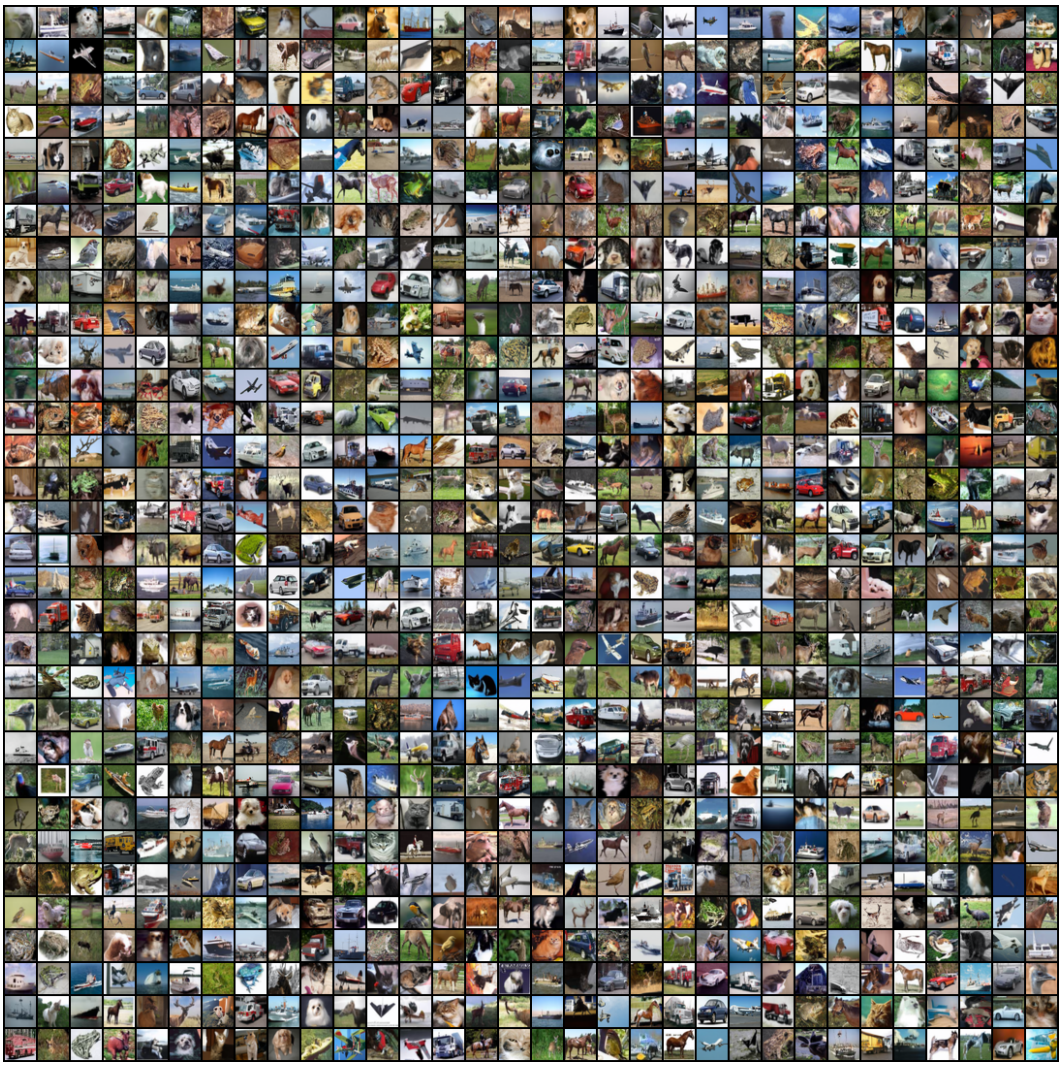

Figure 20: Non cherry-picked random samples from CIFAR-10 trained on INDM (VE, deep, FID).

Figure 21: Non cherry-picked random samples fr om CelebA trained on INDM (VP, FID).